AN EVALUATION OF THE FAST-MIXED SPECTRUM REACTOR

by

WEE TEE LOH

B.S., University of Malaya
(1974)

SUBMITTED IN PARTIAL FULFILLMENT
OF THE REQUIREMENTS FOR THE
DEGREE OF

MASTER OF SCIENCE

at the

MASSACHUSETTS INSTITUTE OF TECHNOLOGY

February 1980

© Massachusetts Institute of Technology 1980

Signature of Author _____
Department of Nuclear Engineering
January 14, 1980

Certified by _____
Michael J. Driscoll
Thesis Supervisor

Certified by _____
David D. Lanning
Thesis Supervisor

Accepted by _____
Allan F. Henry
Chairman, Department Committee
on Graduate Students

ARCHIVES
MASSACHUSETTS INSTITUTE
OF TECHNOLOGY

MAR 20 1980

LIBRARIES

AN EVALUATION OF THE FAST-MIXED SPECTRUM REACTOR

by

WEE TEE LOH

Submitted to the Department of Nuclear Engineering on January 18, 1980, in partial fulfillment of the requirements for the degree of Master of Science.

ABSTRACT

An independent evaluation of the neutronic characteristics of a gas-cooled fast-mixed spectrum reactor (FMSR) core design has been performed. A benchmark core configuration for an early FMSR design was provided by Brookhaven National Laboratory, the originators of the concept.

The results of the evaluation were compared with those of BNL. Points of comparison included system reactivity and breeding ratio, and region-wise power densities and isotopic compositions as a function of burnup. The results are in sufficiently good agreement to conclude that the neutronic feasibility of the FMSR concept has been independently validated. Significant differences, primarily in higher plutonium isotope concentrations, occur only in regions of low neutronic importance, and plausible reasons for the differences are advanced based on sensitivity studies and comparison of spectral indices. While both M.I.T. and BNL calculations tend to predict that the benchmark design is slightly subcritical at the beginning of equilibrium cycle, the margin to $k = 1.0$ is close enough ($\Delta k \leq 0.03$) that the situation can be remedied. Establishment of a consensus fission product cross section set was identified as an objective of merit, since non-negligible differences were found in results computed using various extant sets (BNL, LIB-IV, Japanese).

Non-fission heating by gamma and neutron interactions was evaluated for the reference core design using a coupled neutron/gamma cross section set and S_N calculations. In the unfueled regions of the core, moderator elements in particular, the non-fission heating rate was found to be significant (averaging about 6 kw/liter), but posed no obvious problems. In fueled regions the common assumption of local deposition of all energy at the point of fission was verified to be a good approximation for most engineering purposes.

Thesis Supervisor: Michael J. Driscoll
Title: Associate Professor of Nuclear Engineering

Thesis Supervisor: David D. Lanning
Title: Professor of Nuclear Engineering

ACKNOWLEDGEMENTS

The author wishes to acknowledge the invaluable guidance, advice and encouragement offered by his principal adviser, Professor Michael J. Driscoll. The help of Professor David D. Lanning, who served as co-supervisor, and provided helpful advice, is appreciated.

The advice and assistance of Bahman Atefi, Dale Lancaster, and Rachel Morton on computational problems are gratefully acknowledged.

The Research Assistantship support provided by the Brookhaven National Laboratory subcontract under which this work was done is much appreciated.

Computer calculations were performed at the M.I.T. Information Processing Center and the Laboratory for Nuclear Science. Typing of the manuscript was very ably done by Ms. Annette Holman.

TABLE OF CONTENTS

		Page
ABSTRACT		2
ACKNOWLEDGEMENTS		3
TABLE OF CONTENTS		4
LIST OF FIGURES		6
LIST OF TABLES		8
CHAPTER I.	INTRODUCTION	11
1.1	Foreword	11
1.2	Background	12
	1.2.1 Conventional Fast Breeder Reactor	12
	1.2.2 The Coupled Fast-Thermal Breeder Reactor	12
	1.2.3 The Fast Mixed-Spectrum Reactor Concept	15
1.3	Outline of the Present Work	19
CHAPTER II.	ANALYSIS OF A SIMULATED STEADY-STATE BURNUP CYCLE	21
2.1	Introduction	21
2.2	Reactor Model	22
2.3	Cross Section Preparation	28
2.4	k Calculation and Comparison with BNL Results	34
2.5	Zonewise Comparisons	40
	2.5.1 Spectral Indices	40
	2.5.2 Nuclide Concentrations	51
2.6	Parametric Studies	59
2.7	Conclusions	76

TABLE OF CONTENTS (cont.)

		Page
CHAPTER III.	GAMMA HEATING ANALYSIS	79
3.1	Introduction	79
3.2	Sources of Gammas in a Nuclear Reactor	80
3.3	Gamma Energy Deposition Reactions	82
3.4	The Gamma Format of the Coupled Neutron-Gamma Cross Section Set	83
3.5	Gamma Heating in the Reference Reactor	86
3.6	Neutron Heating	107
3.7	Conclusions	115
CHAPTER IV.	SUMMARY, CONCLUSIONS AND RECOMMENDATIONS	118
4.1	Introduction	118
4.2	Analysis of a Simulated Steady-State Burnup Cycle	119
4.3	Gamma and Neutron Heating Analyses	128
4.4	Conclusions and Recommendations	131
APPENDIX A.	Number Densities of Materials in the Various Core Zones at the BOEC.	134
APPENDIX B.	Tabulation of Data for the Power Distribution in the Reference FMSR	136
REFERENCES		145

LIST OF FIGURES

Figure No.		Page
1.1	Schematic Drawing of a Conventional Fast Breeder Reactor	13
1.2	Schematic Drawing of the Coupled Fast-Thermal Breeder Reactor	16
1.3	Schematic Drawing of the FMSR	18
2.1	Cross-Sectional View of the FMSR	23
2.2	R-Z Model of the Helium-Cooled FMSR	27
2.3	R-Z Model of the Helium-Cooled FMSR Showing Subzones	29
2.4	The One Dimensional Model of the Core Used in Cross Section Collapsing	32
2.5	Location of Core Zones and Subzones	50
2.6	Radial Flux at BOEC Along the Core Midplane (Jap. FP)	52
2.7	Radial Flux at EOEC Along the Core Midplane (Jap. FP)	53
2.8	Radial Flux at BOEC Along the Core Midplane (BNL FP)	54
2.9	Radial Power Distribution at BOEC Along the Core Midplane (Jap. FP)	55
2.10	Radial Power Distribution at EOEC Along the Core Midplane (Jap. FP)	56
2.11	Radial Power Distribution at BOEC Along the Core Midplane (BNL FP)	57
3.1	R-Z Model of the Helium-Cooled FMSR Showing Subzones	91
3.2	One-Dimensional Model of the FMSR Used for Transport Calculations	92
3.3	Total Radial Power Distribution	97
3.4	Gamma Heating Rate in the Reference FMSR Calculated Using the ORNL Coupled Cross Section Set	99
3.5	Ratio of Gamma Heating Rate to Local Fission Power in the Reference FMSR	101
3.6	Local Gamma-Energy Deposition-To-Source Ratio in the Reference FMSR	106
3.7	Neutron Heating Rate in the Reference FMSR	114

LIST OF FIGURES (continued)

Figure No.		Page
4.1	R-Z Model of the Helium-Cooled FMSR Showing Subzones	120
4.2	Fuel Shuffling Strategy	121

LIST OF TABLES

Table No.		Page
2.1	General Design Parameters of the FMSR	25
2.2	Core Region Volume Fractions	26
2.3	Temperatures Used in Cross Section Generation	30
2.4	Group Structure of the 10 Group Cross Section Set	33
2.5	Fission Product Capture Cross Section Ratio JNDC to (LIB IV x 2.7) (50 Groups)	35
2.6	Sequence of Calculations	36
2.7	k_{eff} and Breeding Ratio Comparison Between MIT and BNL Calculations	38
2.8	Comparison of the Spectral Index $\frac{\sigma_f^{28}}{\sigma_f^{49}}$ at the BOEC	42
2.9	Comparison of the Spectral Index $\frac{\sigma_f^{28}}{\sigma_f^{49}}$ at the EOEC	43
2.10	Comparison of the Spectral Index $\frac{\sigma_c^{28}}{\sigma_f^{49}}$ at the BOEC	44
2.11	Comparison of the Spectral Index $\frac{\sigma_c^{28}}{\sigma_f^{49}}$ at the EOEC	45
2.12	Comparison of the Spectral Index $\frac{\sigma_c^{49}}{\sigma_f^{49}}$ at the BOEC	46
2.13	Comparison of the Spectral Index $\frac{\sigma_c^{49}}{\sigma_f^{49}}$ at the EOEC	47
2.14	Comparison of the Spectral Index $\frac{\sigma_a^{FP}}{\sigma_f^{49}}$ at the BOEC	48
2.15	Comparison of the Spectral Index $\frac{\sigma_a^{FP}}{\sigma_f^{49}}$ at the EOEC	49

LIST OF TABLES (continued)

Table No.		Page
2.16	Comparison of the Number Density of U^{28} at the EOEC	60
2.17	Comparison of the Number Density of Pu^{49} at the EOEC (3 σ-sets)	61
2.18	Comparison of the Number Density of Pu^{40} at the EOEC (3 σ-sets)	62
2.19	Comparison of the Number Density of Pu^{41} at the EOEC (3 σ-sets)	63
2.20	Comparison of the Number Density of Pu^{42} at the EOEC (3 σ-sets)	63
2.21	Comparison of σ_a^{40} at BOEC and EOEC	64
2.22	Comparison of σ_a^{40}, from the Zone 1 and Zone 2 Cross Section Sets	65
2.23	k_{eff} and Breeding Ratio Comparison Between M.I.T. (6 Cross Section Sets) and BNL Calculations	68
2.24	Comparison of the Number Density of Pu^{49} at the EOEC (6 σ-sets)	69
2.25	Comparison of the Number Density of Pu^{40} at the EOEC (6 σ-sets)	70
2.26	Comparison of the Number Density of Pu^{41} at the EOEC (6 σ-sets)	71
2.27	Comparison of the Number Density of Pu^{42} at the EOEC (6 σ-sets)	72
2.28	Comparison of $\sigma_{capture}$ of the Plutonium Nuclides in Subzone 3 (Zone 1)	74
2.29	Comparison of $\sigma_{capture}$ of the Plutonium Nuclides in Subzone 7 (Zone 1)	75
3.1	Format of 40-Group ORNL Coupled Neutron-Gamma Cross Section Set	84
3.2	Neutron Energy Group Structures of the ORNL Coupled Cross Section Set	87
3.3	Gamma Energy Group Structures of the ORNL Coupled Cross Section Set	88
3.4	Energy Released per Fission	94
3.5	Summary of Gamma Energy Sources and Sinks in Reference FMSR	102
3.6	Percentage Contributions to the Total Gamma Energy	105

LIST OF TABLES (continued)

Table No.		Page
3.7	Neutron Heating Rate Contributions	116
4.1	k_{eff} and Breeding Ratio Comparison Between M.I.T. and BNL Calculations	124
4.2	Comparison of the Number Density of the Plutonium Isotopes at the EOEC	126
4.3	k_{eff} and Breeding Ratio Comparison Between M.I.T. (6 Cross Section Sets) and BNL Calculations	127
A.1	Number Densities of Materials in the Various Zones at BOEC	134
B.1	Fission Power Density, Gamma Production Rate and Gamma Deposition Rate	137
B.2	Neutron Heating Rate	143

CHAPTER I

INTRODUCTION

1.1 Foreword

Fast breeder reactors have enormous potential for meeting future energy demands. This is due to their ability to breed more fuel than they consume. Research and development programs are underway in the U.S. and abroad on the liquid metal cooled (sodium) fast breeder reactor (LMFBR) and the gas (helium) cooled fast breeder reactor (GCFR).

In recent years, a number of unconventional design concepts related to the fast reactor core have been investigated. The basic objectives of these designs include enhanced safety features, such as less positive sodium void coefficients, and better neutronic performance, such as higher breeding ratio. Several core designs utilizing uranium and thorium blankets have been studied at M.I.T. under DOE support as part of the Nuclear Engineering Department's Fast Reactor Blanket Project. Studies have been carried out on internal blankets; in particular, the "parfait" or internal axial blanket, which have shown that the associated core designs have improved safety features such as decreased sodium void coefficient, decreased sodium temperature coefficient and better neutronic performance--i.e. increased breeding ratio [A-1, D-3, D-2, P-1]. The disadvantages of these cores include increased core fissile inventory,

reduced doppler coefficient and reduced delayed neutron fraction.

The latest efforts on improving the safety and neutronic performance of FBR cores has focussed on internal radial blankets [B-3], and some advanced blanket design concepts such as moderated and fissile-seeded blankets [S-2].

The objective of the present work is to evaluate a new concept in fast reactors for the production of electric power --the Fast-Mixed Spectrum Reactor (FMSR), which has enhancement of proliferation resistance as its major focus.

1.2 Background

The Fast-Mixed Spectrum Reactor concept as proposed by G. S. Fischer et al. at BNL [B-1] is in some ways an extension of the heterogeneous fast breeder reactor, and is also a variation of the coupled fast-thermal reactor studied by R. Avery [A-2, A-3, A-4].

1.2.1 Conventional Fast Breeder Reactor

A fast breeder reactor has a core consisting of tightly-packed hexagonal pitch assemblies. In current state-of-the-art designs the fuel elements are uranium-plutonium dioxide (UO_2/PuO_2) pellets enriched to ~15-20%, clad in stainless steel, and about a quarter of an inch in diameter. Around the core is a blanket of depleted (or natural) uranium oxide pins, which capture core leakage neutrons and thereby permit net breeding to be achieved. Coolants currently proposed for fast breeder reactors are liquid sodium and helium gas. A schematic representation of a fast breeder reactor is shown in Fig. 1.1.

(a) Top View

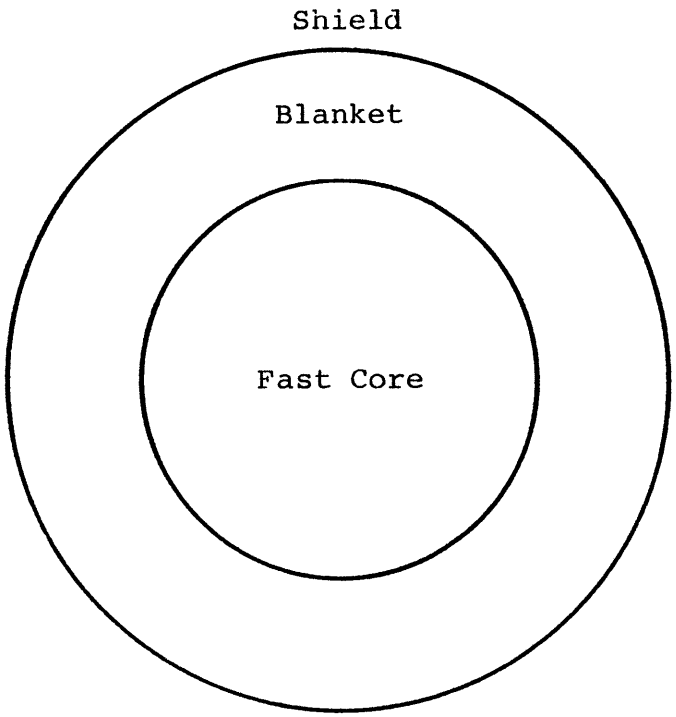

(b) Side View

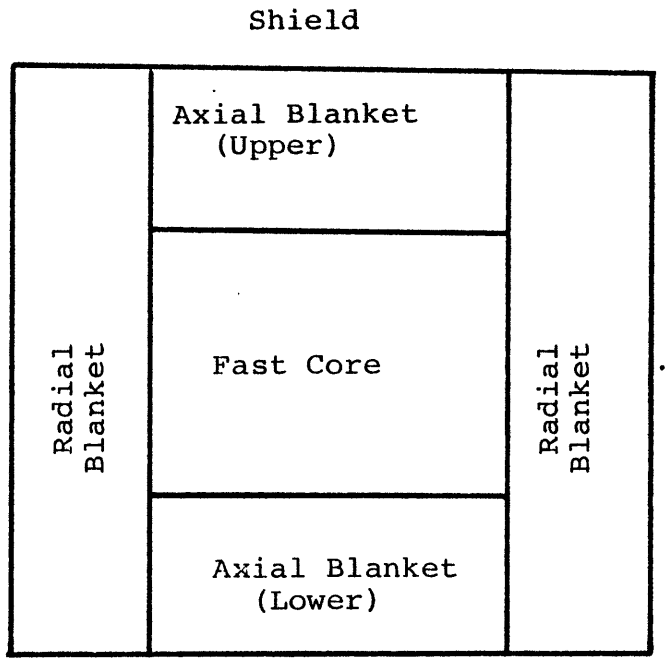

Fig. 1.1 Schematic Drawing of a Conventional Fast Breeder Reactor: (a) Top view, (b) Side View

In fast reactors, neutrons are not slowed down to thermal energies by a moderator. Coolant and other reactor materials however, moderate the neutrons to a certain extent so that the neutron spectrum extends from fission energies, averaging 2 Mev, down to the keV region. In this hard spectrum the value of eta (η) for Pu-239 is high enough (~2.7) to maintain the chain reaction and to breed. On the other hand, the fast fission cross-section is so low at high energies that proportionately more fissile material must be contained in the fuel to maintain criticality. For this reason and also because parasitic capture by core materials is relatively higher in fast reactors, the core requires a relatively high fissile enrichment--approximately 15-20%--as compared with ~3% for a Light Water Reactor (LWR), and 0.7% for a heavy water reactor (CANDU).

FBR cores are compact because of the absence of moderator. They, therefore, have much higher power densities and specific powers, as compared with thermal reactors. This imposes a need for a coolant with good heat transfer properties.

1.2.2 The Coupled Fast-Thermal Breeder Reactor

The coupled fast-thermal system consists of a fast assembly coupled to a thermal assembly in the sense that neutrons born in each of the zones will cause fissions in the other. The system can be designed to have a prompt neutron lifetime characteristic of thermal reactors, and a breeding gain characteristic of fast reactors.

The neutron lifetime can be brought into the thermal range by ensuring that thermal fissions contribute a significant fraction of the total fissions. In addition, these fissions must be important in contributing to the reactivity in the fast assembly. Hence, it is essential that neutrons born in thermal fission have an appreciable probability of entering the fast zone and causing fissions. Until enough reactivity is added to the fast system to bring it close to criticality on its own, the kinetics will be essentially those of a thermal system. The subcriticality of the fast system thus serves as a margin of safety against a prompt excursion.

To achieve a breeding gain characteristic of fast reactors substantial power must be generated in the fast core. Further, we want to shield the fast region from the low energy tail of the neutron spectrum in the thermal region to keep the energy of neutrons absorbed in Pu239 high, in order to attain a low value for the capture to fission ratio, α; and to prevent hot spots at the periphery of the fast region.

A schematic drawing of the coupled fast-thermal reactor is shown in Fig. 1.2.

1.2.3 The Fast-Mixed Spectrum Reactor Concept

Unlike conventional fast breeders, the FMSR would operate on a once-through-and-store fuel cycle. No fuel reprocessing is required and no enrichment is required after the initial core loading. The basic concept of the FMSR is as follows:

The core consists of a central hard spectrum region

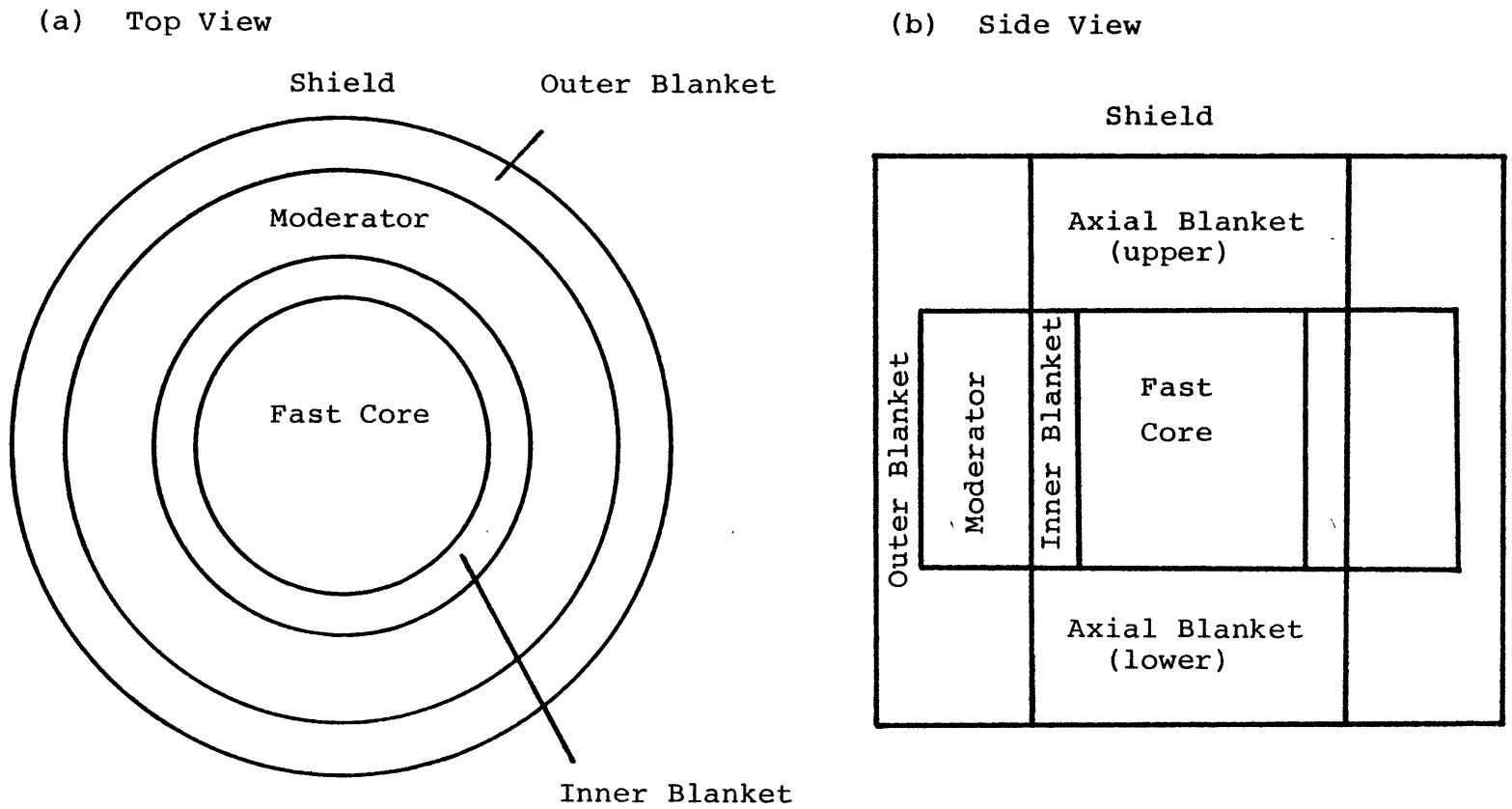

Fig. 1.2 Schematic Drawing of the Coupled Fast-Thermal Breeder Reactor: (a) Top View, (b) Side View.

surrounded by a moderated zone consisting of beryllium. Fig. 1.3 shows a schematic representation of the FMSR. Although the FMSR concept is a variation of the coupled fast-thermal breeder reactor, the present core design is heavily weighted toward the fast region and hence, the prompt life-time is more characteristic of a fast reactor.

The reactor can be started up on medium-enriched uranium (~7% enrichment). Fresh fuel (depleted or natural uranium) is first loaded into the moderated region. The fuel remains in this region until the bred plutonium enrichment reaches approximately 2.7%, at which time the fuel is shuffled to the fast region. In this region the plutonium content increases until it reaches ~7% enrichment at the time of discharge from the (final) region and hence from the reactor. The FMSR is designed to be self-sustaining on an equilibrium feed of natural (or perhaps depleted) uranium alone. No fissile makeup is required. The plutonium burned in the reactor is produced in situ by neutron capture. According to studies made by BNL [B-1], the total burnup of heavy metal during its residence period in the reactor (17 years) would be about 13-15 atom percent. The combination of refuelling with natural or depleted uranium and the high burnup would make the FMSR as much as 15 times as efficient in uranium utilization as a once-through Light Water Reactor (measured in terms of energy per unit mass of natural uranium). The combination of low initial fuel enrichment and the absence of reprocessing, at least for many decades, give the FMSR obvious non-proliferation advantages. The fuel cycle costs should be less than those of a more conventional fast breeder.

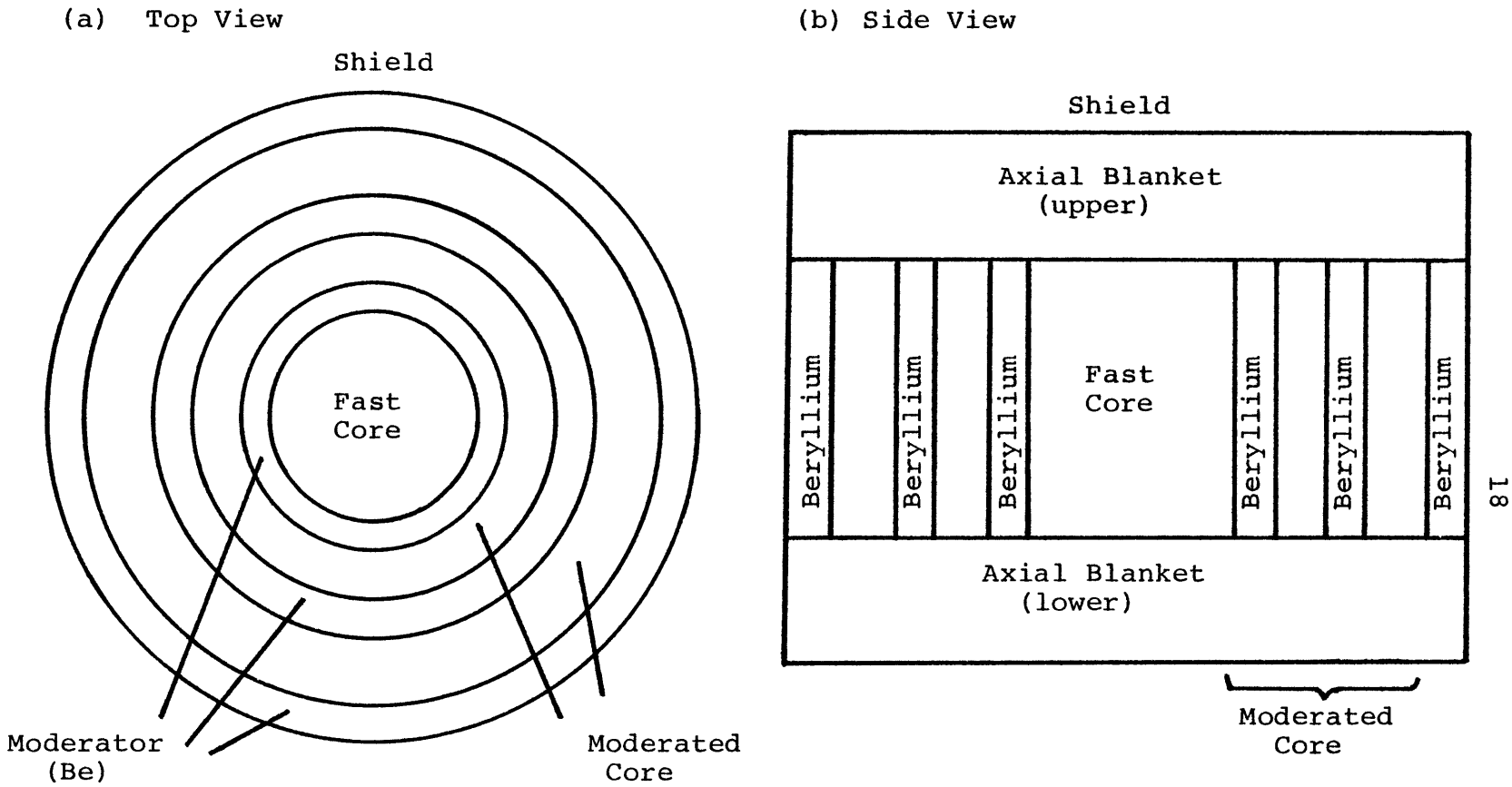

Fig. 1.3 Schematic Drawing of the FMSR: (a) Top View, (b) Side View

1.3 Outline of the Present Work

The objective of the present work is to carry out an independent evaluation of the neutronic characteristics of a gas-cooled FMSR core design in accordance with the terms of a subcontract negotiated between BNL and MIT for this purpose.

Several core design options, with regard to the relative position of fissile and fertile material, and the moderator, are under investigation at BNL, including both gas and sodium-cooled designs. However, for present purposes, a reference configuration of a gas-cooled FMSR was agreed upon for use in benchmark calculations, in particular the version described by BNL in Ref. [B-1]. Thus the objective is to confirm the neutronic feasibility of the steady state fuel cycle, and it is not to be inferred that the system under consideration is an optimized final design.

Chapter Two deals with static beginning-of-equilibrium-cycle reactivity calculations and with fuel burnup studies, carried out using available state-of-the-art computer codes and cross-section sets. A brief account is also given in this chapter of the generation of cross-section sets using a 50 group fast cross-section library, and the selection of a fission-product cross-section (FPCS) set.

Comparisons are made with results obtained at BNL, including zonewise comparisons of spectral indices at the beginning of equilibrium cycle (BOEC) and at the end of equilibrium cycle (EOEC), and the nuclide concentrations at

EOEC. The absorption and capture cross-sections of key nuclides are also compared, since they have considerable influence on the nuclide concentrations, and hence the breeding gain in a cycle. Discrepancies and disagreements in the results are investigated and discussed. The effect of cross section collapse on burnup analysis is also briefly discussed.

Chapter Three considers non-fission heating in the FMSR. This includes gamma heating and neutron heating. The analysis is important since the establishment of the thermal energy source distribution will enable one to determine the temperature field within the reactor, and hence the heat transport, thermal stresses and many other temperature dependent physical and chemical properties of reactor materials. The one-dimensional discrete ordinates transport code ANISN [E-1] and a coupled neutron-gamma cross section set are employed in the gamma heating analysis. The ratio of gammas and neutron heating rates to that of fission heating is examined, and their significance discussed. In addition the distribution of gamma sources will be investigated.

Chapter Four summarizes the results of the present evaluation of the FMSR, reiterating the main conclusions. Recommendations for future work are also outlined.

CHAPTER II

ANALYSIS OF A SIMULATED STEADY-STATE BURNUP CYCLE

2.1 Introduction

The evaluation of the gas-cooled FMSR core design in the present study consists of static beginning-of-equilibrium cycle reactivity calculations and fuel burnup analyses. The primary tool used was the two-dimensional, multigroup, fast-reactor-oriented, diffusion theory burnup code 2DB [L-3]. This program was used to determine fluxes, power densities, and material concentrations as a function of burnup. The reactor model--geometric specifications and zone-wise compositions--were provided by BNL, as addressed in Section 2.2. The 10-group cross section set used in the burnup and k-calculations was developed from the 50-group LIB-IV compilation [K-1]. The 50-group set was first corrected for resonance and spatial self-shielding and then collapsed to ten energy groups using the code SPHINX [D-1]. The cross section preparation is described in Section 2.3. The results obtained from the burnup and $\bar{k}$ calculations were then compared with BNL's calculations. This is done in Section 2.4, while in Section 2.5 zonewise comparisons are made, and the discrepancies and disagreements are noted and discussed. Section 2.6 deals with the effect of using an increased number of zonewise 10-group cross section sets. Conclusions drawn from the evaluations

of the FMSR core design are presented in Section 2.7.

2.2 Reactor Model

The reference configuration of a gas-cooled FMSR used in the benchmark calculations was provided by BNL. A description of this particular reactor configuration is found in Reference [B-1]. However, a summary of important features and design parameters of this gas-cooled FMSR pertinent to the present analysis is given below.

A cross-sectional diagram of the FMSR core is shown in Fig. 2.1. The schematic core layout should be considered as generic, rather than a representation of a specific design layout. The hexagonal subassemblies contain fuel, or moderator, and steel. The nonshaded hexagons surrounding the fuel and moderator subassemblies serve as a radiation shield. Moderator is contained in the hexagons with dots in the center. Hexagons marked "F" are locations of fuel-bearing control rods while those marked "S" are representative locations of shut-down rods. (It should be pointed out that fuel-bearing control rods were not considered or modeled in the k-calculations and burnup analyses done in the present work.) All other hexagons represent fuel-bearing subassemblies. Those marked with "1" are in the moderated zone; those marked with a "2" are in the hard spectrum region, and those marked "3" are in the transition region, where spectrum softening occurs because of the presence of the surrounding moderator.

A number of basic parameters of the FMSR design are listed

FAST-MIXED SPECTRUM REACTOR CONCEPT

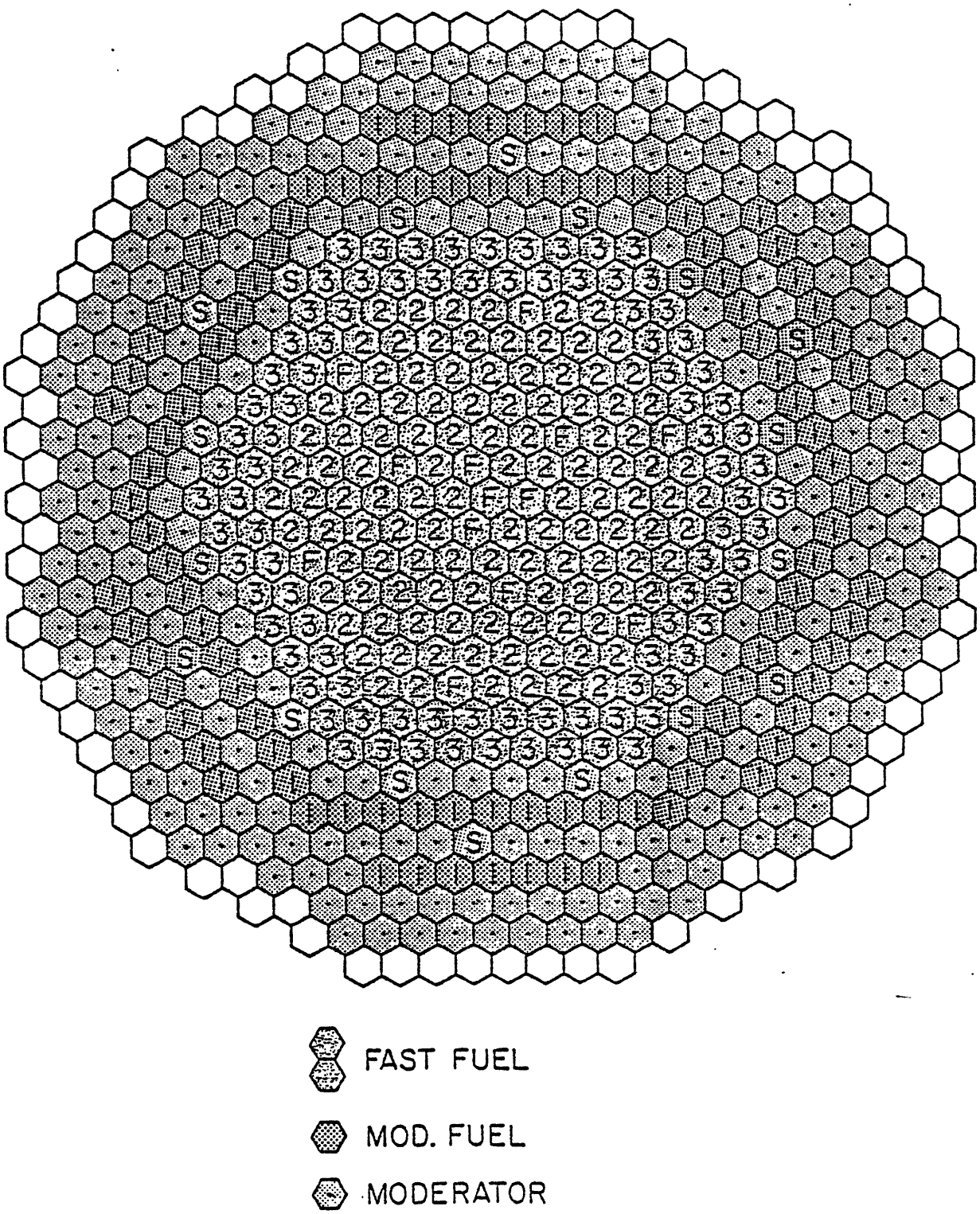

FIGURE 2.1: Cross-Sectional View of the FMSR.

in Table 2.1. Metal fuel is used; and the rationale behind its preference over oxide fuel for the FMSR is discussed in Ref. Ref. [B-1]. The relevant zone compositions are shown in Table 2.2.

Several fuel shuffling strategies were investigated by BNL. The strategy adopted is based on loading fresh fuel first into the outermost ring of the moderated region (see Fig. 2.1). The fresh fuel (natural uranium) acts as a strong absorber of radially leaking neutrons. After a period of residence, the fuel is moved to the inner ring of the moderator region. The fuel remains in this position until the bred plutonium enrichment reaches approximately 3%, at which time the fuel is shuffled to the fast region. It was reported that (Ref. [B-1]) this shuffling strategy results in a lower power swing for the fuel during its first cycle in the fast zone. In addition, this strategy also yields an acceptably flat radial power distribution. The main disadvantage is that the power density in the outer moderated region is low, requiring the fast core to carry a higher power load, and leading to a higher net fluence damage to its cladding.

The R-Z model used in the 2-DB diffusion theory burnup code is shown in Fig. 2.2. Zone 1 represents the fuel in the outer moderated region, Zone 2 represents fuel in the inner moderated region, and Zones 3, 4, 5 and 6 represent the fast core regions. Zones 7 through 12 represent the axial blankets.

Table 2.1

General Design Parameters of the FMSR

Reactor Power, MWe	1000
Active Core Height, cm	160
Cladding OD, cm	0.8804
Cladding Thickness, cm	0.0432
Fuel Pellet OD, cm	0.7940
Fuel-Cladding Gap, cm	0.0
Duct Wall Thickness, cm	0.254
Hexcan Size (Dimensions across flats), cm	18.69
Fuel Volume Fraction	0.39
Flowing Coolant Volume Fraction	0.40
Pitch, cm	1.1354
P/D	1.29
No. of Pins/Subassembly	271
No. of Fuel Subassemblies	408
Number of Spacer Grids	15

Table 2.2

Core Region Volume Fractions*

	Zone 1	Zone 2	Zone 3	Zone 4	Zone 5	Zone 6	Moderator Zones
Fuel	0.39	0.39	0.39	0.39	0.39	0.39	--
Coolant	0.45	0.45	0.45	0.45	0.45	0.45	0.45
Structure	0.16	0.16	0.16	0.16	0.16	0.16	0.16
Control	--	--	--	--	--	--	--
Moderator	--	--	--	--	--	--	0.39
Total	1.00	1.00	1.00	1.00	1.00	1.00	1.00

*See Fig. 2.5 for identification of zone locations.

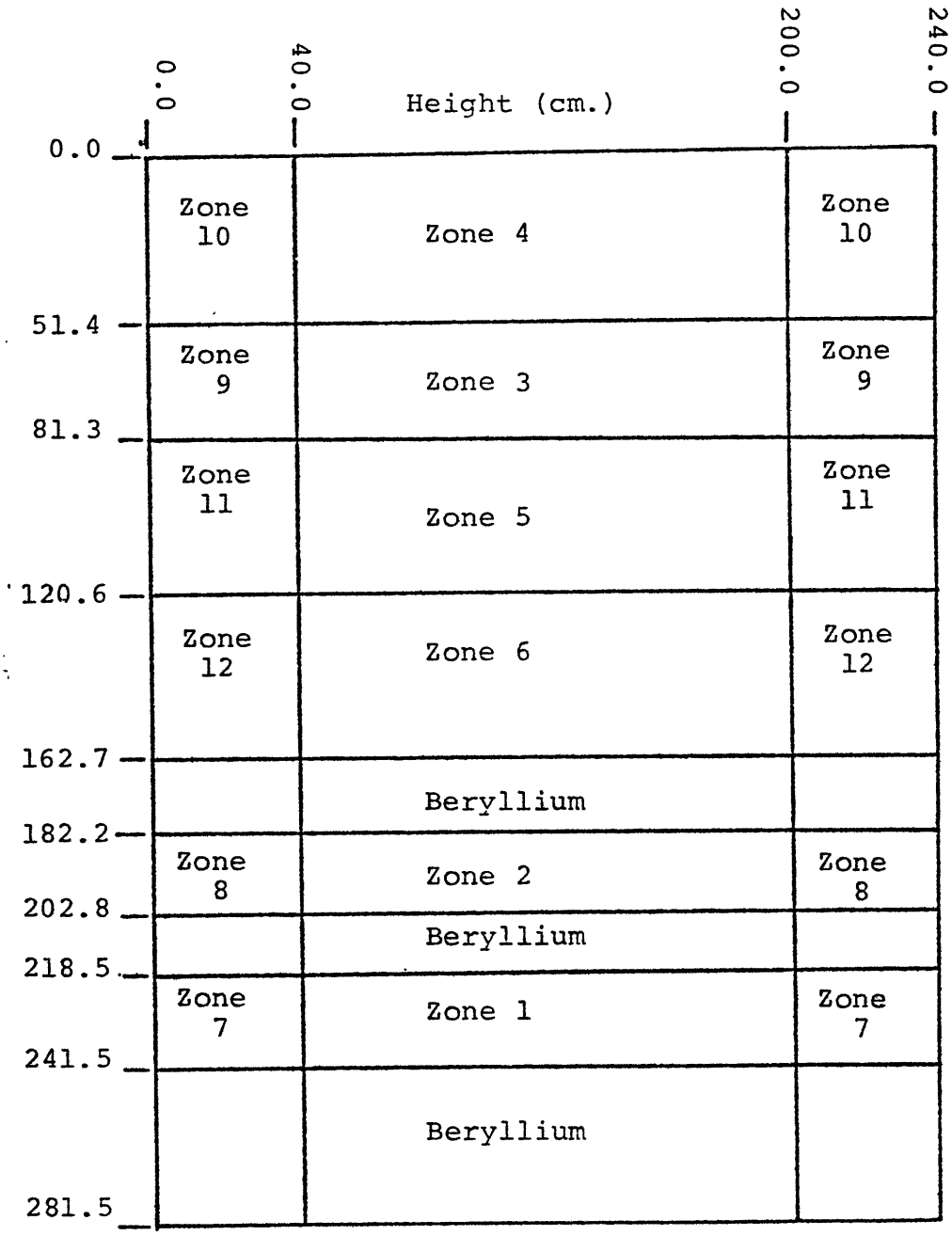

Fig. 2.2 R-Z Model of the Helium-Cooled FMSR

All zones in each horizontal cut through the core are further subdivided into a total of 34 subzones in order to approximate the required fuel shuffling. This is represented in Fig. 2.3 Note that, in the second axial layer, zones 36 and 55 are physical extensions of Zones 1 and 20, respectively.

2.3 Cross-Section Preparation

All calculations were performed using a 10-group cross section set generated using the 50 group LIB IV compilation as the parent cross section set [K-1]. Corrections were made for resonance self-shielding, including spatial shielding and temperature dependence, using the code SPHINX [D-1]. Spatial shielding is not important for the fast spectrum regions of the core, but might be significant for the epithermal regions of the moderated fuel regions. The zonal compositions at the beginning of equilibrium cycle (BOEC) were used in the SPHINX calculations, and were as documented in Appendix A. It should be pointed out that the number densities of the heavy metals in this table were calculated using the BOEC fuel inventory for the core tabulated in Table 3.5 in the FMSR Interim Report by BNL (see Ref. [B-1]). Fuel, cladding and coolant temperatures used in SPHINX are given in Table 2.3. The basis for selecting the fuel, cladding and coolant temperatures is also shown in the table. The maximum fuel centerline temperature of 850°C, maximum cladding-inner-surface temperature of 600°C, etc., are constraints imposed on the FMSR design due to metallurgical, and other Gas Cooled Fast

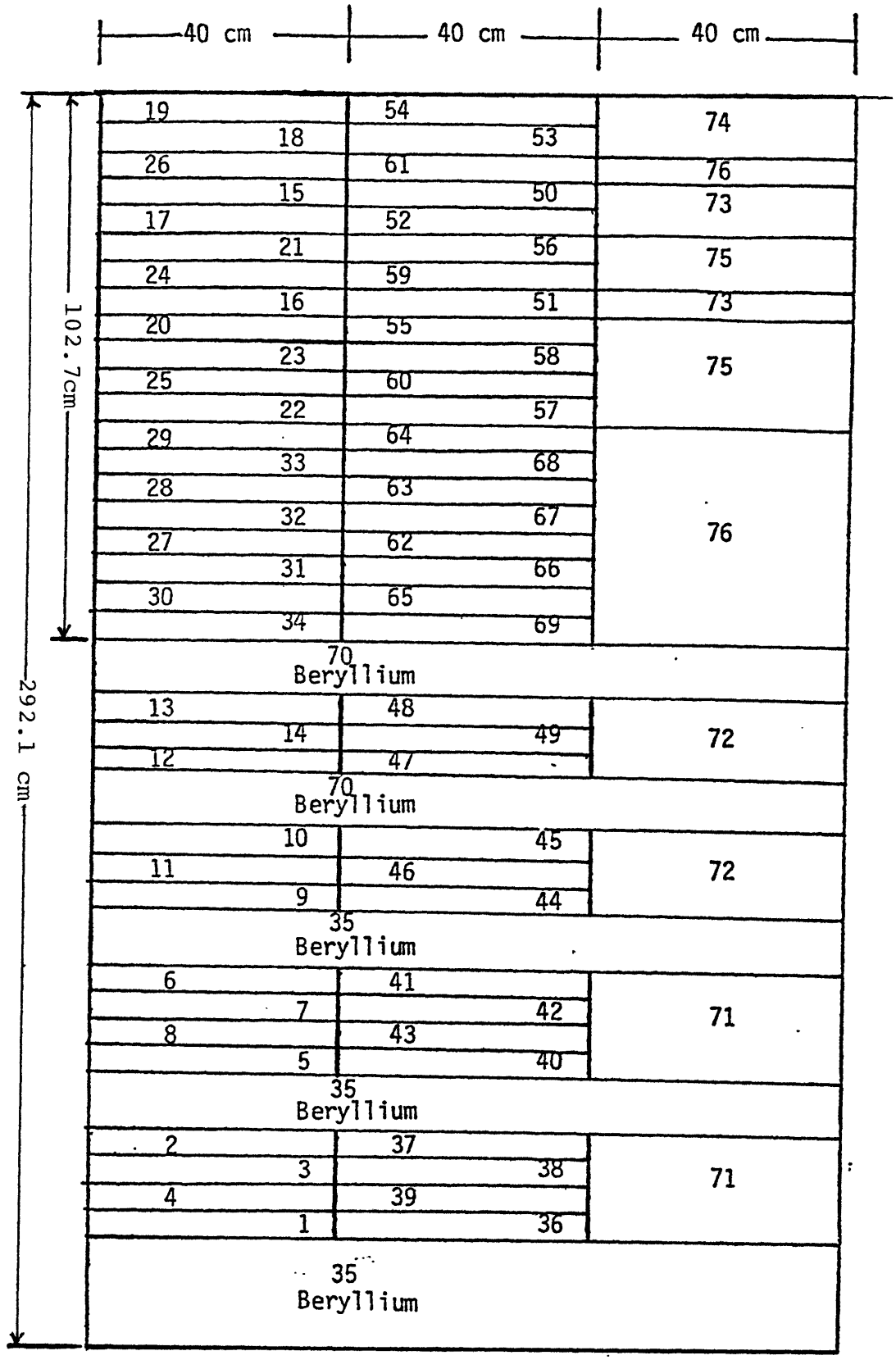

Fig. 2.3 R-Z Model of the Helium-Cooled FMSR

Table 2.3

Temperatures Used in Cross Section Generation

	Temperature	Basis	
Fuel	1000°K = 727°C	T_{CL}	= 850°C
		$T_{clad,max}$	= 600°C
Cladding	800°K = 527°C	$T_{coolant}$	= 400°C
		$T_{clad,max}$	= 600°C
Coolant	673°K = 400°C	T_{out}	= 530°C
		ΔT_{core}	= 230°C

Reactor (GCFR) design requirements.

The one dimensional model of the core used for the group collapsing in SPHINX is shown in Fig. 2.4. Table 2.4 shows the structure of the 10 group cross section set used. This group structure is based on a 9 group cross section set used by Westinghouse, with the addition of one extra group in the thermal region [L-1]. All the cross sections are based on the LIB-IV set except for the fission products. It must be pointed out that several fission product cross section (FPCS) libraries have been published in recent years. Each includes a different number of isotopes. It was shown by Bustraan [B-1] that, when using these data to evaluate the reactivity worth of fission-product mixtures in fast cores, different values are obtained depending on the library used. The differences range from 20 to 40% in various neutron spectra.

In the present work a new 50 group cross section set for the fission products was generated based on the results reported by the Japanese Nuclear Data Committee (JNDC) [J-1]. The JNDC evaluated in detail 28 of the most important fission product nuclides, which constitute about 80% of the total capture by fission products. This was supplemented with 165 nuclides evaluated by Cook [C-1]. The concentrations of these 198 nuclides were determined for fast reactor burnups of 1, 30, 60, 180, 360 and 720 days. These concentrations were then used to produce lumped fission products in 70 groups and 47 down-scattering terms. The variations in one-group-collapsed

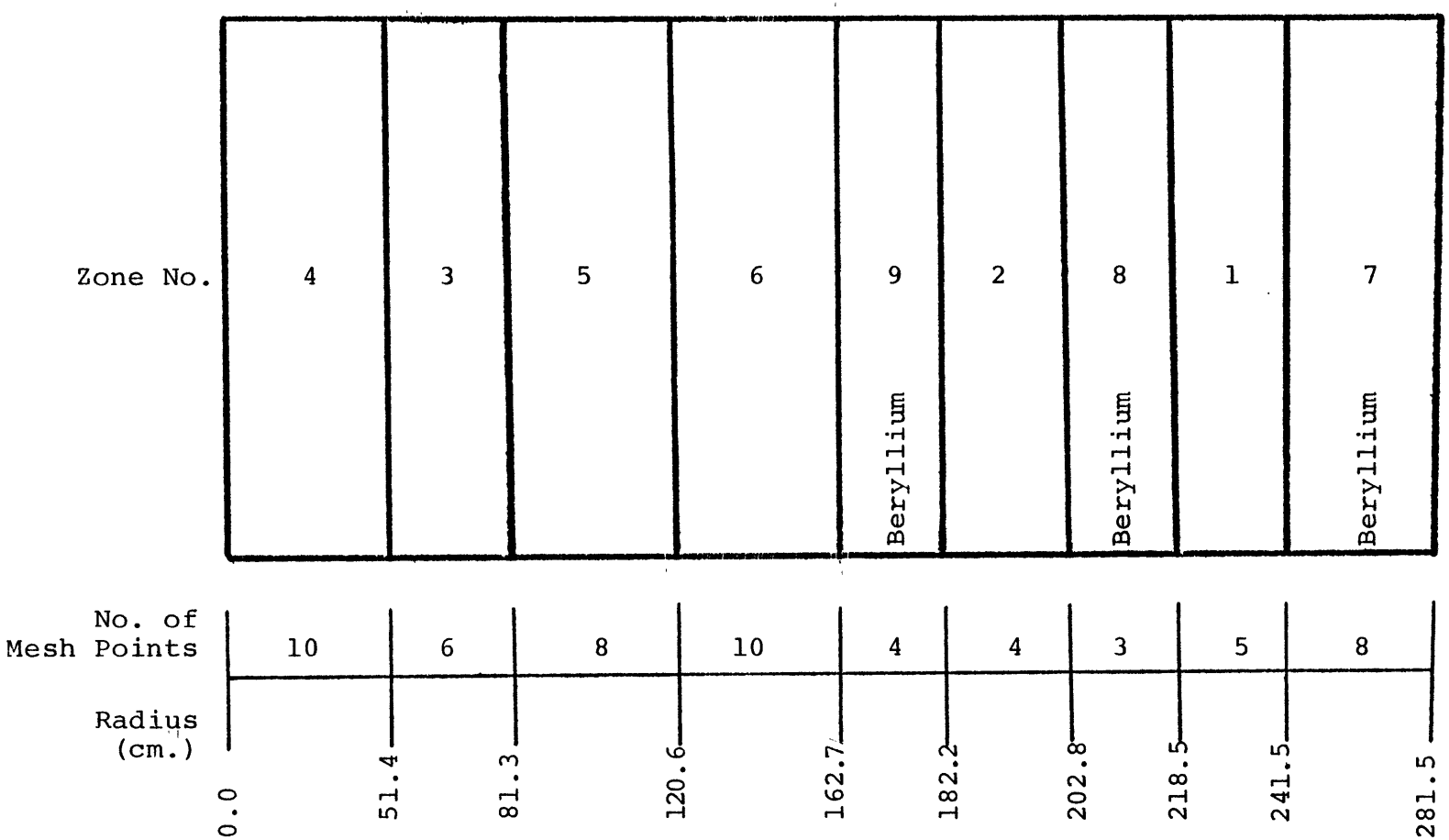

Fig. 2.4 The One Dimensional Model of the Core Used in Cross Section Collapsing

Table 2.4

Group Structure of the 10 Group Cross Section Set

Group	Upper Energy (ev)	
1	15.0	E6
2	2.231	E6
3	0.821	E6
4	0.183	E5
5	0.408	E4
6	0.911	E4
7	0.203	E4
8	0.454	E3
9	0.504	E1
10	0.682	E0

cross sections (in a 1000 MW fast reactor spectrum) was less than 2% over the interval from 180 to 720 days. Benchmark calculations of measured central reactivity worth for different FP mixture samples and the reactivity worths of some separated FP isotope samples by Kikuchi et al. [J-12] using the JNDC, Cook and ENDF/B-4 sets, showed that the JNDC set gave better results than the other two sets when compared with the experimental values measured in various cores of the STEK facility in RCN, Petten, the Netherlands. Detailed descriptions of the experiments and the associated results are given in Refs. [B-6] and [G-2]. For the present work the 70 group lumped JNDC σ-set was collapsed to the LIB-IV 50 group energy structure using typical fission and 1/E spectra [L-2].

Table 2.5 shows the ratio of the JNDC 50 group fission product capture cross sections to the LIB-IV cross section set multiplied by a factor of 2.7 (i.e., the set used by BNL).

The LIB-IV version of JNDC's 50 group fission product cross section was next collapsed to a 10-group set in the same manner as for other LIB-IV cross sections. The 10 group cross sections generated by the above procedure were used in the two dimensional diffusion theory burnup code 2DB for all burnup and k calculations.

2.4 k Calculations and Comparison with BNL Results

The sequence of calculations is shown in Table 2.6. The simulated steady state k calculations for the beginning and end of equilibrium cycle were performed on an R-Z model of the

Table 2.5

Fission Product Capture Cross Section Ratio of JNDC to (LIB IV x 2.7) (50 Groups)

Group	$\sigma_c^{JNDC}/\sigma_c^{LIB\ IV}$	Group	$\sigma_c^{JNDC}/\sigma_c^{LIB\ IV}$
1	0.07937	26	1.15834
2	0.18915	27	1.18386
3	0.53271	28	1.23698
4	0.96746	29	1.20836
5	1.17042	30	1.22464
6	1.20366	31	1.26440
7	1.24069	32	1.29982
8	1.27833	33	1.59619
9	1.29605	34	1.52277
10	1.29803	35	1.07200
11	1.23524	36	0.72979
12	1.16735	37	1.40743
13	1.14966	38	1.40306
14	1.14659	39	2.78448
15	1.14898	40	0.96248
16	1.15344	41	3.03949
17	1.15711	42	1.58189
18	1.15979	43	9.35697
19	1.16517	44	10.68521
20	1.18013	45	1.90879
21	1.18096	46	72.22638
22	1.17810	47	18.38698
23	1.17150	48	31.07376
24	1.16405	49	61.69649
25	1.16184	50	7.24559

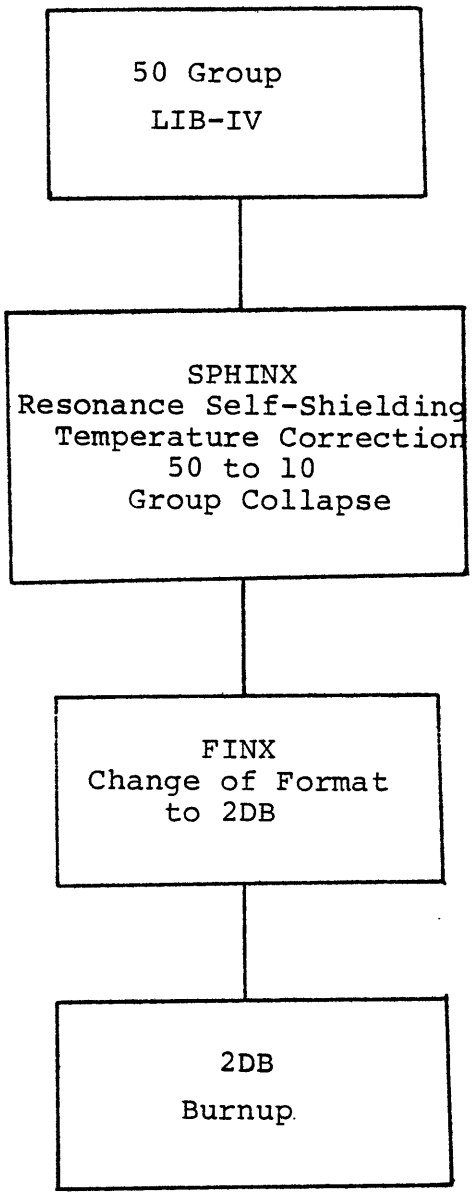

Table 2.6 Sequence of Calculations

core using the two dimensional diffusion theory burnup code 2DB. The R-Z model used in these calculations has been described in Section 2.2 (see Fig. 2.2).

To be consistent, all specifications with regard to the core in the 2DB calculation, e.g. number of mesh points in each zone, dimension of each mesh interval, number of mixtures used, etc., are similar to those in the BNL calculations. Three 10-group cross section sets were used for the fuel zones. An additional set was used for the moderator zones. More specifically, in the present work, the set developed for Zone 2, was used for Zones 1 and 2. The Zone 2 set, determined at the beginning of cycle, was chosen as a compromise between trying to match Zone 1 at the BOEC and Zone 2 at EOEC, and also to favor the zone having the greater effect on key system integral properties. The effect of this selection on the results of the calculations is discussed briefly in Section 2.5.

Two sets of k calculations were performed, one with the Japanese fission products and one with the BNL fission products (LIB-IV nonsaturating plutonium fission products times the factor 2.7).

Table 2.7 shows the results of the MIT and BNL calculations. Also shown is a set of results for the case of no fission products. (These results can be used to find the total net worth of the fission products for both sets). As can be seen, the MIT (BNL FP) and the BNL k_{eff} calculations are in good agreement. The difference in breeding ratio is due to

Table 2.7

k_{eff} and Breeding Ratio Comparison Between M.I.T. and BNL Calculations

	k_{Eff}		BR	
	BOEC	EOEC	BOEC	EOEC
M.I.T. (Japanese FP)	0.969	0.987	1.68	1.61
M.I.T. (BNL FP)	0.986	1.004	1.67	1.60
BNL	0.982	1.000	1.57 (1.67)	1.51 (1.61)*
M.I.T. (no FP)	1.020	1.039	1.64	1.58

*Values in parentheses exclude U-235 absorption; otherwise M.I.T. values exclude, while BNL values include U-235 absorptions (see text for discussion).

differences in the definition of the breeding ratio used. In our calculations the breeding ratio is calculated by using the relation

$$BR = \frac{U^{238}_{capture} + Pu^{240}_{capture}}{Pu^{239}_{absorption} + Pu^{241}_{absorption}} \qquad (2.1)$$

An alternative definition, as adopted by BNL, would also include U^{235} absorption in the denominator, which in turn will reduce the breeding ratio. This is evident in the BNL results in Table 2.7. Using the previous definition for breeding ratio (without U^{235} absorption in the denominator) BNL gives the values shown in parenthesis ( ) in Table 2.7, which are in good agreement with those reported by MIT. Although it is still not established which definition of breeding ratio will be universally adopted, it is clear that a consistent definition must be employed.

It can be seen, from Table 2.7 that the Japanese fission products are worth around 5% ΔK and the BNL fission products are worth around 3.5% ΔK. Another interesting point to note is the reduction in breeding ratio when the lower worth fission products are used. From the three MIT calculations it can be seen that the highest breeding ratio is for the case of Japanese fission products, and the lowest value is with no fission products. One explanation could be that since fission products have high absorption cross sections at low energies, the higher the fission product cross section, the lower the low energy

part of the spectrum, and the harder the overall spectrum. A harder spectrum would lead to a higher breeding ratio.

2.5 Zonewise Comparisons

To identify the nature of the differences between the calculations done at M.I.T. and those done at BNL, a detailed zonewise comparison between the two sets of calculations was performed.

2.5.1 Spectral Indices

Several spectral indices were calculated for the different zones. These include:

$$\frac{\sigma_f^{28}}{\sigma_f^{49}}, \quad \frac{\sigma_c^{28}}{\sigma_f^{49}}, \quad \frac{\sigma_c^{49}}{\sigma_f^{49}}, \text{ and } \frac{\sigma_a^{FP}}{\sigma_f^{49}}$$

The results are given in Tables 2.8 through 2.15. For each zone, two or three subzones were chosen to represent the particular zone. Locations of the core zones and subzones are shown in Fig. 2.5. Referring to Table 2.8, the first column gives the value of $\frac{\sigma_f^{28}}{\sigma_f^{49}}$ based on the MIT-Japanese fission product results. The second column gives the results for the BNL 50 group calculations and the third column gives the MIT-BNL fission product results. Columns 4 and 5 show the ratio of the indices: BNL to MIT with BNL fission products, and BNL to MIT with Japanese fission products respectively. Any difference in the basic cross section treatments should show up in Column 4, while Column 5 indicates the difference when a higher worth fission product cross section set is used. Looking at Tables 2.8 and 2.9 it can be seen that the agreement is good in the regions of hard spectrum, i.e., in the fast

core regions. In the zones close to the moderator MIT calculations show a lower value for σ_f^{28}. This is most pronounced in subzones 11 and 14. Referring to Tables 2.10 and 2.11, it can be seen that the reverse is true, i.e., again the agreement is good in the hard spectrum subzones but in the softer spectrum subzones MIT calculates a higher σ_c^{28}. The basic conclusion from this examination is that in the vicinity of the moderator, M.I.T. calculations show evidence of a softer spectrum than indicated by the BNL results. This conclusion is based on the fact that σ_f^{28} is sensitive to the higher energy flux while σ_c^{28} is sensitive to the neutron flux at lower energies. This behavior could also in part be due to the lower number of fast groups ($\geq$1MeV) used in the M.I.T. 10 group calculations compared to the BNL 50 group calculations. Tables 2.12 and 2.13 show the spectral index $\frac{\sigma_c^{49}}{\sigma_f^{49}}$, confirming a generally good agreement between M.I.T. and BNL calculations. Finally, Tables 2.14 and 2.15 give the values of $\frac{\sigma_a^{FP}}{\sigma_f^{49}}$. M.I.T. calculates a higher σ_a^{FP} due to higher fission product absorption at lower energies. This result supports the previous argument. The last column of Table 2.14 is also interesting because it shows the differences due to the two sets of fission products used.

Figures 2.6 and 2.7 show the beginning and end of equilibrium cycle radial flux profiles for the M.I.T. and BNL calculations. The M.I.T. calculations shown in these figures

Table 2.8

Comparison of the Spectral Index $\frac{\sigma f^{28}}{\sigma_f^{49}}$ at the BOEC

Zone*	Subzone**	1 M.I.T. (Japanese FP)	2 BNL 50 Group	3 M.I.T. (BNL FP)	4 BNL/M.I.T. (BNL FP)	5 BNL/M.I.T. (JFP)
1	3	1.6605E-3	1.681E-3	1.669E-3	1.007	1.012
1	7	2.5453E-3	2.610E-3	2.551E-3	1.023	1.025
2	11	3.8677E-3	4.073E-3	3.864E-3	1.054	1.053
2	14	7.2720E-3	7.940E-3	7.380E-3	1.075	1.091
3	17	2.063 E-2	2.101E-2	2.106E-2	0.997	1.018
4	19	2.180 E-2	2.226E-2	2.214E-2	1.005	1.021
5	20	2.359 E-2	2.424E-2	2.457E-2	0.986	1.027
5	24	2.316 E-2	2.360E-2	2.389E-2	0.987	1.018
6	29	2.645 E-2	2.878E-2	2.884E-2	0.9979	1.088
6	32	2.728 E-2	3.027E-2	3.015E-2	1.003	1.109
6	34	1.367 E-2	1.478E-2	1.437E-2	1.0285	1.081

*see Fig. 2.5.
**Selected Subzones

Table 2.9

Comparison of the Spectral Index $\frac{\sigma f^{28}}{\sigma_f^{49}}$ at the EOEC

Zone*	Subzone	M.I.T. (Japanese FP)	BNL 50 Group	M.I.T. (BNL FP)	BNL/M.I.T. (BNL FP)	BNL/M.I.T. (J FP)
1	3	1.767 E-3	1.815 E-3	1.751 E-3	1.037	1.027
1	7	2.844 E-3	3.008 E-3	2.833 E-3	1.062	1.058
2	11	4.433 E-3	4.857 E-3	4.430 E-3	1.096	1.096
2	14	8.081 E-3	9.057 E-3	8.208 E-3	1.103	1.121
3	17	2.133 E-2	2.178 E-2	2.187 E-2	0.996	1.021
4	19	2.235 E-2	2.270 E-2	2.281 E-2	0.995	1.016
5	20	2.384 E-2	2.469 E-2	2.496 E-2	0.989	1.036
5	24	2.351 E-2	2.410 E-2	2.439 E-2	0.988	1.025
6	29	2.619 E-2	2.875 E-2	2.870 E-2	1.002	1.098
6	32	2.695 E-2	3.018 E-2	2.988 E-2	1.010	1.120
6	34	1.351 E-2	1.478 E-2	1.423 E-2	1.039	1.094

Table 2.10

Comparison of the Spectral Index $\frac{\sigma c^{28}}{\sigma_f^{49}}$ at the BOEC

Zone	Subzone	M.I.T. (Japanese FP)	BNL 50 Group	M.I.T. (BNL FP)	BNL/M.I.T. (BNL FP)	BNL/M.I.T. (Jap. FP)
1	3	3.886 E-2	3.505 E-2	3.880 E-2	0.903	0.902
1	7	5.198 E-2	4.703 E-2	5.184 E-2	0.907	0.905
2	11	6.763 E-2	6.283 E-2	6.733 E-2	0.933	0.929
2	14	9.409 E-2	9.356 E-2	9.385 E-2	0.997	0.994
3	17	1.195 E-1	1.184 E-1	1.183 E-1	1.001	0.991
4	19	1.195 E-1	1.176 E-1	1.185 E-1	0.992	0.984
5	20	1.144 E-1	1.129 E-1	1.125 E-1	1.004	0.987
5	24	1.158 E-1	1.148 E-1	1.141 E-1	1.006	0.991
6	29	1.108 E-1	1.074 E-1	1.077 E-1	0.997	0.969
6	32	1.123 E-1	1.091 E-1	1.094 E-1	0.997	0.972
6	34	1.109 E-1	1.116 E-1	1.059 E-1	1.054	1.006

Table 2.11

Comparison of the Spectral Index $\frac{\sigma c^{28}}{\sigma_f^{49}}$ at the EOEC

Zone	Subzone	M.I.T. (Japanese FP)	BNL 50 Group	M.I.T. (BNL FP)	BNL/M.I.T. (BNL FP)	BNL/M.I.T. (Jap. FP)
1	3	4.026 E-2	3.684 E-2	4.027 E-2	0.914	0.915
1	7	5.570 E-2	5.198 E-2	5.578 E-2	0.932	0.933
2	11	7.313 E-2	7.060 E-2	7.320 E-2	0.964	0.965
2	14	9.841 E-2	9.932 E-2	9.830 E-2	1.010	1.009
3	17	1.185 E-1	1.169 E-1	1.170 E-1	0.999	0.986
4	19	1.185 E-1	1.166 E-1	1.174 E-1	0.993	0.984
5	20	1.141 E-1	1.121 E-1	1.119 E-1	1.001	0.982
5	24	1.152 E-1	1.138 E-1	1.133 E-1	1.004	0.988
6	29	1.110 E-1	1.072 E-1	1.077 E-1	0.995	0.9 6
6	32	1.127 E-1	1.091 E-1	1.097 E-1	0.995	0.968
6	34	1.112 E-1	1.120 E-1	1.063 E-1	1.054	1.007

Table 2.12

Comparison of the Spectral Index $\frac{\sigma c^{49}}{\sigma_f^{49}}$ at the BOEC.

Zone	Subzone	M.I.T. (Japanese FP)	BNL 50 Group	M.I.T. (BNL FP)	BNL/M.I.T. (BNL FP)	BNL/M.I.T. (Jap. FP)
1	3	5.486 E-1	5.448 E-1	5.473 E-1	0.995	0.993
1	7	5.722 E-1	5.658 E-1	5.721 E-1	0.989	0.989
2	11	6.056 E-1	5.963 E-1	6.050 E-1	0.986	0.985
2	14	6.144 E-1	6.048 E-1	6.116 E-1	0.989	0.984
3	17	1.589 E-1	1.554 E-1	1.565 E-1	0.993	0.978
4	19	1.588 E-1	1.540 E-1	1.564 E-1	0.985	0.970
5	20	1.522 E-1	1.467 E-1	1.485 E-1	0.988	0.964
5	24	1.546 E-1	1.498 E-1	1.516 E-1	0.988	0.969
6	29	1.464 E-1	1.381 E-1	1.413 E-1	0.977	0.943
6	32	1.542 E-1	1.506 E-1	1.531 E-1	0.984	0.977
6	34	4.228 E-1	4.270 E-1	4.202 E-1	1.016	1.010

Table 2.13

Comparison of the Spectral Index $\frac{\sigma c^{49}}{\sigma_f^{49}}$ at the EOEC

Zone	Subzone	M.I.T. (Japanese FP)	BNL 50 Group	M.I.T. (BNL FP)	BNL/M.I.T. (BNL FP)	BNL/M.I.T. (Jap. FP)
1	3	5.505 E-1	5.489 E-1	5.507 E-1	0.997	0.997
1	7	5.777 E-1	5.736 E-1	5.787 E-1	0.991	0.993
2	11	6.125 E-1	6.067 E-1	6.124 E-1	0.991	0.991
2	14	6.122 E-1	6.014 E-1	6.095 E-1	0.987	0.982
3	17	1.571 E-1	1.529 E-1	1.546 E-1	0.989	0.973
4	19	1.570 E-1	1.528 E-1	1.545 E-1	0.989	0.973
5	20	1.516 E-1	1.448 E-1	1.473 E-1	0.983	0.955
5	24	1.534 E-1	1.479 E-1	1.497 E-1	0.988	0.964
6	29	1.464 E-1	1.375 E-1	1.414 E-1	0.972	0.939
6	32	1.549 E-1	1.507 E-1	1.538 E-1	0.980	0.973
6	34	4.239 E-1	4.273 E-1	4.210 E-1	1.015	1.008

Table 2.14

Comparison of the Spectral Index $\frac{\sigma a^{FP}}{\sigma_f^{49}}$ at the BOEC.

Zone	Subzone	M.I.T. (Japanese FP)	BNL 50 Group	M.I.T. (BNL FP)	BNL/M.I.T. (BNL FP)	BNL/M.I.T. (Jap. FP)
1	3	4.756 E-1	1.582 E-1	1.692 E-1	0.935	0.333
1	7	5.641 E-1	2.084 E-1	2.208 E-1	0.944	0.369
2	11	6.505 E-1	2.754 E-1	2.835 E-1	0.971	0.423
2	14	6.642 E-1	3.574 E-1	3.458 E-1	1.034	0.538
3	17	1.765 E-1	1.467 E-1	1.471 E-1	0.997	0.831
4	19	1.763 E-1	1.458 E-1	1.473 E-1	0.990	0.827
5	20	1.684 E-1	1.389 E-1	1.389 E-1	1.000	0.825
5	24	1.706 E-1	1.418 E-1	1.413 E-1	1.004	0.831
6	29	1.627 E-1	1.318 E-1	1.327 E-1	0.993	0.810
6	32	1.695 E-1	1.401 E-1	1.402 E-1	0.999	0.827
6	34	4.384 E-1	2.817 E-1	2.656 E-1	1.061	0.643

Table 2.15

Comparison of the Spectral Index $\frac{\sigma a^{FP}}{\sigma_f^{49}}$ at the EOEC.

Zone	Subzone	M.I.T. (Japanese FP)	BNL 50 Group	M.I.T. (BNL FP)	BNL/M.I.T. (BNL FP)	BNL/M.I.T. (Jap. FP)
1	3	4.861 E-1	1.654 E-1	1.749 E-1	0.946	0.340
1	7	5.870 E-1	2.277 E-1	2.351 E-1	0.969	0.388
2	11	6.698 E-1	3.032 E-1	3.028 E-1	1.001	0.453
2	14	6.502 E-1	3.677 E-1	3.529 E-1	1.042	0.566
3	17	1.747 E-1	1.446 E-1	1.453 E-1	0.995	0.828
4	19	1.746 E-1	1.443 E-1	1.457 E-1	0.990	0.826
5	20	1.677 E-1	1.377 E-1	1.381 E-1	0.997	0.821
5	24	1.696 E-1	1.408 E-1	1.401 E-1	1.005	0.853
6	29	1.629 E-1	1.314 E-1	1.327 E-1	0.990	0.888
6	32	1.699 E-1	1.400 E-1	1.404 E-1	0.997	0.851
6	34	4.378 E-1	2.816 E-1	2.662 E-1	1.058	0.643

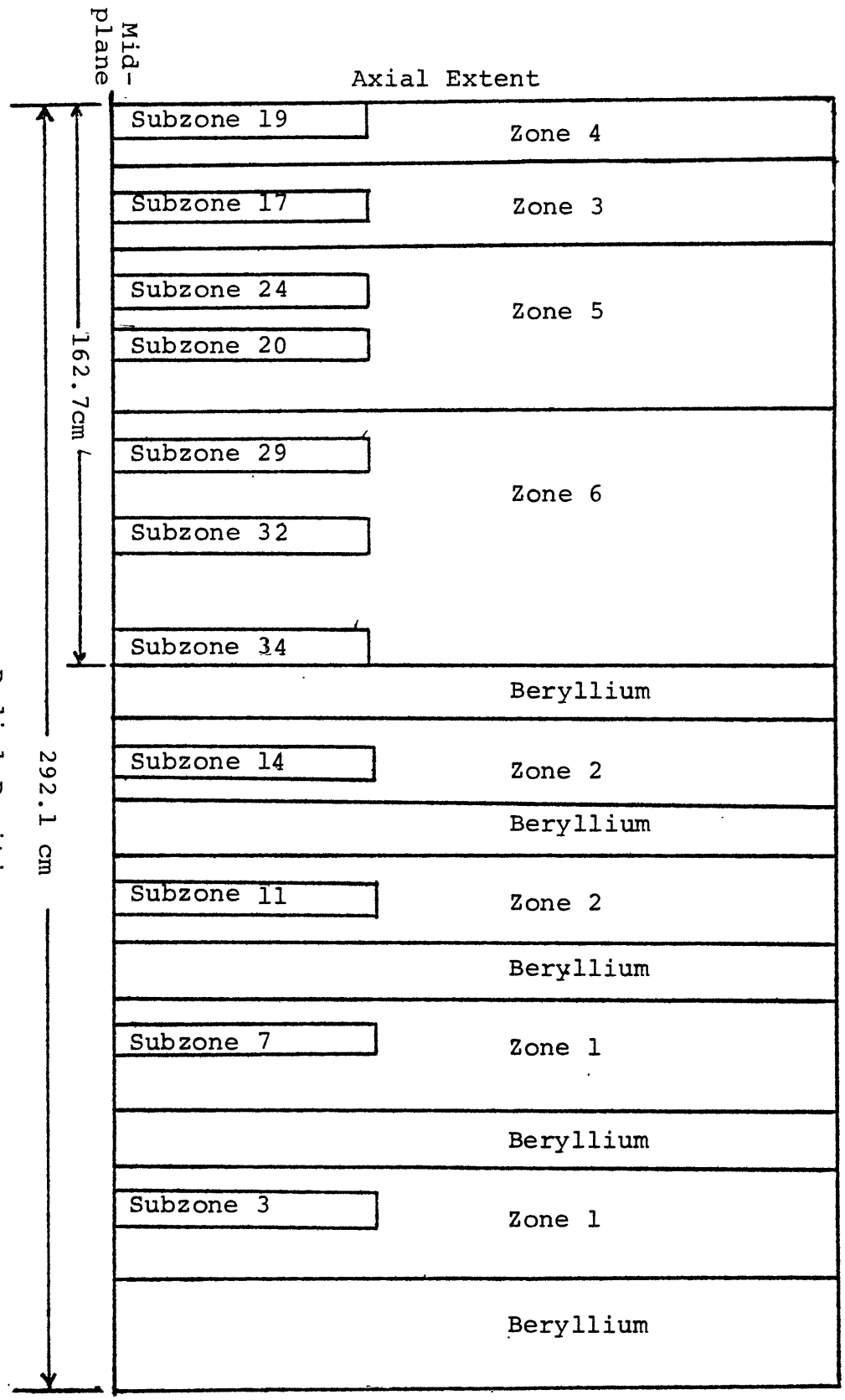

Fig. 2.5 Location of Core Zones and Subzones

are with the Japanese fission products. Figure 2.8 shows the beginning of the equilibrium cycle radial flux for BNL and for M.I.T. results with BNL fission products. Figure 2.8 shows the beginning of the equilibrium cycle radial flux for BNL and for M.I.T. results with BNL fission products. It can be seen from Fig. 2.8 that when the same fission product cross sections are used the radial fluxes are almost identical. Figures 2.6 and 2.7 indicate the shift in flux when a higher worth fission product set is used.

Figures 2.9 and 2.10 show the M.I.T. (Japanese fission products) and BNL radial power distributions at the beginning and end of equilibrium cycle. Figre 2.11 shows the M.I.T. (BNL fission products) and BNL radial power distribution at the beginning of equilibrium cycle. There is excellent agreement evidenced in this figure. Looking at Figs. 2.9 and 2.10 it can be seen that the power peaking in the zone next to the first ring of beryllium is much higher in BNL calculations compared to M.I.T.'s (Japanese fission products) results. The BNL power density in this zone appears to be higher than the limiting power density of 0.36 MW/liter set by thermal hydraulic considerations

2.5.2 Nuclide Concentrations

The number densities of all the materials used in the M.I.T. and BNL calculations at the beginning of equilibrium cycle are the same. The nuclide concentrations of the heavy

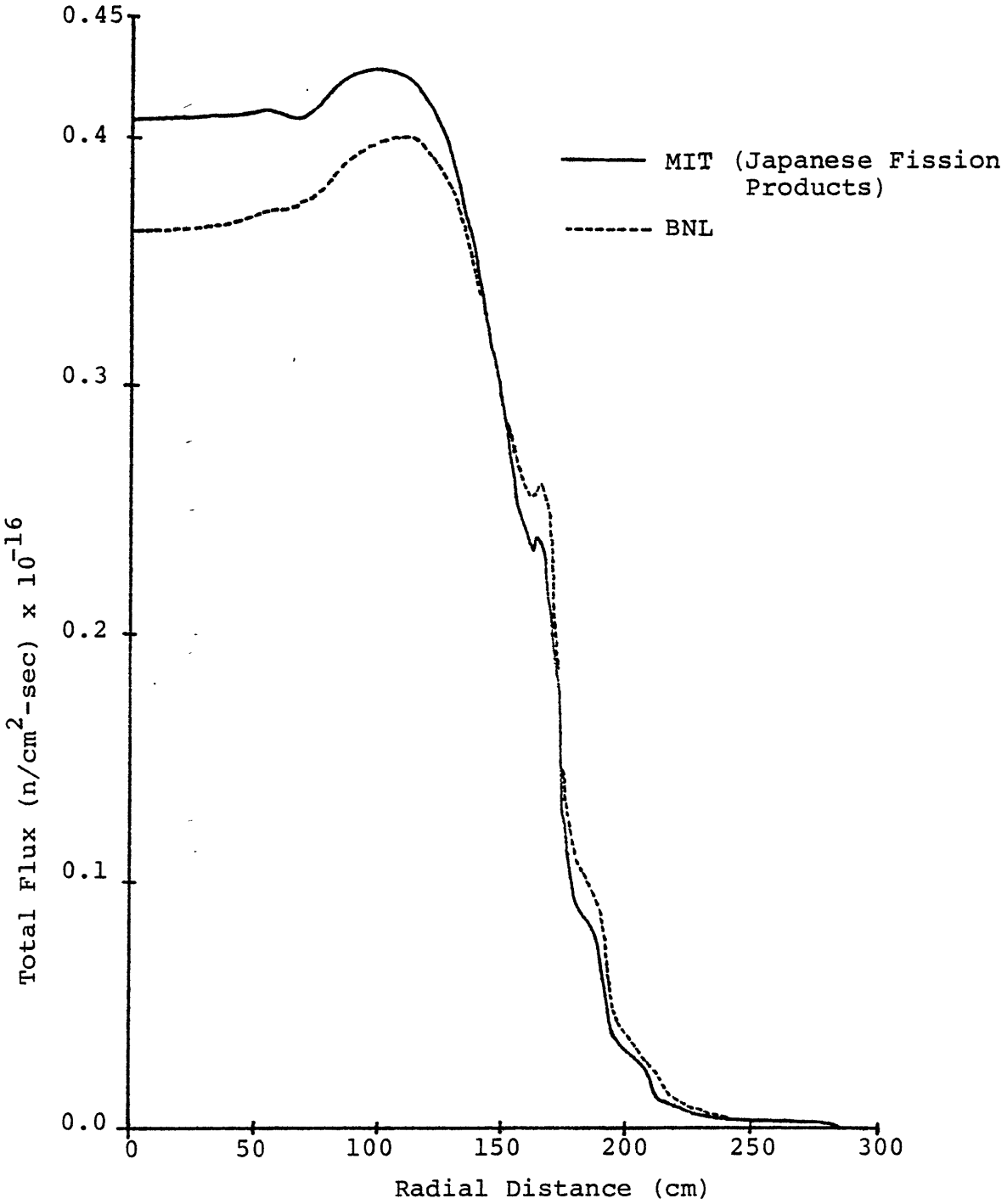

Fig. 2.6 Radial Flux at BOEC along the Core Midplane

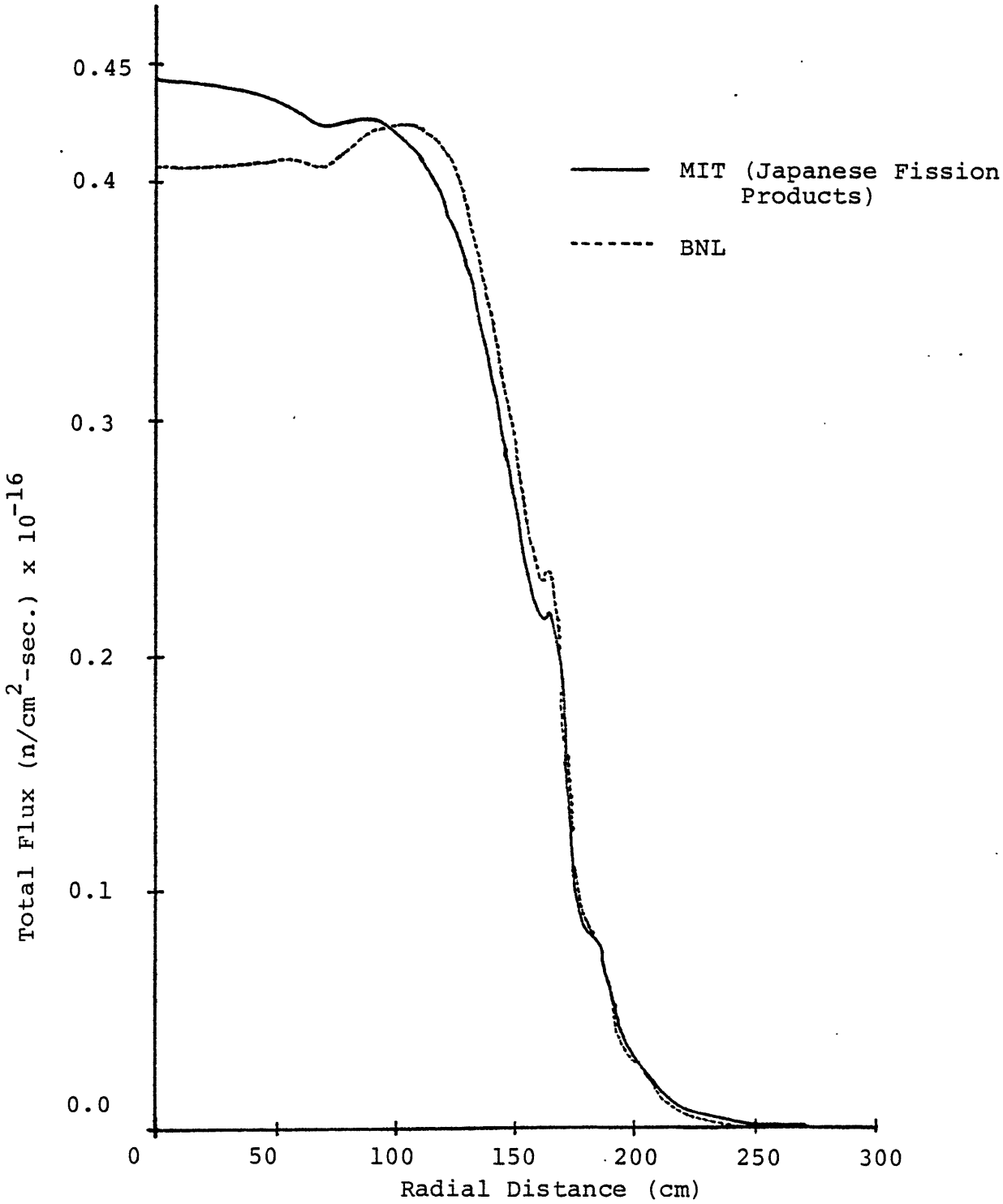

Fig. 2.7 Radial Flux at EOEC along the Core Midplane

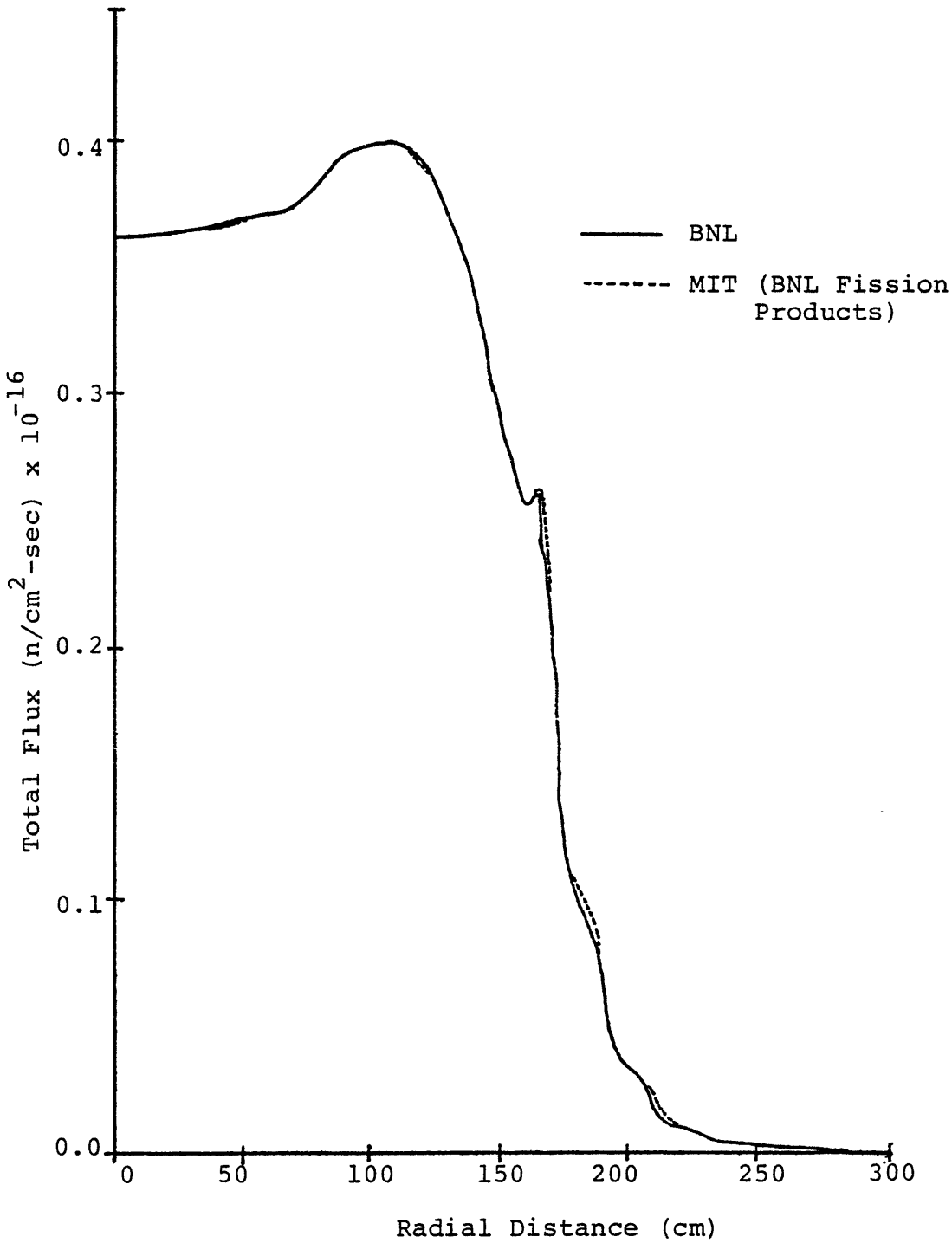

Fig. 2.8 Radial Flux at BOEC along the Core Midplane

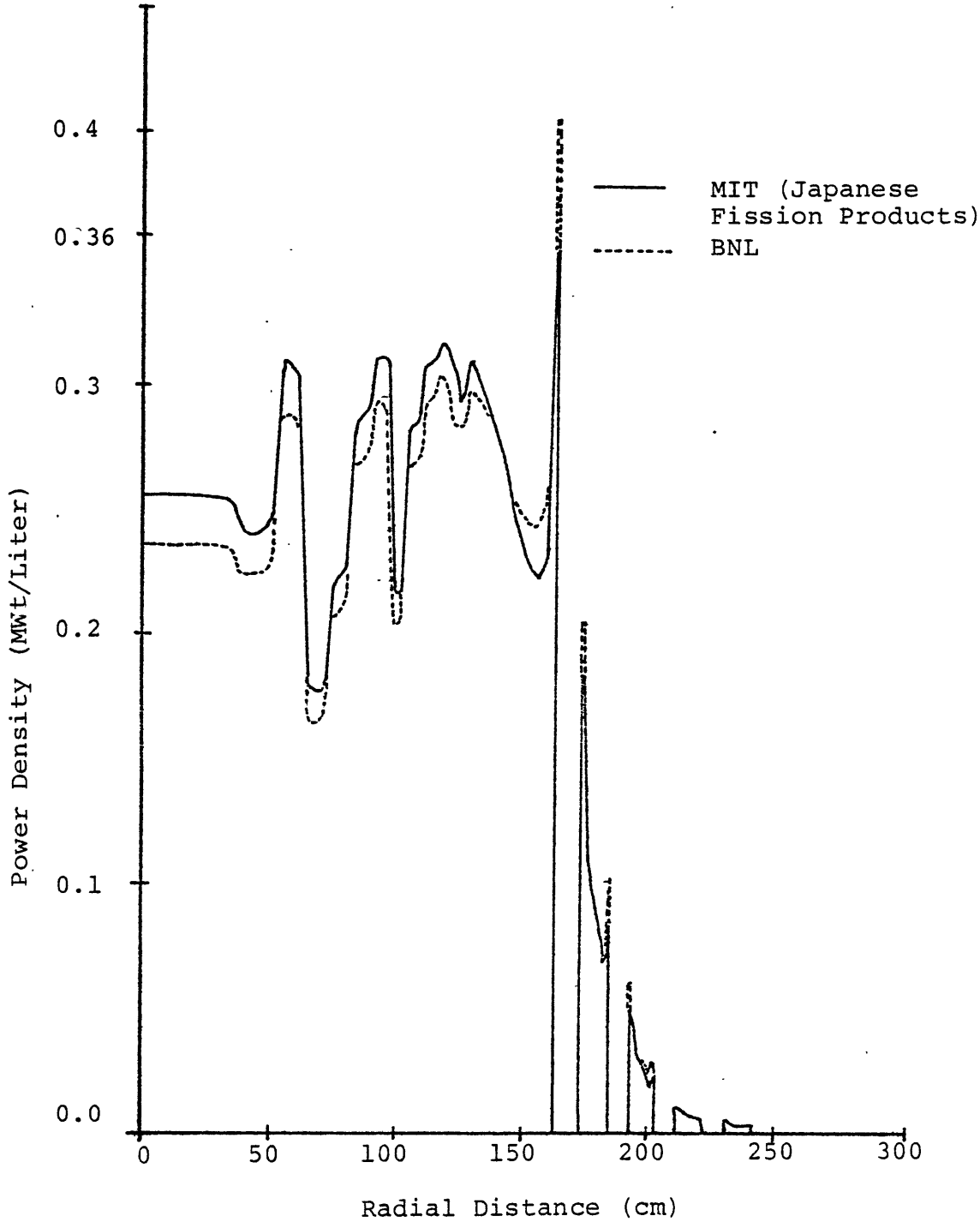

Fig. 2.9 Radial Power Distribution at BOEC along the Core Midplane

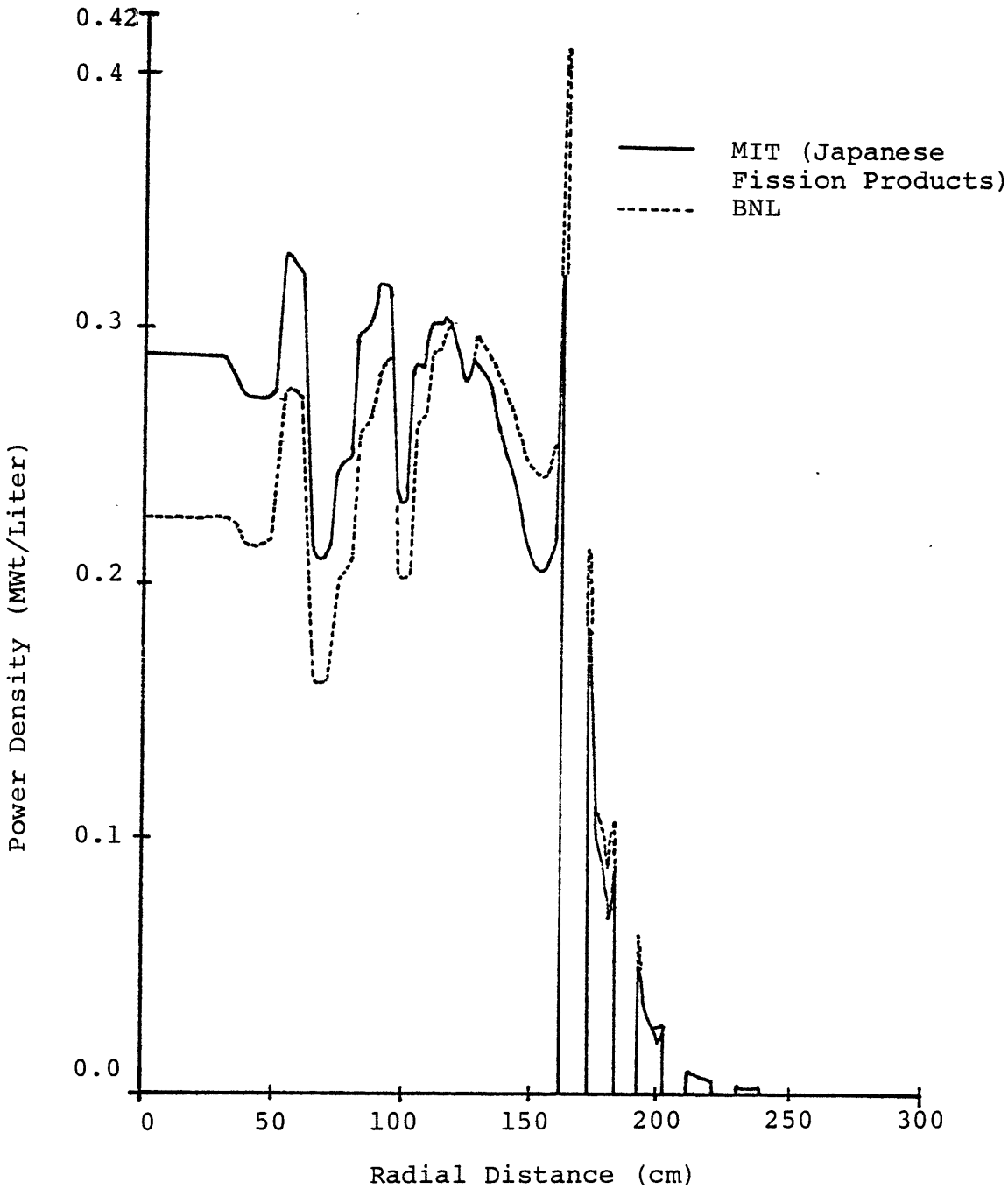

Fig. 2.10 Radial Power Distribution at EOEC Along the Core Midplane

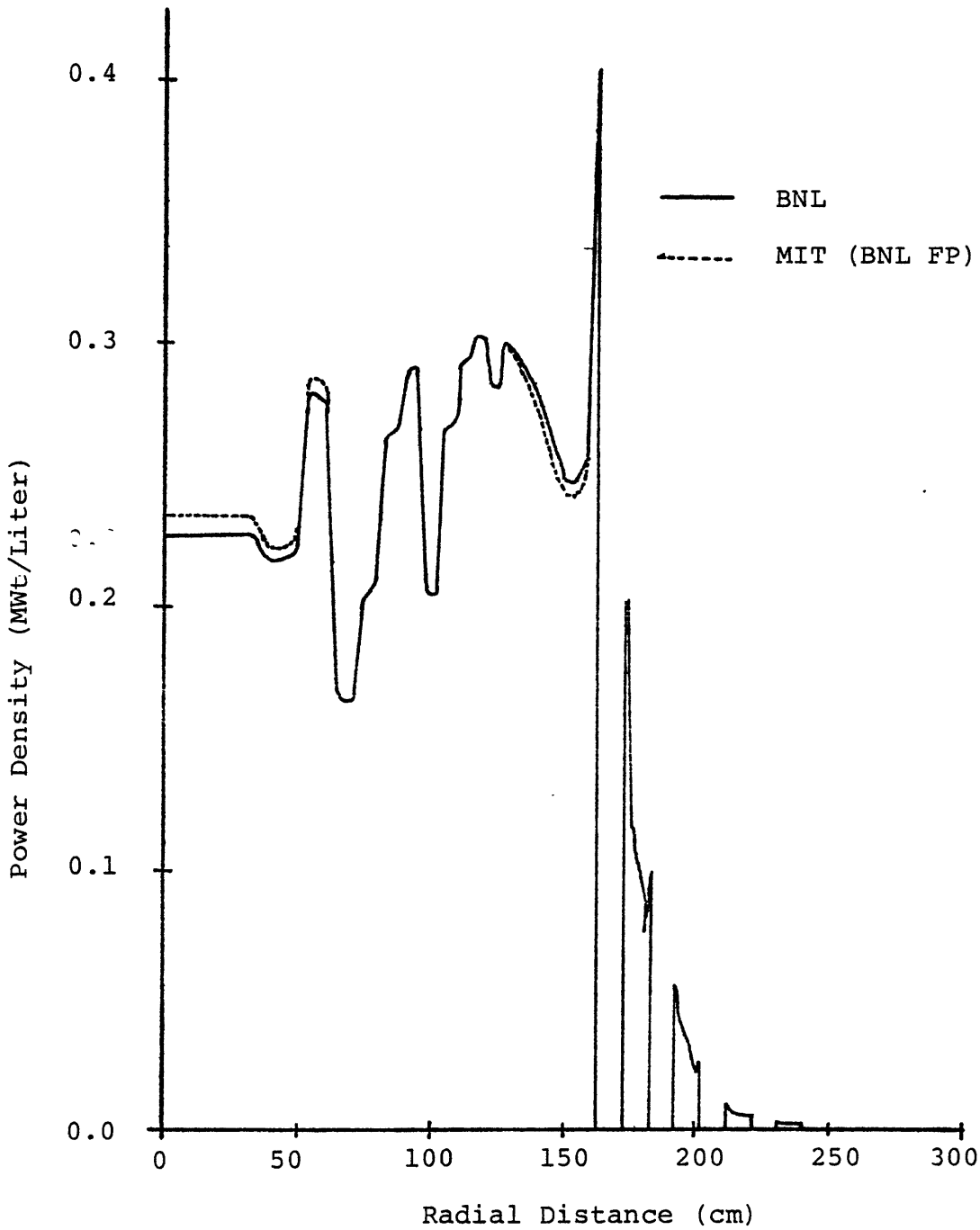

Fig. 2.11 Radial Power Distribution at BOEC along the Core Midplane

metals change during burnup. This section will compare the end-of-equilibrium-cycle (EOEC) nuclide concentrations from the BNL calculations with those from the M.I.T. calculations.

Tables 2.16 through 2.20 record the EOEC nuclide concentrations for U-238 and the four major plutonium isotopes. The format is similar to that of Table 2.8: the first column gives the M.I.T. results using the Japanese fission product cross section set; Column 2 gives the BNL 50-group results; Column 3 the M.I.T. results using BNL fission products; and Columns 4 and 5 are ratios of the preceding columns, as indicated.

Basically there is good agreement. The most important disagreement is the discrepancy in the soft-spectrum blanket zone, Zone No. 1. There is a progressively larger discrepancy between BNL and M.I.T. as one moves up the plutonium chain.

While there is also a systematic effect of fission product cross section sets, the cause of the discrepancy becomes clearer if one examines the space and spectrum-averaged one group cross sections for each zone. Table 2.21 shows the absorption cross section for Pu-240. The larger value of σ_a^{40} for BNL in Zone 1 will generate more Pu-241 in that zone than the M.I.T. case, as shown in Column 4 of Table 2.18. This difference in nuclide concentration will propagate up the plutonium chain.

The large differences between M.I.T. and BNL absorption cross sections are due to the use of a restricted number of zonewise 10-group sets in the M.I.T. calculations. As already

mentioned in Section 2.4, three 10-group sets were used, and the set developed for Zone 2 was used for Zones 1 and 2. The reasons for selecting the Zone 2 cross section set was also given. As shown in Table 2.22, the difference in σ_a^{40} between the true Zone 1 and Zone 2 cross-section sets is substantial, but the former is in slightly better agreement with BNL.

It should be pointed out that if the Zone 1 cross section set is used instead of the Zone 2 set in the burnup calculations we would expect greater nuclide concentrations for the plutonium isotopes in Zone 1 compared to the BNL results, because of the greater value of σ_a^{40} in the Zone 1 set. This is discussed further in Section 2.6. Looking at Tables 2.17 through 2.20, we notice that Zone 2 agreement, while considerably better than for Zone 1, still exhibits a substantial mismatch. This could be reduced by collapsing the zone-wise sets over the middle-of-cycle spectrum instead of beginning of cycle, or by going to more energy groups as BNL has done, or by subdividing the zones.

2.6 Parametric Studies

The k calculations previously performed employed only three 10-group cross section sets for the six fuel zones. More specifically, the set developed for Zone 2 was used for Zones 1 and 2; that developed for Zone 4 was used for Zones 3 and 4 and the cross section set used for Zones 5 and 6 was developed only for Zone 6. The reasons for such a selection were given in Section 2.4. The analysis will be more accurate if six

Table 2.16

Comparison of the Number Density of U^{28} at the EOEC

Zone	Subzone	1 M.I.T. (Japanese FP)	2 BNL 50 Group	3 M.I.T. (BNL FP)	4 BNL/M.I.T. (BNL FP)	5 BNL/M.I.T. (Jap. FP)
1	3	1.404E-2	1.404E-2	1.404E-2	1.000	1.000
1	7	1.399E-2	1.399E-2	1.399E-2	1.000	1.000
2	11	1.383E-2	1.382E-2	1.382E-2	1.000	0.999
2	14	1.346E-2	1.344E-2	1.344E-2	1.000	0.999
3	17	1.288E-2	1.289E-2	1.290E-2	0.999	1.001
4	19	1.252E-2	1.254E-2	1.254E-2	1.000	1.002
5	20	1.235E-2	1.236E-2	1.236E-2	1.000	1.001
5	24	1.167E-2	1.168E-2	1.168E-2	1.000	1.001
6	29	1.093E-2	1.093E-2	1.093E-2	1.000	1.000
6	32	1.054E-2	1.054E-2	1.054E-2	1.000	1.000
6	34	1.026E-2	1.023E-2	1.024E-2	0.999	0.997

Table 2.17

Comparison of the Number Density of Pu^{49} at the EOEC

Zone	Subzone	1 M.I.T. (Japanese FP)	2 BNL 50 Group	3 M.I.T. (BNL FP)	4 BNL/M.I.T. (BNL FP)	5 BNL/M.I.T. (Jap. FP)
1	3	1.423E-5	1.511E-5	1.477E-5	1.023	1.062
1	7	6.098E-5	6.329E-5	6.249E-5	1.013	1.038
2	11	1.881E-4	1.921E-4	1.914E-4	1.004	1.021
2	14	4.189E-4	4.254E-4	4.239E-4	1.004	1.016
3	17	7.096E-4	7.041E-4	7.031E-4	1.002	0.992
4	19	8.333E-4	8.268E-4	8.270E-4	1.000	1.004
5	20	8.778E-4	8.747E-4	8.736E-4	1.001	0.996
5	24	9.947E-4	9.930E-4	9.919E-4	1.001	0.998
6	29	1.042E-3	1.039E-3	1.039E-3	1.000	0.997
6	32	1.051E-3	1.049E-3	1.049E-3	1.000	0.998
6	34	1.013E-3	1.008E-3	1.003E-3	1.005	0.995

Table 2.18

Comparison of the Number Density of Pu^{40} at the EOEC

Zone	Subzone	1 M.I.T. (Japanese FP)	2 BNL 50 Group	3 M.I.T. (BNL FP)	4 BNL/M.I.T. (BNL FP)	5 BNL/M.I.T. (Jap. FP)
1	3	4.952E-8	6.841E-8	5.765E-8	1.187	1.381
1	7	1.196E-6	1.285E-6	1.270E-6	1.012	1.074
2	11	9.076E-6	8.835E-6	9.494E-6	0.931	0.973
2	14	3.939E-5	4.032E-5	4.036E-5	0.999	1.024
3	17	6.132E-5	6.056E-5	6.053E-5	1.001	0.988
4	19	7.970E-5	7.851E-5	7.856E-5	0.999	0.985
5	20	8.927E-5	8.836E-5	8.840E-5	1.000	0.990
5	24	1.278E-4	1.268E-4	1.268E-4	1.000	0.992
6	29	1.698E-4	1.688E-4	1.689E-4	0.999	0.994
6	32	1.988E-4	1.983E-4	1.983E-4	1.000	0.997
6	34	2.318E-4	2.309E-4	2.308E-4	1.000	0.996

Table 2.19

Comparison of the Number Density of Pu^{41} at the EOEC

Zone	Subzone	1 M.I.T. (Japanese FP)	2 BNL 50 Group	3 M.I.T. (BNL FP)	4 BNL/M.I.T. (BNL FP)	5 BNL/M.I.T. (Jap. FP)
1	3	5.999E-10	2.172E-9	7.923E-10	2.741	3.621
1	7	1.575E-7	2.691E-7	1.684E-7	1.598	1.709
2	11	2.650E-6	3.975E-6	2.828E-6	1.406	1.500
2	14	1.323E-5	1.450E-5	1.413E-5	1.026	1.096
3	17	9.032E-6	9.036E-6	9.040E-6	1.000	1.000
4	19	8.971E-6	8.941E-6	8.949E-6	0.999	0.997
5	20	9.182E-6	9.140E-6	9.148E-6	0.999	0.995
5	24	1.094E-5	1.087E-5	1.087E-5	1.000	0.994
6	29	1.453E-5	1.444E-5	1.446E-5	0.999	0.994
6	32	1.865E-5	1.867E-5	1.878E-5	0.994	1.001
6	34	2.910E-5	3.545E-5	3.366E-5	1.053	1.218

Table 2.20

Comparison of the Number Density of Pu^{42} at the EOEC

Zone	Subzone	1 M.I.T. (Japanese FP)	2 BNL 50 Group	3 M.I.T. (BNL FP)	4 BNL/M.I.T. (BNL FP)	5 BNL/M.I.T. (Jap. FP)
1	3	6.903E-13	3.204E-12	1.037E-12	3.090	4.641
1	7	1.033E-9	1.858E-9	1.218E-9	1.525	1.799
2	11	3.933E-8	6.355E-8	4.615E-8	1.377	1.616
2	14	6.805E-7	7.108E-7	7.235E-7	0.982	1.045
3	17	1.034E-6	1.023E-6	1.022E-6	1.001	0.989
4	19	1.319E-6	1.305E-6	1.305E-6	1.000	0.989
5	20	1.418E-6	1.409E-6	1.408E-6	1.001	0.994
5	24	1.932E-6	1.921E-6	1.919E-6	1.001	0.994
6	29	2.550E-6	2.535E-6	2.536E-6	1.000	0.994
6	32	3.074E-6	3.052E-6	3.060E-6	0.997	0.993
6	34	3.691E-6	3.847E-6	3.637E-6	1.058	1.042

Table 2.21

Comparison of σ_a^{40}(b) at BOEC and EOEC

BOEC

zone	subzone	M.I.T. (BNL FP)	BNL 50 Group	BNL/M.I.T. (BNL FP)
1	3	5.408E+1	1.136E+2	2.101
1	7	4.252E+1	9.167E+1	2.156

EOEC

zone	subzone	M.I.T. (BNL FP)	BNL 50 Group	BNL/M.I.T. (BNL FP)
1	3	5.308E+1	1.091E+2	2.055
1	7	4.031E+1	7.883E+1	1.956

Table 2.22

Comparison of σa^{40}, from the Zone 1 and Zone 2 Cross Section Sets

Subzone	M.I.T. (Zone 1 Cross-Section Set)	M.I.T. (Zone 2 Cross-Section Set)	BNL Zone 1
3	1.675E+2	5.408E+1	1.136E+2
7	1.366E+2	4.252E+1	9.167E+1

10-group cross section sets, each being developed for each of the six fuel zones, respectively, are used instead of only three sets.

The burnup and k-calculations were therefore repeated using the 10-group cross section sets. Again, both the Japanese and the BNL fission product cross section sets were used. Table 2.23 shows the results of the calculations. The values of the breeding ratio and k_{eff} are slightly lower compared to the previous calculations.

It was mentioned in Section 2.5.2 that by going from three to six 10-group cross section sets in the burnup and k-calculations we should obtain results which are in better agreement with BNL especially with regard to the nuclide concentrations of the plutonium isotopes in Zones 1 and 2. Tables 2.24 through 2.27 compare number densities of the plutonium isotopes at the EOEC in Zones 1 and 2. Looking at these tables, we notice that the results of the 6-set calculations are in much better agreement with the BNL calculations, than were the 3-set calculations. However, referring back to Tables 2.25 through 2.27, we see that the number densities of Pu^{40}, Pu^{41} and Pu^{42} in Zone 1 from the six-set calculations are greater than those from the BNL calculations. The reason for this finding will become apparent by examining the space and spectrum-averaged one group capture cross sections of the plutonium nuclides in Zone 1 from the 3 sets of calculations, namely M.I.T. calculations using three and six cross section

Table 2.23

k_{eff} and Breeding Ratio Comparison Between M.I.T. (6 Cross Section Sets) and BNL Calculations

	k_{eff}		BR	
	BOEC	EOEC	BOEC	EOEC
BNL (50 group)	0.982	1.000	1.67	1.61
MIT (6 x-section sets) Japanese FP	0.971	0.987	1.66	1.59
MIT (6 x-section sets) BNL FP	0.976	0.994	1.65	1.58

Table 2.24

Comparison of the Number Density of Pu^{49} at the EOEC

Zone	Subzone	MIT (Japanese FP 3 sets)	MIT (Japanese FP 6 sets)	BNL 50 Group	BNL/MIT (3 sets)	BNL/MIT (6 sets)
1	3	1.423 E-5	1.471 E-5	1.511 E-5	1.062	1.027
1	7	6.098 E-5	6.142 E-5	6.329 E-5	1.038	1.030
2	11	1.881 E-4	1.879 E-4	1.921 E-4	1.021	1.022
2	14	4.189 E-4	4.174 E-4	4.254 E-4	1.016	1.019

Zone	Subzone	MIT (BNL FP 3 sets)	MIT (BNL FP 3 sets)	BNL 50 group	BNL/MIT (3 sets)	BNL/MIT (6 sets)
1	3	1.477 E-5	1.504 E-5	1.511 E-5	1.023	1.005
1	7	6.249 E-5	6.209 E-5	6.329 E-5	1.013	1.019
2	11	1.914 E-4	1.890 E-4	1.921 E-4	1.004	1.016
2	14	4.239 E-4	4.187 E-4	4.254 E-4	1.004	1.016

Table 2.25

Comparison of the Number Density of Pu^{40} at the EOEC

Zone	Subzone	MIT (Japanese FP 3 sets)	MIT (Japanese FP 6 sets)	BNL 50 Group	BNL/MIT (3 sets)	BNL/MIT (6 sets)
1	3	4.952 E-8	7.546 E-8	6.841 E-8	1.381	0.907
1	7	1.196 E-6	1.262 E-6	1.285 E-6	1.074	1.018
2	11	9.076 E-6	9.006 E-6	8.835 E-6	0.973	0.981
2	14	3.939 E-5	3.572 E-5	4.032 E-5	1.024	1.129

Zone	Subzone	MIT (BNL FP 3 sets)	MIT (BNL FP 6 sets)	BNL 50 Group	BNL/MIT (3 sets)	BNL/MIT (6 sets)
1	3	5.765 E-8	8.161 E-8	6.841 E-8	1.187	0.838
1	7	1.270 E-6	1.293 E-6	1.285 E-6	1.012	0.994
2	11	9.494 E-6	9.136 E-6	8.835 E-6	0.931	0.9167
2	14	4.036 E-5	3.593 E-5	4.032 E-5	0.999	1.122

Table 2.26

Comparison of the Number Density of Pu^{41} at the EOEC

Zone	Subzone	MIT (Japanese FP 3 sets)	MIT (Japanese FP 6 sets)	BNL 50 Group	BNL/MIT (3 sets)	BNL/MIT (6 sets)
1	3	5.999 E-10	3.434 E-9	2.173 E-9	3.621	0.633
1	7	1.575 E-7	2.285 E-7	2.691 E-7	1.709	0.819
2	11	2.650 E-6	3.172 E-6	3.975 E-6	1.500	1.253
2	14	1.323 E-5	1.634 E-5	1.450 E-5	1.096	0.887

Zone	Subzone	MIT (BNL FP 3 sets)	MIT (BNL FP 6 sets)	BNL 50 Group	BNL/MIT (3 sets)	BNL/MIT (6 sets)
1	3	7.923 E-10	3.963 E-9	2.172 E-9	2.741	0.548
1	7	1.684 E-7	3.448 E-7	2.691 E-7	1.598	0.781
2	11	2.828 E-6	3.243 E-6	3.975 E-6	1.405	1.225
2	14	1.413 E-5	1.661 E-5	1.450 E-5	1.026	0.873

Table 2.27

Comparison of the Number Density of Pu^{42} at the EOEC

Zone	Subzone	MIT (Japanese FP 3 sets)	MIT (Japanese FP 6 sets)	BNL 50 Group	BNL/MIT (3 sets)	BNL/MIT (6 sets)
1	3	6.903 E-13	5.377 E-12	3.204 E-12	4.641	0.596
1	7	1.033 E-9	2.124 E-9	1.858 E-9	1.799	0.875
2	11	3.933 E-8	5.251 E-8	6.355 E-8	1.616	1.211
2	14	6.805 E-7	7.168 E-7	7.108 E-7	1.045	0.992

Zone	Subzone	(BNL FP 3 sets)	(BNL FP 6 sets	BNL 50 Group	BNL/MIT (3 sets)	BNL/MIT (6 sets)
1	3	1.037 E-12	6.633 E-12	3.204 E-12	3.090	0.483
1	7	1.218 E-9	2.312 E-9	1.858 E-9	1.525	0.804
2	11	4.615 E-8	5.526 E-8	6.355 E-8	1.377	1.149
2	14	7.235 E-7	7.301 E-7	7.108 E-7	0.982	0.974

sets, and the BNL calculations. Refer to Tables 2.28 and 2.29. We notice that the capture cross sections of the plutonium nuclides from the six-set calculations are greater than those from the BNL calculations. This will lead to the production of more plutonium nuclides, and hence higher nuclide concentrations, as observed.

It is not clear that increasing the degree of sophistication in the M.I.T. calculations will lead to exact duplication of the BNL results. However, use of 6 zonewise cross section sets in the burnup and k-calculations considerably improved the agreement in the plutonium composition at EOEC in the blanket or moderated fuel zones between the 2 sets of calculations (i.e. the M.I.T. and the BNL). It should also be pointed out that our spectrum-averaged cross sections are slightly larger than those of the BNL results, which is consistent with the finding that in the moderated regions our calculations showed a softer spectrum than BNL. This could in large part be due to the different number of energy groups used in the analyses. The point should also be made that neither set of calculations can be relied upon to give true-to-life results, since both used infinite-medium resonance shielding, which is not appropriate near interfaces of dissimilar media. Fortunately, since the blanket or moderated fuel zones are not especially productive of either power or bred fuel, one would not expect these discrepancies to have much impact on the overall analysis. It can be concluded that the k calculations

Table 2.28

Comparison of $\sigma_{capture}$ of the Plutonium Nuclides in Subzone 3 (Zone 1)

At BOEC	MIT (3 sets)	MIT (6 sets)	BNL (50 Group)
σ_c^{49}	0.857 E+1	1.093 E+1	0.931 E+1
σ_c^{40}	0.538 E+2	1.662 E+2	1.134 E+2
σ_c^{41}	0.742 E+1	0.873 E+1	0.762 E+1

At EOEC	MIT (3 sets)	MIT (6 sets)	BNL (50 Group)
σ_c^{49}	0.825 E+1	1.039 E+1	0.882 E+1
σ_c^{40}	5.276 E+1	1.624 E+2	1.088 E+2
σ_c^{41}	0.711 E+1	0.787 E+1	0.718 E+1

Table 2.29

Comparison of $\sigma_{capture}$ of the Plutonium Nuclides in Subzone 7 (Zone 1)

At BOEC	MIT (3 sets)	MIT (6 sets)	BNL (50 Group)
σ_c^{49}	0.639 E+1	0.783 E+1	0.684 E+1
σ_c^{40}	4.219 E+1	1.325 E+2	9.132 E+1
σ_c^{41}	0.530 E+1	0.575 E+1	0.544 E+1

At EOEC	MIT (3 sets)	MIT (6 sets)	BNL (50 Group)
σ_c^{49}	0.592 E+1	0.711 E+1	0.615 E+1
σ_c^{40}	3.998 E+1	1.217 E+2	7.848 E+1
σ_c^{41}	0.486 E+1	0.516 E+1	0.484 E+1

and burnup analyses performed by MIT using ten energy groups are sufficiently accurate when compared against the 50-group calculations done by BNL. Using fewer energy groups reduces computational cost and storage requirements substantially.

2.7 Conclusions

In the present work static BOEC reactivity calculations and fuel burnup analyses were performed for a gas cooled FMSR using the two-dimensional multigroup diffusion theory burnup code 2DB. The 10-group cross section set used in the calculations was developed from the 50-group LIB-IV compilation using the code SPHINX. The reactor model used had geometric specifications and zonewise compositions provided by BNL. In the BNL calculations, the uncollapsed 50-group cross section set from the LIB-IV library was used. The other difference between the M.I.T. and the BNL k calculations and burnup analyses was the use of "Japanese" fission product cross sections [J-1] by M.I.T. instead of those from the LIB-IV compilation as used by BNL. The results from the M.I.T. calculations were then compared with BNL's calculations.

The differences in the results from M.I.T. and BNL's analyses can be attributed to, basically, two factors. First, the number of energy groups used in the analyses were different--10 groups in the M.I.T. calculations and 50 groups in the BNL calculations. The softer spectrum in the moderated regions observed in the M.I.T. results is probably due to the

fewer number of energy groups in the calculations. The softer spectrum is responsible to a considerable extent for the disagrement in the plutonium nuclide concentrations at the EOEC in the moderated fuel regions. Spectrum softening in going from fine to coarser energy groups was observed by Wood [W-1] in his computations of capture rates for uranium and thorium in the blanket regions of a fast breeder reactor.

The second factor which contributed to the disagreement in the results was the choice of the fission product cross section set. M.I.T. used a set generated using the results reported by the JNDC [J-1], whereas, BNL employed the set corresponding to the LIB-IV nonsaturating plutonium fission products times a factor of 2.7. The JNDC fission product worth in the analysis was around 5.0% Δk, while the BNL fission products were worth around 3.5% Δk. It was found that the breeding ratio of an equilibrium cycle was reduced when lower worth fission products were used. One explanation for this could be that the higher fission product cross sections harden the overall spectrum, leading to a higher breeding ratio. There are still uncertainties with regard to the choice of any particular fission product cross section set in the burnup analysis of a fast reactor, especially the FMSR. It is important to develop a cross section set for the fission products in the FMSR suitable to its analysis. This will eliminate many, if not most, differences in the results of the burnup and k calculations performed by M.I.T. and BNL.

Clearly, in any benchmark calculations the careful selection and preparation of cross section sets can never be over-emphasized.

Finally, it can be concluded that sufficiently accurate static BOEC reactivity calculations and fuel burnup analyses can be performed using only ten energy groups instead of 50 energy groups, particularly if several ten group sets are used, each tailored to a particular zone of the reactor. The computational cost and storage requirements will be reduced substantially by using fewer energy groups.

CHAPTER III

GAMMA HEATING ANALYSIS

3.1 Introduction

In any reactor, it is important to know the distribution of the thermal energy source, since the temperature field within the reactor, and hence the heat transport, thermal stresses and many other temperature-dependent physical and chemical properties of reactor materials, are determined by the thermal energy source distributions. We can ultimately associate the thermal energy source in a reactor with the slowing down of fission fragments, which are heavy charged particles, alpha and beta particles, neutrons and recoil nuclei and atoms. The difference between energy deposition by charged and uncharged particles must be pointed out. It is generally accepted that the initial kinetic energy of the charged particles is immediately converted into thermal energy locally [A-5], whereas the mean free path of photons and neutrons is of the order of several centimeters, and hence requiring in general a detailed transport calculation.

It should also be noted that a fraction of the kinetic energy of charged particles, especially in the case of energetic beta particles, as they decelerate via coulomb interactions can be re-emitted in the form of Bremsstrahlung radiation. If this process is important or significant in a particular

medium, then the assumption of local deposition of the total kinetic energy of these charged particles will not be valid, because the secondary photons thus created can travel a significant distance away from the point of origin in the medium.

Investigation of the production of photons and their subsequent interaction with reactor materials, finally leading to energy deposition, usually referred to as Gamma Heating, is an important consideration in the FMSR design activity.

3.2 Sources of Gammas in a Nuclear Reactor

Gamma-Sources in a reactor are: [K-2]

1. Nuclear Fission Gammas
   a. Prompt fission gamma
   b. Short-lived fission product decay gammas
   c. Long-lived fission product decay gammas
2. Capture Gammas
   a. Prompt capture gammas
   b. Post-capture decay gammas
3. Inelastic Scattering Gammas
4. Gammas from (n, 2n) and (n, charged particle) reactions
5. Annihilation gammas
6. Bremsstrahlung gammas

Prompt gammas and, for all practical purposes, short-lived fission product decay gammas are emitted at the time of fission; whereas for long-lived fission product decay gammas the time involved is so long that they constitute a significant source of radiation after shutdown. They are of little importance during reactor operation.

The next most important source of gammas after fission is the radiative capture of neutrons, i.e. the (n,γ) reaction. When a neutron is absorbed, the energy level of the resultant nucleus is raised by an amount equal to the binding energy (E_B) of the neutron plus the kinetic energies (E_k) of the neutron and the target nucleus in the center-of-mass system. The reaction is immediately followed by the release of this excitation energy through the emission of gammas. It should be pointed out that if the product nucleus is radioactive, or is formed in an isomeric state, its post-capture decay gamma-energy may be treated separately, or may be included in the binding energy E_B of the neutron. It may also be noted that a very small fraction of the excitation energy (E_B+E_K) goes into the recoil of the nucleus as the gamma(s) is (are) emitted. This is true for all gamma emission processes. The recoil energy of the nucleus or atom is deposited locally.

Inelastic scattering can occur if E_K is greater than ε_1, the energy of the first excited state of the target nucleus, and almost instantaneously (on the order of 10^{-14} sec after the scattering) the nucleus loses its energy of excitation by emitting one or more gammas.

Reactions such as (n,p), (n,α) and $(n, 2n)$ can lead to excited residual nuclei which lose their excitation energy by photon emission. However, the thresholds for these reactions are high and the cross-sections low, making their contribution negligible in most situations.

Annihilation gammas are produced mainly from electron-positron pairs arising from pair production events at higher gamma energies. (Positron sources other than pair production events are rare in the reactor since neutron and fission reactions usually lead to nuclei which are on the excess-neutron side of the stability line and, therefore, decay by β^- emission). Since the pair production process is a significant form of gamma energy deposition in the reactor, annihilation radiation is quite important. In the coupled neutron-gamma cross-section sets used in the gamma heating analysis, this process is appropriately accounted for as a gamma down-scatter event.

Kalra [K-2] in his evaluation of the importance of Bremsstrahlung in a FBR, especially in the reflector region, concluded that for gamma heating calculations, neglecting the effects of Bremsstrahlung radiation is justified.

3.3 Gamma Energy Deposition Reactions

The three types of gamma interactions with matter relevant to the gamma heating analysis are:

1. the photoelectric effect
2. Compton scattering, and
3. pair production

These are the mechanisms by which gammas deposit their energy in the reactor medium. In the photoelectric process, all the energy, $h\nu$, of the incident photon is transferred to a bound electron which is ejected from the atom with a kinetic

energy $T = h\nu - I$, where I is the ionization potential of the electron. This kinetic energy is immediately converted to heat locally, via Coulomb interactions. The photoelectric effect is dominant at low energies (< 100 keV). As the energy of the radiation increases, Compton Scattering becomes more important, especially in the range from 0.1 to 2.0 MeV. In this interaction, the energy of the gamma is reduced without the extinction of the gamma itself. The energy thus lost is imparted to an electron. Pair production can occur only if the energy of the photon is greater than 1.02 MeV, which is the minimum required to create an electron-positron pair, the excess being available as the kinetic energy of the pair and the interacting nucleus. As mentioned above, the kinetic energy of these charged particles is then converted to thermal energy locally.

3.4 The General Format of the Coupled Neutron-Gamma Cross Section Set

An updated (as of 1974) 40-group coupled neutron-gamma cross section library (22 groups of neutrons and 18 groups of gammas) compiled at Oak Ridge National Laboratory (ORNL) [O-1] was used in the present study of gamma heating in the FMSR. At M.I.T., Wood [W-1], Brown [B-4], and Scheinert [S-1] used the original version of this cross section library for gamma heating analysis of LMFBR blankets and blanket assemblies. Both versions (the original and the updated one) were used by Kalra [K-2] in his gamma heating analysis of fast reactors.

The format of the 40-group ORNL cross section set is given in Table 3.1. The first column lists the discrete

Table 3.1

Format of 40-Group ORNL Coupled Neutron-Gamma Cross Section Set

Cross Section	Neutron Groups						Gamma Groups			
	1	2	----	----	----	22	23	----	39	40
σ_a or $\overline{E\sigma_a}$			σ_a					$\overline{E\sigma_a}$		
$\overline{\nu\sigma_f}$							$\overline{\nu\sigma_f}$ (Gammas) = 0			
σ_t		Neutron Transport					Gamma Transport			
σ_{gg}	$\sigma_{1\to1}$		Cross Sections				$\sigma_{23\to23}$	Cross Sections		
$\sigma_{g-1\to g}$	0	$\sigma_{1\to2}$					$\sigma_{22\to23}$			
⋮	0	0	----						----	
$\sigma_{g-17\to g}$	0	0	0						$\sigma_{22\to39}$	$\sigma_{23\to40}$
⋮	0	0	0	0	----		Gamma Production			----
$\sigma_{g-21\to g}$	0	0	0	0	0	$\sigma_{1\to22}$		Cross Sections		
$\sigma_{g-22\to g}$	0	0	0	0	0	0	$\sigma_{1\to23}$			
⋮	0	0	0	0	0	0	0			
$\sigma_{g-38\to g}$	0	0	0	0	0	0	0	0	$\sigma_{1\to39}$	
$\sigma_{g-39\to g}$	0	0	0	0	0	0	0	0	0	$\sigma_{1\to40}$

ordinate format for cross sections used in the code ANISN (E-1), i.e., $E\sigma_a$, $\nu\sigma_f$, σ_t, σ_{gg}, $\sigma_{g-1\to g}$, $\sigma_{g-2\to g}$ . . . $\sigma_{g-39\to g}$. The table length in the vertical direction is 43. The 22 neutron and 18 gamma group members are labelled along the top. Photofission (γ,f) and photoneutron (γ,n) reactions and energy upscatter mechanisms for neutrons or gammas are not allowed for.

Gamma production cross-sections are entered as down-scattering events from 22 groups of neutrons to 18 groups of gammas. These cross-sections were generated at ORNL using the POPOP4 code [F-1], and are documented in Ref.[O-1].

Gamma scattering cross sections are expanded in a P_3 Legendre expansion using the Klein-Nishina approximation [W-2]. The zeroth moment photon transfer cross sections are modified for the pair production event as follows [K-3]:

$$\sigma^m_{so}\ (E\to E') = \sigma_{so}(E\to E) + \sigma_{pp}(E)\ \cdot\ 2\delta\ (E'-0.51). \qquad (3.1)$$

where

$\sigma^m_{so}(E\to E')$ is the modified zeroth moment photon transfer cross section

$\sigma_{so}(E\to E')$ is the zeroth moment photon transfer cross section as given by the Klein-Nishina approximation,

$\sigma_{pp}(e)$ is the pair production cross section,

E is the energy of the incident photon,

E' is the energy of the scattered photon, and

δ is the Kronecker delta.

Use of the modified zeroth moment photon transfer cross sections in transport codes takes care of annihilation radiation subsequent to pair production events.

The total cross section for a given group is obtained from the sum of the Klein-Nishina total scattering cross section (unmodified) for that group plus the group average cross sections for the photoelectric effect and pair production.

The energy absorption cross section $\bar{E}\sigma_a$ (MeV-barn) is defined by [K-3]:

$$\bar{E}\sigma_a(E) = (E-1.02)\sigma_{pp}(E) + E\sigma_{pe}(E) + \sum_{E'}(E-E')\sigma_{so}(E\rightarrow E'), \tag{3.2}$$

where $\sigma_{pe}(E)$ is the cross section for the photoelectric effect, and all other symbols are the same as in Eq. 3.1.

MUG (K-3] and GAMLEG 69, an updated version of GAMLEG [L-4], are suitable codes for preparing the gamma transport cross sections in this format.

It should be noted that the term (2L+1) in higher order Legendre expansions is included in the ORNL cross sections.

Table 3.2 lists the neutron group structure and Table 3.3 gives the gamma group structure for the cross section set.

3.5 Gamma Heating in the Reference Reactor

3.5.1 Introduction

The 40-group ORNL coupled neutron-gamma cross section set has essentially all the information needed to do neutron-

Table 3.2

Neutron Energy Group Structure of the ORNL Coupled Cross Section Set

Group g	E_{max} = 15.0 MeV Lower Energy Boundary Group g
1	12.2 Mev
2	10.0 MeV
3	8.18 MeV
4	6.36 MeV
5	4.96 MeV
6	4.06 MeV
7	3.01 MeV
8	2.46 MeV
9	2.35 MeV
10	1.83 MeV
11	1.11 MeV
12	0.55 MeV
13	0.111 MeV
14	3.35 KeV
15	0.583 KeV
16	0.101 KeV
17	29.0 eV
18	10.7 eV
19	3.06 eV
20	1.12 eV
21	0.414 eV
22	Thermal

Table 3.3

Gamma Energy Group Structure of the ORNL Coupled Cross Section Set

Group g	E_{max} = 10.0 MeV Lower Energy Boundary Group g, MeV
23	8.0
24	6.5
25	5.0
26	4.0
27	3.0
28	2.5
29	2.0
30	1.66
31	1.33
32	1.00
33	0.80
34	0.60
35	0.40
36	0.30
37	0.20
38	0.10
39	0.05
40	0.01

induced gamma heating calculations. The gamma production cross sections, entered as down-scattering events from, for example, neutron groups 1 and 2 to gamma groups 23 and 24, include the production cross sections for all gamma-producing neutron reactions, i.e.,

$$\sigma_{1\to23} = \sigma^{c}_{1\to23} + \sigma^{f}_{1\to23} + \sigma^{in}_{1\to23} + \sigma^{n,2n}_{1\to23} + \ldots\text{etc.} \quad (3.3)$$

$$\sigma_{1\to24} = \sigma^{c}_{1\to24} + \sigma^{f}_{1\to24} + \sigma^{in}_{1\to24} + \sigma^{n,2n}_{1\to24} + \ldots\text{etc.} \quad (3.4)$$

$$\sigma_{2\to23} = \sigma^{c}_{2\to23} + \sigma^{f}_{2\to23} + \sigma^{in}_{2\to23} + \sigma^{n,2n}_{2\to23} + \ldots\text{etc.} \quad (3.5)$$

$$\sigma_{2\to24} = \sigma^{c}_{2\to24} + \sigma^{f}_{2\to24} + \sigma^{in}_{2\to24} + \sigma^{n,2n}_{2\to24} + \ldots\text{etc.} \quad (3.6)$$

where

σ	denotes the microscopic cross section in barns,
c	denotes capture
f	denotes fission
in	denotes inelastic scattering, and
n,2n	denotes the (n,2n) reaction.

The corresponding neutron reaction cross sections can be written as:

$$\sigma_{a1} = \sigma_{c1} + \sigma_{f1} - \sigma^{n,2n}_{1} + \ldots \text{ etc.} \quad (3.7)$$

$$\sigma_{a2} = \sigma_{c2} + \sigma_{f2} - \sigma^{n,2n}_{2} + \ldots \text{ etc.} \quad (3.8)$$

and

$$\sigma_{1\to2} = \sigma^{e}_{1\to2} + \sigma^{in}_{1\to2} \quad (3.9)$$

where e denotes elastic scattering and other symbols are as in the preceding equations.

In the present work, the one-dimensional discrete ordinate Sn transport calculation was done using the code ANISN [E-1].

3.5.2 Reference Reactor

The reactor configuration employed in the gamma heating analysis is the same as that used in the k-calculations and burnup studies discussed in Chapter 3. As mentioned in Chapter 2, this reference configuration of a gas-cooled FMSR was provided by BNL for use in benchmark calculations. Figure 3.1 shows the R-Z model of the reactor, the numbers indicating the locations of the different subzones. The positions of the subzones are determined in accordance with the fuel management strategy for the reactor.

The one-dimensional model of the core used in transport calculations is shown in Fig. 3.2. There are 39 subzones in this model, 20 fuel subzones in the core region, 14 fuel subzones in the moderated region and 5 zones of moderator (beryllium). The radial dimensions of the subzones in this 1-D model are identical to those in the 2-D model.

The number densities of the materials in each subzone used in the transport calculation are exactly the same as in those selfsame radial fuel subzones in the first axial layer of the 2-D model, i.e. subzones 1 to 34 in Fig. 3.1. The number densities of the materials were provided by BNL [B-1]; the number density of the moderator was also given.

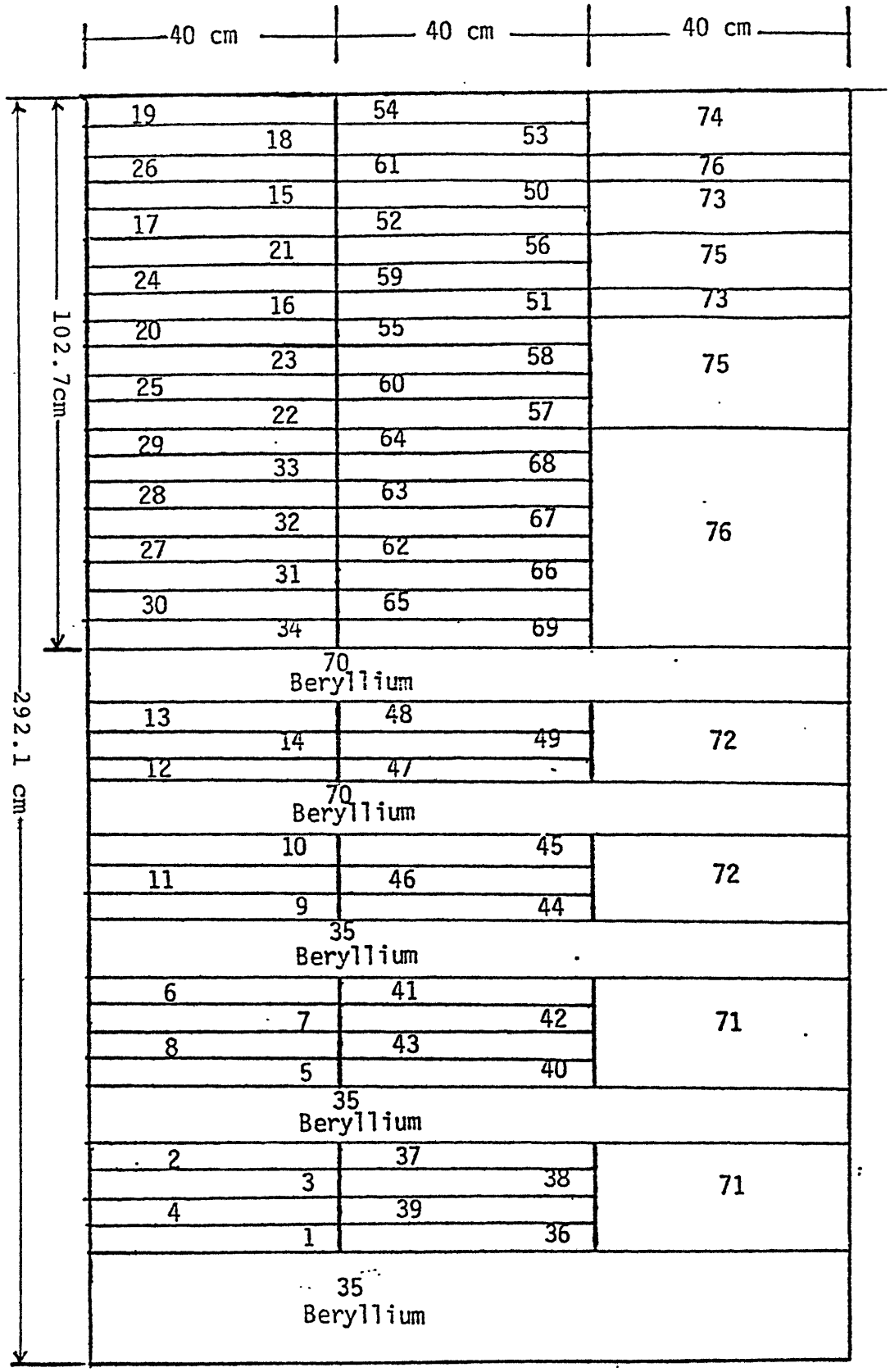

Fig. 3.1 R-Z Model of the Helium-Cooled FMSR

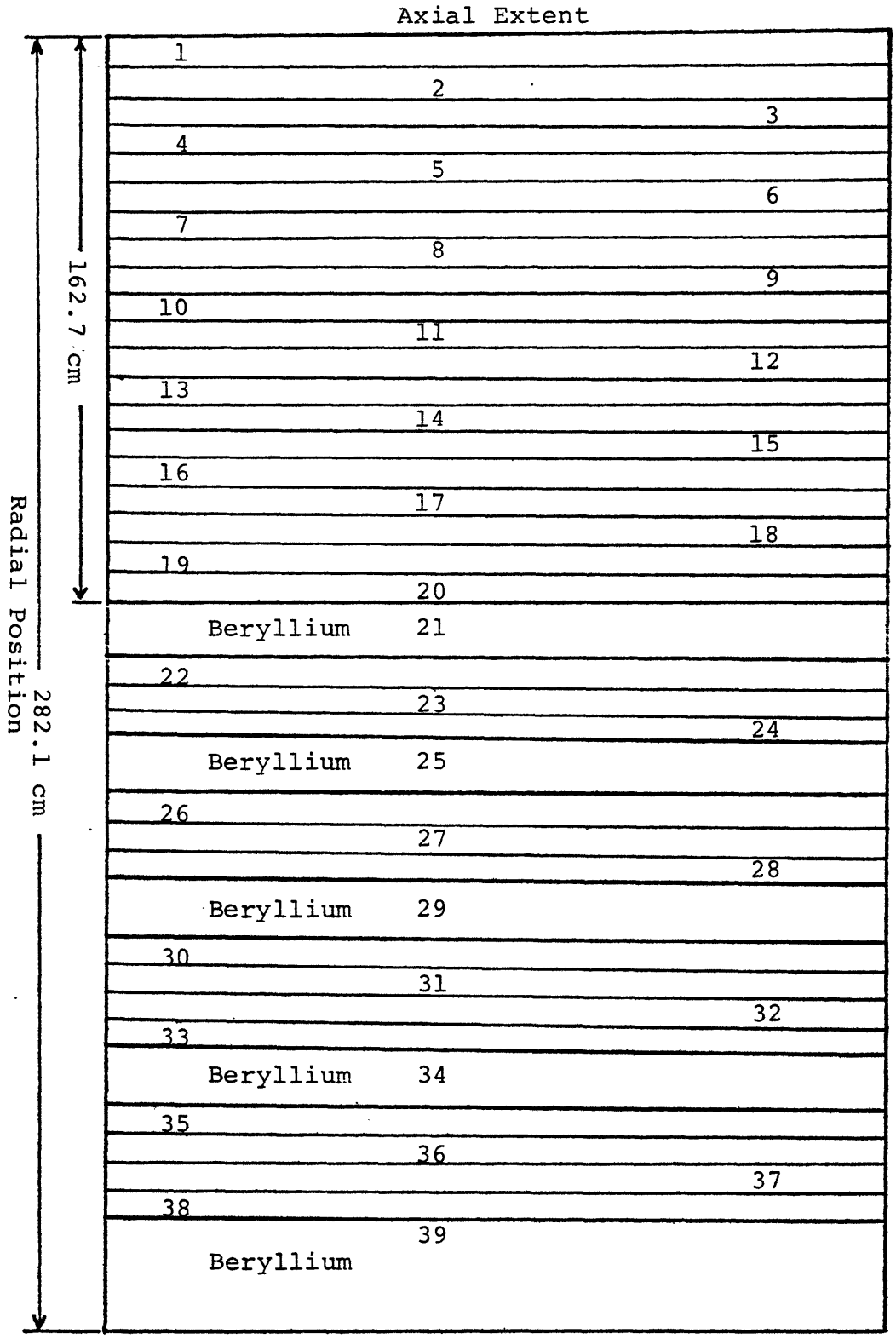

Fig. 3.2 One-Dimensional Model of the FMSR Used for Transport Calculations

3.5.3 Gamma Heating

The computation of gamma energy production and deposition requires the neutron and gamma fluxes and the coupled neutron-gamma cross section set. The fluxes were determined by one dimensional transport calculations using the code ANISN [E-1]. In this problem the S_8 approximation was employed and only P_1 scattering was considered. It was shown by Kalra [K-2] in his work on gamma heating in LMFBRs that the S_8P_1 approximation is adequate. K. N. Grimm and D. Meneghetti [G-1] calculated that in the gamma environment of EBR-II, the average absolute percentage error over a region for S_8P_1 calculations as compared to S_8P_3 calculations is 0.26% over the core and 0.20% over the blanket. Thus using the S_8P_1 approximation in the present work should be acceptable.

ANISN also provides the fission density (cm^{-3} sec^{-1}) at every mesh interval, from which we can evaluate the radial fission power density distribution. This is done by multiplying the fission density at each mesh interval by that part of the energy released from fission which will be deposited locally. In the present work a "standard" value of 176 MeV/fission local energy deposition has been employed for all ANISN associated calculations (2DB has its own built-in values). As shown in Table 3.4, the value of this parameter actually varies with isotopic composition. Thus to be more precise we would have to estimate values for all isotopes undergoing fission (also as a function of the energy of the neutron causing

Table 3.4

Energy Released per Fission [K-2]

Form	U235	Pu239
Light fragments (av)	99.8 ±1 (MeV)*	101.8 ± 1*
Heavy fragments (av)	68.4 ± 0.7*	73.2 ± 0.7*
Prompt neutrons	4.8	5.8
Prompt γ-rays	7.5	7
Fission-product decay:		
β rays	7.8*	~8
γ rays	6.8	~6.2
Total (not including neutrinos)	195	202

*Total local deposition: 176 MeV for U-235 and 183 MeV for Pu-239

fission) and appropriately weight the results to define a local mean value. This was not considered justifiable in view of the uncertainties in both MeV/fission data and other parameters (cross sections, neutron flux) involved in determining local energy sources and sinks. Moreover, if found desirable, the present results can readily be scaled to any other MeV/fission value deemed appropriate.

The gamma energy deposition rate (in units of MeV/cm^3-sec) in material k at a point r in the reactor is given by

$$E_\gamma^k(r) = \sum_j \phi_j(r) \cdot \overline{E\sigma}_{aj}^k \cdot N^k(r) \tag{3.10}$$

where

j	denotes the gamma group
$\phi_j(r)$	denotes the gamma group flux at point r
$\overline{E\sigma}_{aj}^k$	denotes the energy absorption cross section of material k for group j
$N^k(r)$	denotes the number density of material k at point r

Summing Eq. 3.10 over all materials will give us the volumetric energy deposition rates--the gamma heating rates (MeV/cm^3-sec) at a particular point r, i.e.,

$$H_\gamma(r) = \sum_k E_\gamma^k(r) \tag{3.11}$$

The gamma energy <u>production</u> rate (in units of MeV/cm^3-sec) in material k at a point r in the reactor is given by

$$E^k_{prod.}(r) = \sum_{i=1}^{N} \sum_{j=1}^{G} \phi_i(r) \cdot \sigma^k_{i\to j} \cdot E_j \cdot N^k(r) \qquad (3.12)$$

where

i denotes the neutron group

$\phi_i(r)$ denotes the neutron group flux at point r

E_j denotes the mean gamma energy in group j, and

$\sigma^k_{i\to j}$ are the gamma production cross sections for material k: gammas produced in gamma group j due to neutron events in neutron group i

Again, summing Eq. 3.12 over all materials will give us the gamma energy production rate at a point r.

$$H_{prod.}(\bar{r}) = \sum_k E^k_{prod.}(r) \qquad (3.13)$$

Figure 3.3 shows the radial power distribution determined using ANISN and the 40-group ORNL coupled neutron-gamma cross section set. The power distribution is normalized to the centerline-core midplane power density of 0.255 MW/L. The unnormalized radial power distribution from ANISN is obtained by summing the fission power density, the gamma heating rate, and the neutron heating rate. In these calculations the neutron heating was assumed to be local and its contribution to the total power density at the center of the core was assumed to be 3%.

In Fig. 3.3 we also have the radial power distribution computed using the code 2DB [L-3], which assumes all energy is

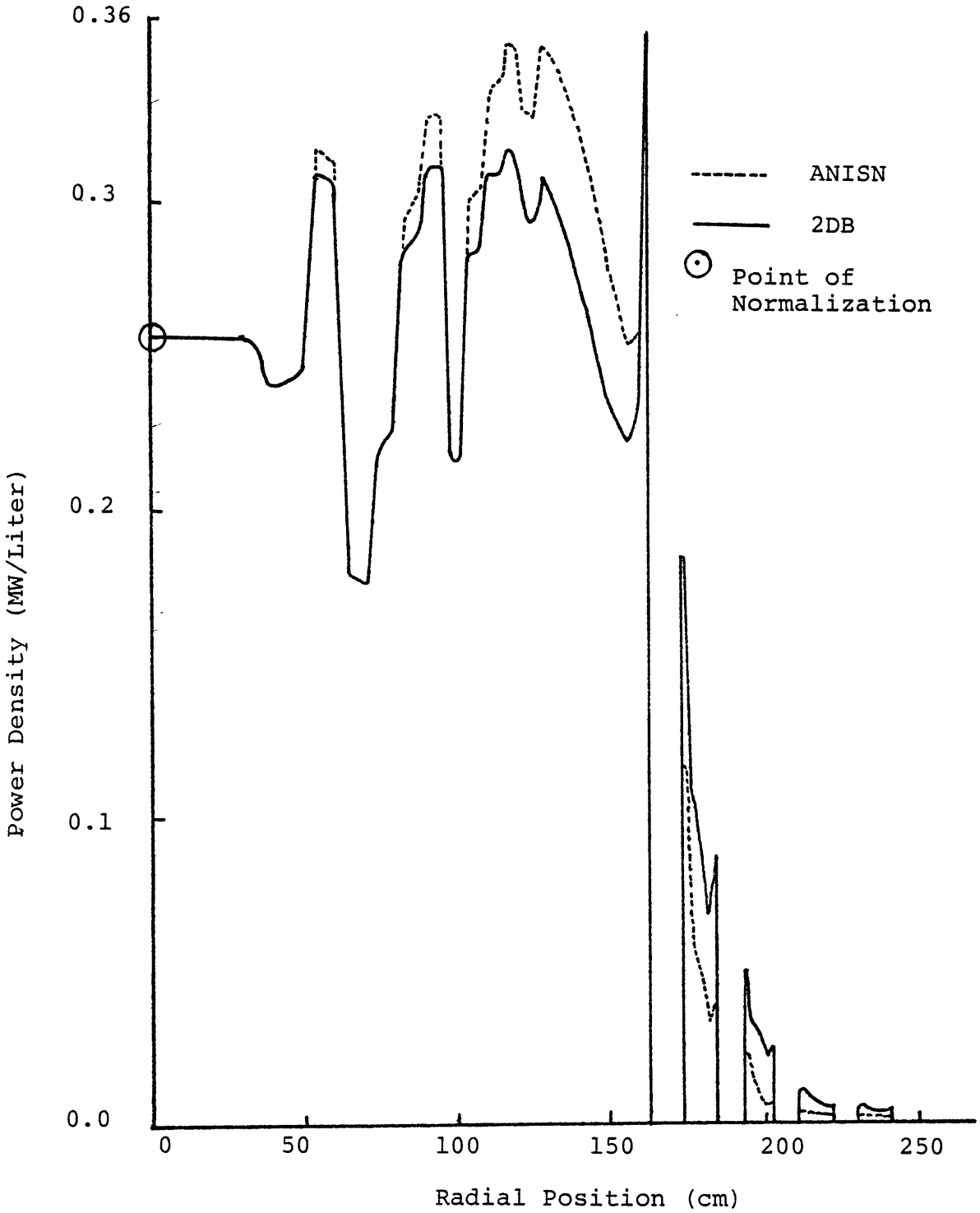

Fig. 3.3 Total Radial Power Distribution

deposited locally. This power distribution is the core mid-plane radial power density distribution. The shapes of both power distributions (i.e. from ANISN and 2DB) are the same. The mismatch in the power distributions can be attributed to the differences between ANISN and 2DB calculations, and the different cross section sets employed in the calculations. ANISN performs a one dimensional transport theory calculation (with the S_8P_1 approximation in the present work), whereas 2DB is a two-dimensional diffusion theory code. The 10-group cross section set used in the 2DB computations was generated using the 50 group LIB-IV compilation as the parent set. Resonance self-shielding and group collapsing (i.e. from 50 groups to 10 groups) were done using the code SPHINX. On the other hand the 40 group coupled neutron-gamma cross section set used in the ANISN calculations was not custom-shielded, and the "representative" cross section values for U-238 were prepared by Kalra [K-2], who self-shielded the cross sections using a typical LMFBR model. The magnitude of the disagreement at large radii is also accentuated by the choice of the core center as the point of normalization.

The gamma heating rate (normalized to the centerline-core midplane power density of 0.255 MW/liter) in the fast core, the moderated regions and the beryllium zones of the gas (helium) cooled FMSR is shown in Fig. 3.4. In the fast core the heating rate due to gammas is approximately constant, averaging about 16 KW/liter. The dip in gamma heating rate in the moderator

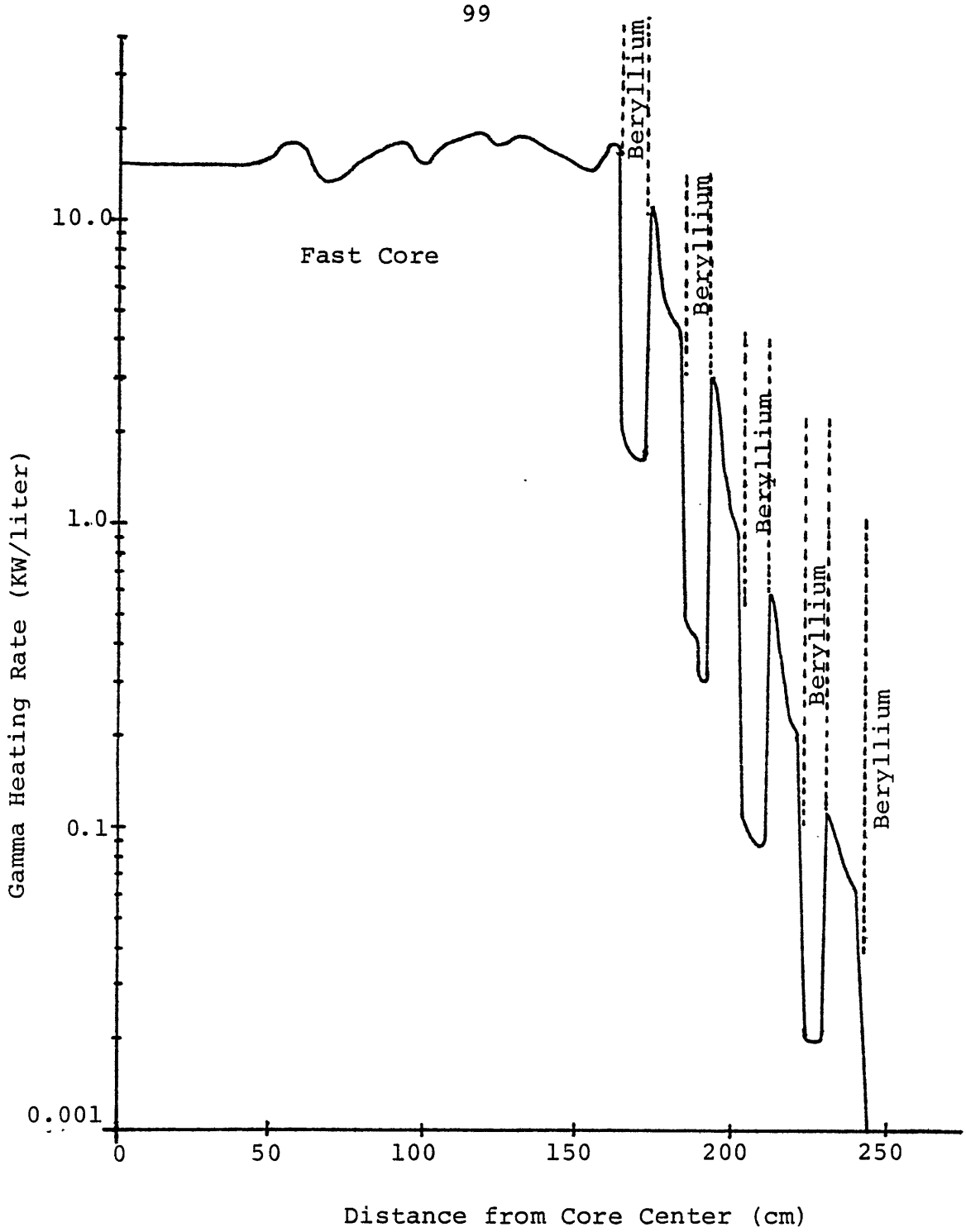

Fig. 3.4 Gamma Heating Rate in the Reference FMSR Calculated using the ORNL Coupled Cross Section Set

zones is due to the superior gamma production and absorption characteristics of the fuel materials in the moderated core regions. Gamma heating in the moderator zone adjacent to the fast core is quite significant (~2 KW/liter).

Figure 3.5 gives the ratio of gamma heating rate to local fission power in the reference FMSR. As shown, the gamma heating rate in the fast core is from 6 to 9 percent of the fission heating rate. In the moderated zones, however, the gamma heating rate varies from about 15% at the inner moderated zone to about 35% at the outer moderated zone. This might be expected because of the greatly reduced fission rate in these zones and from the large relative increase in fertile capture rate compared to the fission rate at increased distances from the fast core. It should be noted that the relative heating rates in Fig. 3.5 are for beginning-of-equilibrium cycle conditions. As fissile material builds in, the relative contribution of gamma heating to the total heating rate will be reduced.

Table 3.5 summarizes the gamma energy sources and sinks in the various regions of the reference reactor. It can be seen that the coolant (helium) plays no part in the production and deposition of gammas in the reactor. In the fast core the structure contributes less than 4% to the gamma energy source, but absorbs up to 9% of the gamma energy. In the moderator zones, however, the structure absorbs about 25 to 38% of the gamma energy and contributes about 77 to 86% to the

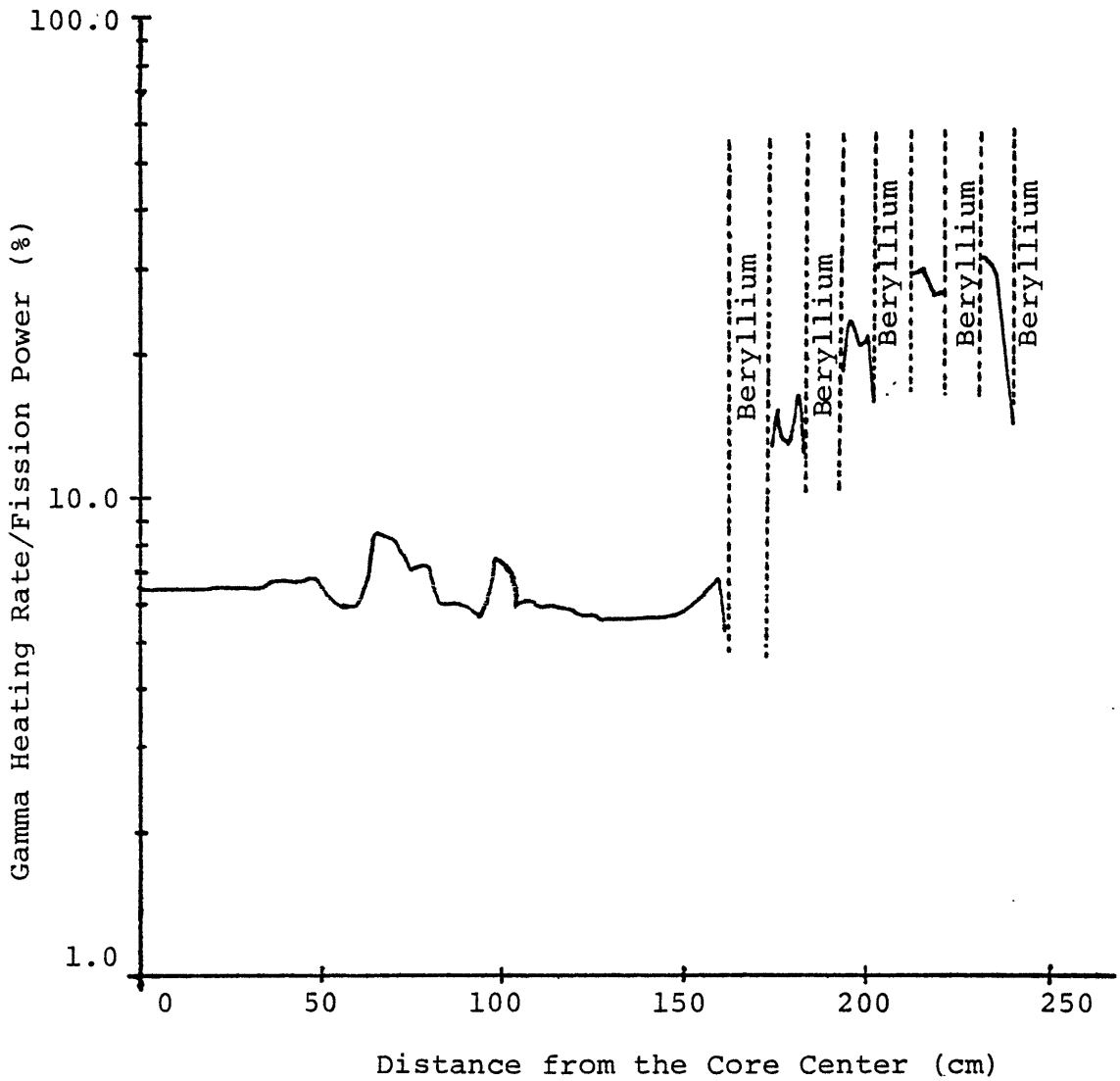

Fig. 3.5 Ratio of Gamma Heating Rate to Local Fission Power in the Reference FMSR

Table 3.5

Summary of Gamma Energy Sources and Sinks in Reference FMSR

Region		Percentage Contribution to Total Gamma Energy Source/Sink						
		Be	He	Fe,Cr, Ni	U235 U238	Pu239	Pu240	Total
Fast Core	Source	--	--	3.8	55.4	37.8	3.0	100.0
	Sink	--	--	9.4	83.7	6.2	0.7	100.0
Moderator Row 1	Source	22.2	--	77.8	--	--	--	100.0
	Sink	67.2	--	32.8	--	--	--	100.0
Blanket Row 1	Source	--	--	3.4	85.8	10.2	0.6	100.0
	Sink	--	--	9.9	89.0	1.1	0.05	100.0
Moderator Row 1	Source	22.9	--	77.1	--	--	--	100.0
	Sink	74.9	--	25.1	--	--	--	100.0
Blanket Row 2	Source	--	--	6.9	80.7	11.4	1.1	100.0
	Sink	--	--	18.3	80.6	1.0	0.1	100.0

Table 3.5

Summary of Gamma Energy Sources and Sinks in Reference FMSR (cont.)

Region		Percentage Contribution to Total Gamma Energy Source/Sink						
		Be	He	Fe,Cr, Ni	U235 U238	Pu239	Pu240	Total
Moderator Row 4	Source	17.1	--	82.9	--	--	--	100.0
	Sink	68.6	--	31.4	--	--	--	100.0
Blanket Row 3	Source	--	--	9.6	88.8	1.6	0.03	100.0
	Sink	--	--	20.9	78.9	0.2	--	100.0
Moderator Row 4	Source	16.2	00	88.8	--	--	--	100.0
	Sink	68.1	--	31.9	--	--	--	100.0
Blanket Row 4	Source	--	--	12.3	84.9	2.8	0.04	100.0
	Sink	--	--	20.9	79.0	0.1	--	100.0
Moderator Outermost Row	Source	13.5	--	86.5	--	--	--	100.0
	Sink	61.7	--	38.3	--	--	--	100.0

gamma energy source. Beryllium accounts for the rest of the gamma energy, both absorbed and produced in the moderator zones.

Table 3.6 gives the percentage contribution to the total gamma energy of the reactor by the different regions. As shown, more than 90% of the gamma energy comes from fission and capture reactions in the fast core of the reactor.

Figure 3.6 shows the ratio of gamma heating (gamma energy deposition) to the local gamma energy source at each spatial point in the reference FMSR, as calculated using the ORNL 40-group coupled cross section set. It can be seen that the heating due to gamma deposition in the fast core, and to a certain extent in the moderated fuel regions, is local, since the gamma-energy deposition-to-source ratio in these regions is equal to unity. This in a way justifies the assumption in the 2DB calculations, that total energy deposition (i.e., fission heating plus gamma heating) is localized.

It can also be seen that leakage of gamma energy from the fast core and moderated fuel regions, to the moderator zones (with the exception of the outermost moderator zone) can increase the gamma heating rate in these zones by a factor of 3.5 to 4. On the other hand, leakage from the outermost beryllium zone decreases the gamma heating rate in the zone by about 40 to 50%; the net leakage is from the beryllium zone to the exterior of the reactor core.

Table 3.6

Percentage Contributions to Total Gamma Energy

Region	Fast Core	Mod. Row 1	Row 1	Row 2	Row 2	Row 3	Row 3	Row 4	Row 4	Mod Outer-most Row	Total
Source	92.6	0.4	5.3	0.07	1.5	0.01	0.2	--	0.04	0.01	100.0
Sink	91.6	1.1	5.3	0.3	1.4	0.05	0.2	0.01	0.04	--	100.0

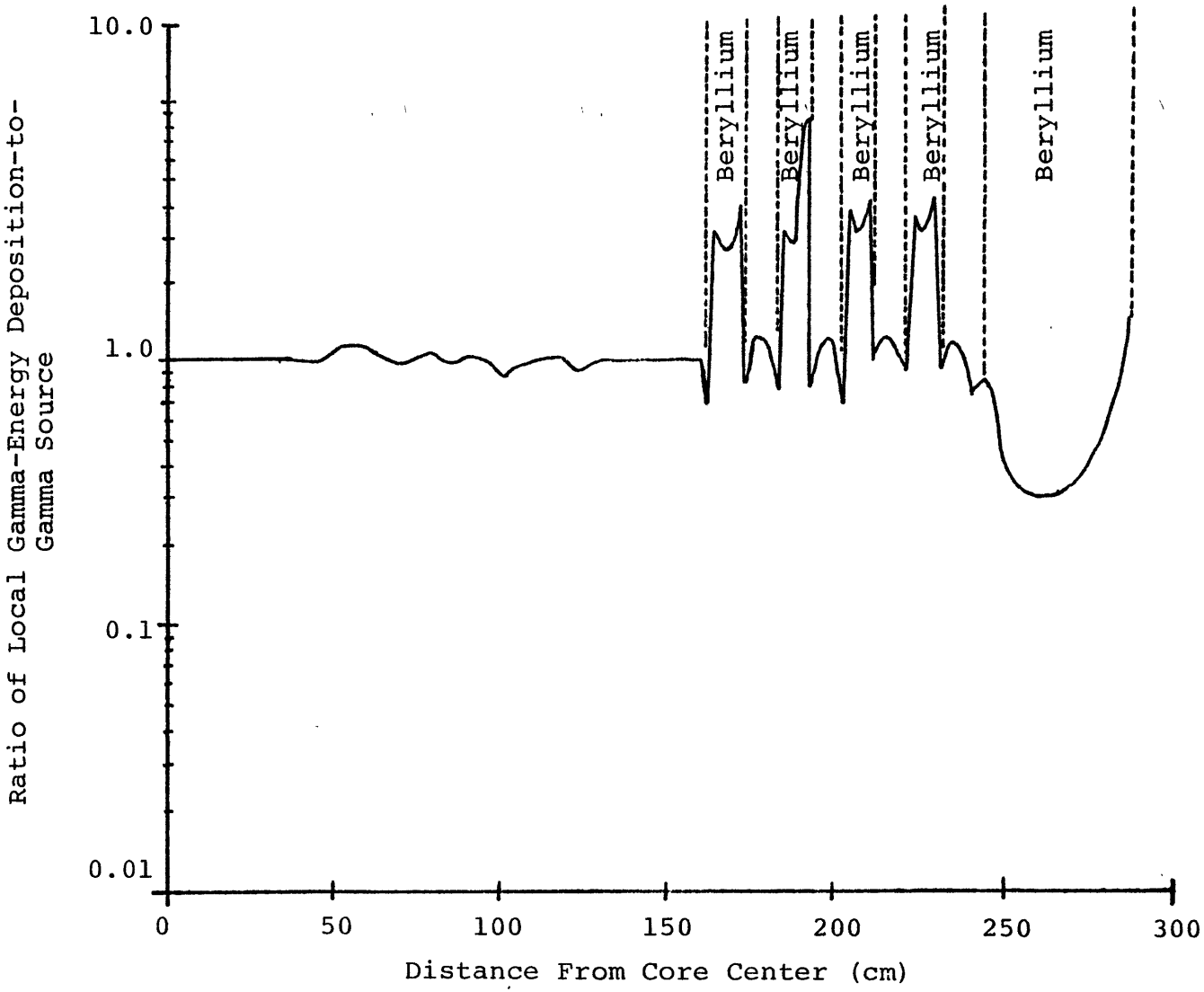

Fig. 3.6 Local Gamma-Energy Deposition-To-Source Ratio in the Reference FMSR

3.6 Neutron Heating

In the determination of the total radial power distribution in Section 3.5.3 from the one dimensional transport theory code ANISN and the 40-group ORNL coupled neutron-gamma cross section set, the normalization of the power distribution was done by first summing the fission power density, the gamma heating rate and the neutron heating rate and then equating this value to the centerline-core midplane power density of 0.255 MW/liter to obtain the normalization factor. The neutron heating was assumed to be local and its contribution to the total power density at the core center was assumed to be ~ 3%.

Neutron heating in the fast and moderated core regions of the FMSR is not important because of its small contribution. This is due to the fact that the materials present in these regions have high mass number, and the energy loss by the neutrons due to elastic scattering (which is shown below to be the most important contributor to the total neutron heating) with these materials is very small. In the moderator regions, however, neutron heating is expected to be significant because of the presence of the beryllium.

Neutron heating is considered to involve the after effects of elastic scattering, inelastic scattering, nuclear recoil following neutron capture, and nuclear recoil following capture gamma emission. The general procedure followed in neutron heating calculations was to use the neutron cross sections from the 26-group Bondarenko (ABBN) cross section set [B-5] to

generate energy absorption cross sections for the processes of interest. In addition, calculations utilizing conservation of momentum were necessary to define energy deposition resulting from nuclear recoil following neutron capture, inelastic scatter, and capture gamma emission. Table 3.7 gives the group structure of the ABBN cross section set.

The first and most important contribution to the total neutron heating rate in the reactor core is elastic scattering. The contribution of elastic scattering events to the total heating rate is given by [W-1]

$$E^n_{es}(r) = \sum_j \phi_j(r) \left[\sum_k N_k(r) (\sigma^e_{kj} \Delta\bar{E}_{kj}) \right] \qquad (3.14)$$

where

$E^n_{es}(r)$	denotes the volumetric heating rate from elastic scattering events at point r
$\phi_j(r)$	denotes the neutron flux in group j at point r
$N_k(r)$	denotes the number density of material k at point r
σ^e_{kj}	denotes the elastic scatter cross section for material k in the energy group j
ΔE_{kj}	denotes the average energy lost in an elastic collision between a neutron in the energy group j and the material k.

The average energy lost per elastic collision is [L-3, p. 175]:

$$\Delta\bar{E}_{kj} = E_j(1-e^{-\xi}). \tag{3.15}$$

where

$$\bar{E}_j = (E_j - E_{j+1})/\ln\,(E_j/E_{j+1})$$

$$\xi = 1 + [\alpha/(1-\alpha)]\ln\,\alpha$$

$$\alpha = [(A-1)/(A+1)]^2$$

A is the mass number of the material k

E_j is the upper energy bound for group j

E_{j+1} is the lower energy bound for group j .

In the equations above, $\bar{E}_j$ is the average energy in group j for a 1/E intragroup spectrum. In the ABBN cross section set cross sections for all but the top three groups have been generated using a 1/E weighting spectrum. The cross sections in the three highest energy groups, where elastic scattering contributes a very small amount to neutron slowing down, were averaged over a fission neutron spectrum. For the purpose of this analysis the $\bar{E}_j$ defined above has been used for all energy groups. This introduces a very small error in the overall totals of the energy loss per elastic collision. The quantity in brackets, [ ], in Eq. 3.14 is an elastic scatter energy deposition cross section which can be evaluated for each neutron energy group in any region of the reactor.

Consider next inelastic scattering. The heating rate resulting from inelastic scattering has two components: energy

associated with the nuclear recoil when the compound nucleus is formed, and the nuclear recoil energy following breakup of the compound nucleus (i.e., neutron emission), conservation of momentum in these two processes gives the following recoil energies:

$$E_{RI} = [\frac{1}{A+1}]\ \bar{E}_{inc} \tag{3.16}$$

$$E_{RF} = [\frac{1}{A}]\ \bar{E}_{n} \tag{3.17}$$

where

E_{RI} denotes the nuclear recoil energy on formation of the compound nucleus

E_{RF} denotes the nuclear recoil energy on disintegration of the compound nucleus

A denotes the mass number of the initial nucleus

$\bar{E}_{inc}$ denotes the incident neutron energy

$\bar{E}_{n}$ denotes the neutron energy on departure from the nucleus.

The microscopic cross sections associated with these processes were available in the Bondarenko cross section set in the form of an inelastic downscatter matrix. This form allowed separation of the two components of neutron heating due to inelastic scattering. An equation similar to Eq. 3.14 can be written to describe neutron heating in the inelastic scattering process:

$$E_{in}^{n}(r) = \sum_{j} \phi_j(r) \left[\sum_{k} N_k(r) \; (\sigma_{kj}^{in} \; E_{RI}) \right]$$

$$+ \sum_{j} \phi_j(r) \left[\sum_{k} N_k(r) \; \{ (\sum_{n} \sigma_{k(j\to n)}^{in}) \; E_{RF} \} \right]$$

(3.18)

where

$E_{in}^{n}(r)$ denotes the volumetric heating rate from inelastic scattering events at point r.

σ_{kj}^{in} denotes the total inelastic scattering cross section of isotope k in group j

$\sigma_{k(n\to j)}^{in}$ denotes the inelastic scattering cross section for material k for events in which the initial neutron is in group j and the final neutron is in group n.

Again, the quantities in brackets, [ ], can be thought of as inelastic energy absorption cross sections according to neutron energy group for any particular region in the reactor.

In a neutron capture event, energy is deposited locally by the recoil of the product nucleus following the capture event. The recoil energy following a capture event can be written in the same form as that following the compound nucleus formation in inelastic scattering, as in Eq. 3.16. The capture recoil heating rate can therefore be written:

$$E_c^n(r) = \sum_j \phi_j(r) \left[\sum_k N_k(r) \ (\sigma_{kj}^c \ E_{RI}) \right]$$

where

$E_c^n(r)$ denotes the heating rate resulting from nuclear recoil following neutron capture

σ_{kj}^c denotes the microscopic capture cross section for material k in energy group j.

The quantity in brackets is the energy deposition cross section for nuclear recoil following neutron capture. This quantity can be computed for each neutron energy group in any region within the reactor.

In the present neutron heating calculations, the last and least important of the neutron energy deposition mechanisms, i.e., the nuclear recoil following decay gamma emission of an isotope formed by neutron capture, was neglected. This is because the contribution to the total neutron heating rate by this process is insignificant compared to the other processes just enumerated.

The total neutron heating cross sections (designated earlier in brackets) as well as their component parts were generated from the unshielded ABBN cross section set. Use of unshielded cross sections will result in a slight overprediction of the neutron heating rate in the fuel regions but it will have a negligible effect on the results in the moderator region. The fluxes used in conjunction with the local neutron

heating cross sections were calculated using the code 1DX [H-1]. The one dimensional model of the core used in the 1DX calculations is similar to that used in the self-shielding and group collapsing calculations in SPHINX, as discussed in Section 2.3 (see Fig. 2.4). The zonal compositions used here are again similar to those used in the SPHINX calculations, as documented in Appendix A. The cross section set used in the generation of the fluxes was the same ABBN set used to generate the neutron heating cross sections. The total core power used in the normalization was 3000 MWt or 18.75 MW/cm. axial, since the active core height is 160 cm.

Figure 3.7 shows the neutron heating rate in the gas (helium) cooled FMSR. Neutron heating in the fast core is not significant. It varies from ~0.27 kw/liter to about 0.50 kw/liter. As expected, the peak neutron heating occurs in the first moderator zone (i.e., the zone lying next to the fast core). It is about 5.6 kw/liter. This much neutron heating in the beryllium moderator zone might have some influence on the thermal/hydraulic/mechanical design of the moderator subassembly.

The average neutron heating rate in the first beryllium zone is approximately 4.0 kw/liter. This is much higher than the gamma heating rate (as calculated in Section 3.6) in the same region, which is ~2.0 kw/liter. This is also true in the other beryllium zones, which indicates that the most important heating process taking place in the moderator zones of the

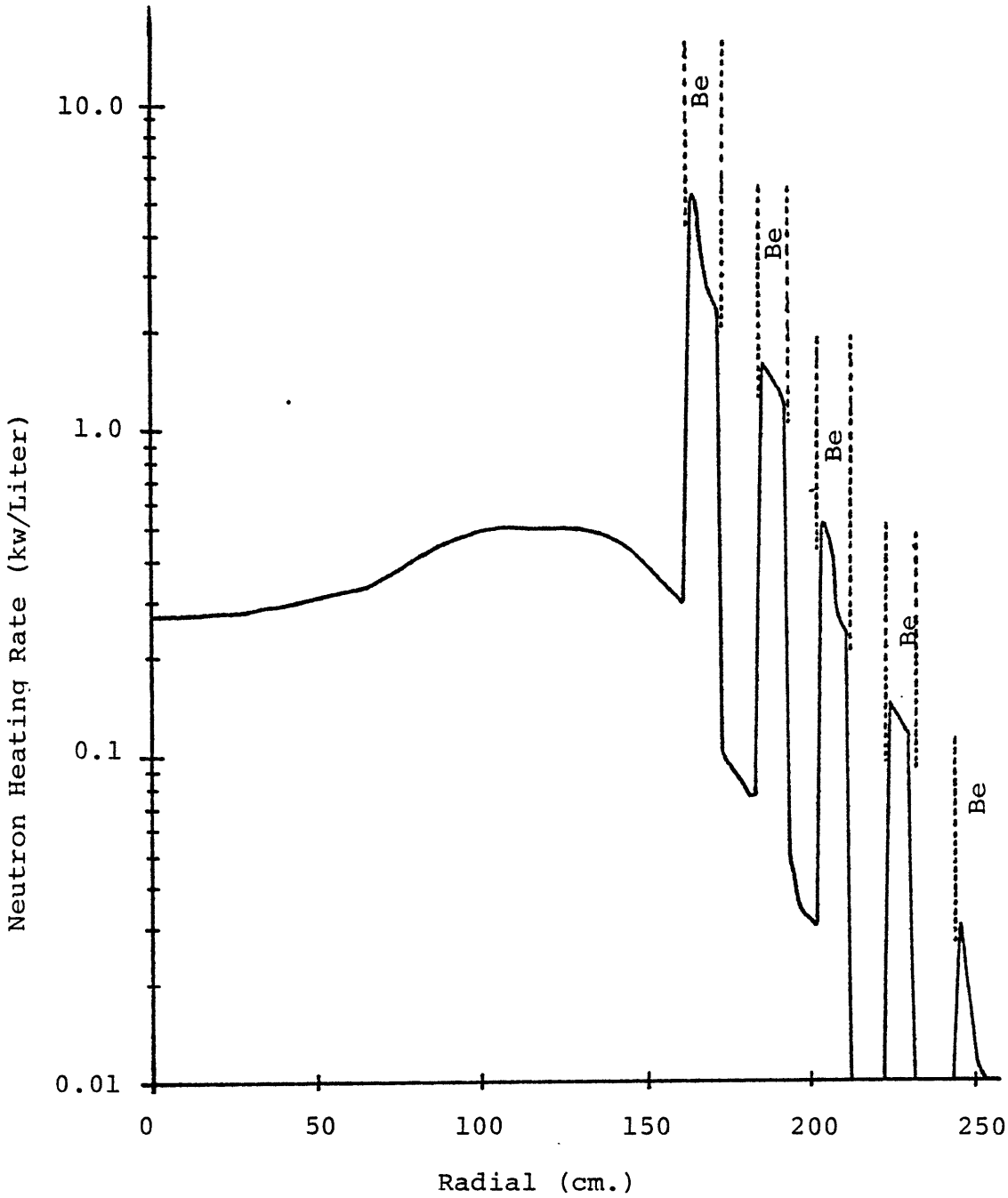

Fig. 3.7 Neutron Heating Rate in the Reference FMSR

FMSR is the neutron heating.

To allow an evaluation of the relative contribution of the different components entering into the neutron heating calculation, Table 3.7 has been included. This table clearly shows that the largest contributing factor to the neutron heating rate is elastic scattering.

3.7 Conclusions

Gamma and neutron heating are not important in the fast core because of their small contributions to the total power density in this region. Gamma heating averages about 16 kw/liter in the fast core and the neutron heating rate varies from ~ 0.35 kw/liter to about 0.65 kw/liter in the same region. The main contribution to the average total power density of 260 kw/liter in the fast core came from the local fission heating (i.e., heating due to energy deposition by fission fragments and β particles). It was also shown that gamma heating in the same region is local, and this result justifies the use of 2DB calculations, which assume that the total energy deposition (i.e., fission plus gamma heating) is localized. Near the boundaries between fuel and moderator zones, however, transport effects must be considered.

In the moderated fuel zones, the contributions of gamma heating to the total power density were rather significant, varying from about 15% at the inner moderated fuel zone to approximately 35% at the outer moderated fuel zone. This is

Table 3.7

Neutron Heating Rate Contributions

Mean Radial Distance from the Center of the Core (cm)	Heating Rate Contributions (KW/Liter)			
	Elastic Scatter	Inelastic Scatter	Capture Recoil	Total
Fast Core				
4.5	0.218	0.058	0.001	0.277
31.8	0.228	0.061	0.001	0.290
60.1	0.255	0.065	0.001	0.321
90.0	0.343	0.099	0.002	0.444
122.0	0.380	0.117	0.002	0.499
151.1	0.290	0.099	0.002	0.391
1st Beryllium Zone				
163.7	5.133	0.453	0.030	5.616
109.6	2.387	0.195	0.014	2.596
1st Moderated Fuel Zone				
175.4	0.069	0.025	0.000	0.094
181.0	0.058	0.019	0.000	0.077

due to the greatly reduced fission rate in these zones. In the beryllium zones, neutron heating is the dominant process. For example, in the first beryllium zone the neutron heating rate averages about 4.0 kw/liter while the contribution from gamma heating is ~ 2.0 kw/liter. Although comparison of these two heating rates may not be precise on a quantitative basis because of differences in the calculational procedures and data employed, the values quoted should give an acceptable indication of their relative contributions. It should be pointed out that the neturon heating rates determined for the moderator zones, especially the first moderator zone, might be sufficiently high to have some influence on moderator sub-assembly design.

The above heating analysis will provide a good first order approximation to the gamma and neutron heating rates in the reference FMSR. More accurate gamma heating analyses can be performed by using more recent cross section sets, such as the MATXS 2 [M-1] set currently under preparation at the Los Alamos Scientific Laboratory. The neutron heating analysis can be improved by using the calculational methods for nuclear heating developed by M. A. Abdou and C. W. Maynard [A-6], and recently developed cross section sets.

CHAPTER IV

SUMMARY, CONCLUSIONS AND RECOMMENDATIONS

4.1 Introduction

The purpose of the research summarized here has been to carry out an independent evaluation of the neutronic characteristics of a gas-cooled Fast-Mixed Spectrum Reactor (FMSR) core design. This is a new concept in fast reactors for the production of electric power. Unlike conventional fast breeders, the FMSR would operate on a once-through-and-store fuel cycle. No reprocessing is required. In addition, the FMSR is designed to be self-sustaining on an equilibrium feed of natural uranium alone. No fissile makeup is required and the plutonium burned in the reactor is bred in situ. During the fuel's residence time in the reactor ($\sim$ 17 years), its total burnup would be high ($\sim$ 13-15 atom percent) [B-1]. These characteristics of the FMSR make it highly proliferation resistant, and its cumulative fuel cycle costs should, in the long term, be less than those of a more conventional fast breeder.

The reference configuration of the FMSR used in benchmark calculations, together with its geometric specifications and the zonewise compositions of the reactor model were provided by BNL [B-1].

It must be pointed out that the system under consideration is not an optimized final design, but an early, convenient representative of a family of designs suitable for proof-of principle studies. The work carried out at MIT, as summarized in the remainder of this chapter, assists in the confirmation of the neutronic feasibility of the steady state FMSR fuel cycle.

Finally, non-fission heating, which includes gamma and neutron heating, was amalyzed for the FMSR core design. This will allow the temperature field within the reactor, especially in the moderator regions, to be determined.

4.2 Analysis of a Simulated Steady-State Burnup Cycle

The evaluation of the given gas-cooled FMSR core design consists essentially of static BOEC k calculations and fuel burnup analyses. The two-dimensional multigroup, fast-reactor-oriented, diffusion theory burnup code 2DB [L-3] was the main tool used in the present work. This program calculates flux and power density distributions and material concentrations as a function of burnup. The R-Z model of the FMSR core design used in the 2DB diffusion theory burnup code is shown in Fig. 4.1. Zones 1 and 2 are the moderated fuel regions and zones 3 through 6 represent the fast core regions. The axial blankets are represented by zones 7 through 12. All zones in each horizontal cut through the core are further subdivided into a total of 34 subzones in order to approximate the required fuel shuffling (see Fig. 2.3). Fig. 4.2 summarizes

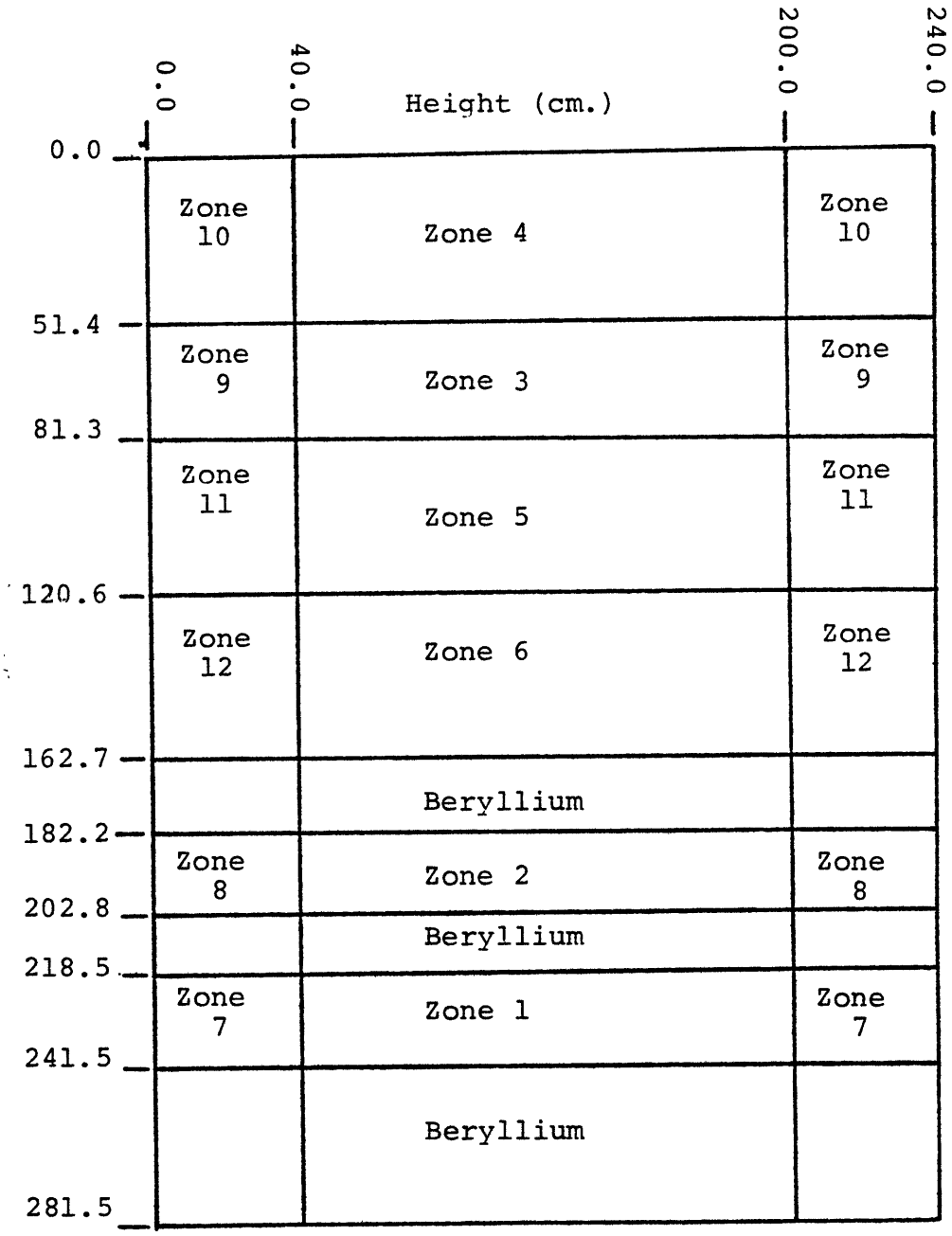

Fig. 4.1 R-Z Model of the Helium-Cooled FMSR

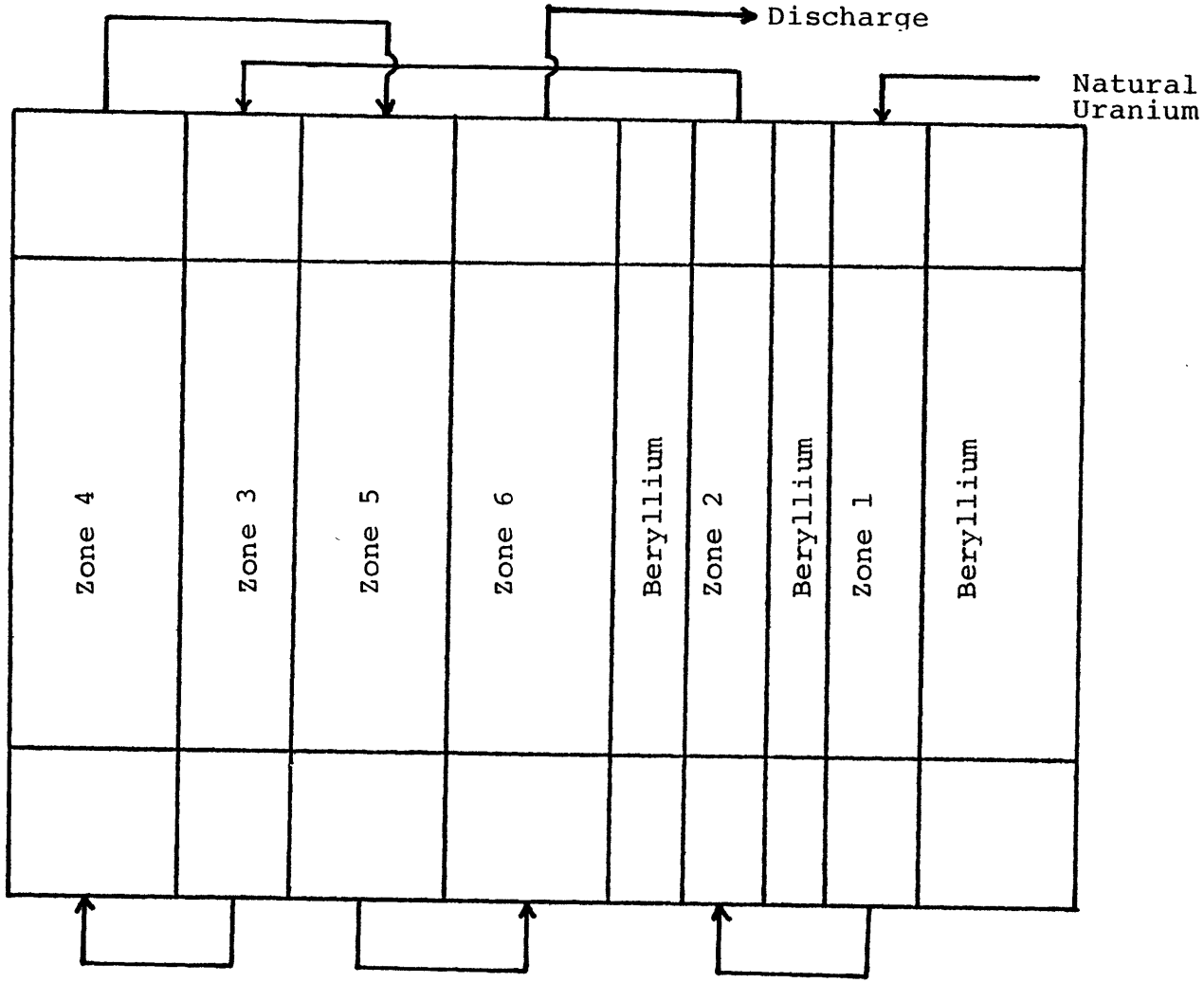

Fig. 4.2 Fuel Shuffling Strategy

the fuel shuffling strategy adopted in the present design.

A 10-group cross section set was employed in all calculations performed in the analyses. All the cross sections, with the exception of the fission product cross sections, were generated using the 50 group LIB IV compilation as the parent cross section set [K-1]. In the present work a new 50 group cross section set for the fission products was generated based on the results reported by the Japanese Nuclear Data Committee (JNDC) [J-1]. In the same report it was shown that the results of reactivity worth calculations using the JNDC set were better than those of the ENDF/B-4 and Cook sets, when compared with the experimental values measured in various cores of the STEK facility in RCN, Petten, the Netherlands [B-6, G-2]. The 50-group cross section set (including the fission products) was collapsed to 10 using the code SPHINX [D-1]. Corrections in the cross sections were made for resonance self-shielding and temperature dependence using the same program.

In the first part of the k and burnup calculations, three 10-group cross section sets were used for the fuel zones, and an additional set was employed for the moderator zones. Two sets of calculations were performed, using the 2DB program, the first, using "Japanese" fission products and the second, using the LIB-IV nonsaturating plutonium fission products times the factor 2.7 (the cross section set used by BNL). The Japanese fission products were converted at MIT

from their original format [J-1] into the LIB-IV format used in the present work, and collapsed to 10 groups.

Table 4.1 shows the results of the MIT and BNL calculations. The breeding ratios evaluated in this table exclude U-235 absorption. As can be seen the MIT (BNLFP) and BNL k_{eff} calculations are in good agreement. The Japanese fission products are worth ∿5% Δk and the BNL fission products are worth around 3.5% Δk.

To identify the nature of the differences between the calculations done at MIT and those done at BNL, a detailed zonewise comparison between the two sets of calculations was performed. Several spectral indices (including $\frac{\sigma_f^{28}}{\sigma_f^{49}}$, $\frac{\sigma_c^{28}}{\sigma_f^{49}}$, $\frac{\sigma_c^{49}}{\sigma_f^{49}}$ and $\frac{\sigma_a^{FP}}{\sigma_f^{49}}$) and the EOEC nuclide concentrations for U^{238}, and the four major plutoniums, belonging to a few selected subzones, were compared between the MIT and BNL calculations. In the vicinity of the moderator (i.e. in subzones 3, 7, 11 and 14; refer to Fig. 2.5), MIT calculations show evidence of a softer spectrum than indicated by the BNL results. This behavior could in part be due to the lower number of fast groups ($\geq$1 Mev) used in the MIT 10 group calculations compared to the BNL 50 group calculations.

With regard to the nuclide concentration comparisons, basically there is good agreement. The most important disagreement is the discrepancy in the moderated fuel zones.

Table 4.1

k_{eff} and Breeding Ratio Comparison Between M.I.T. and BNL Calculations

	k_{eff}		BR	
	BOEC	EOEC	BOEC	EOEC
M.I.T. (Japanese FP)	0.969	0.987	1.68	1.61
M.I.T. (BNL FP)	0.986	1.004	1.67	1.60
BNL (50 group)	0.982	1.000	1.67	1.61
M.I.T. (no FP)	1.020	1.039	1.64	1.58

As one moves up the plutonium chain, there is a progressively larger discrepancy. This is partly due to the systematic effect of differences in fission product cross section sets and partly due to the restricted number of zonewise 10-group sets used in the MIT calculations. By going from three to six 10-group cross section sets for the fuel zones in the burnup and k-calculations, we obtained results which are in better agreement with BNL, especially with regard to the nuclide concentrations of the plutonium isotopes in Zone 1: as shown in Table 4.2. It can also be seen that the number densities of Pu^{40}, Pu^{41} and Pu^{42} in Zone 1 from the six-set calculations are greater than those from the BNL calculations. The reason for this observation is that the capture cross sections of the plutonium nuclides from the six-set calculations are greater than those from the BNL calculations. Table 4.3 shows the k_{eff} and breeding ratios of the calculations employing six 10-group cross section sets, compared to the BNL calculations. It is not clear that increasing the degree of sophistication in the MIT calculations will lead to exact duplication of the BNL results. However, use of 6 zonewise cross section sets in the analysis produced much better agreement in the plutonium composition at EOEC in the moderated fuel zones between the 2 sets of calculations, and for that reason use of the larger number of zone-wise sets would be recommended for future work.

Table 4.2

Comparison of the Number Density of the Plutonium Isotopes at the EOEC

Zone	Subzone	M.I.T. (Japanese FP 3 sets)	M.I.T. (Japanese FP 6 sets)	BNL (50 group)	BNL/M.I.T. (3 sets)	BNL/M.I.T. (6 sets)
Pu^{49}						
1	3	1.423E-5	1.471E-5	1.511 E-5	1.062	1.027
1	7	6.098E-5	6.142E-5	6.329E-5	1.038	1.030
Pu^{40}						
1	3	4.952E-8	7.546E-8	6.841E-8	1.381	0.907
1	7	1.196E-6	1.262E-6	1.285E-6	1.074	1.018
Pu^{41}						
1	3	5.999E-10	3.434E-9	2.172E-9	3.621	0.633
1	7	1.575E-7	3.285E-7	2.691E-7	1.709	0.819
Pu^{42}						
1	3	6.903E-13	5.377E-12	3.204E-12	4.641	0.596
1	7	1.033E-9	2.124E-9	1.858E-9	1.799	0.875

Table 4.3

k_{eff} and Breeding Ratio Comparison Between M.I.T. (6 Cross Section Sets) and BNL Calculations

	k_{eff}		BR	
	BOEC	EOEC	BOEC	EOEC
BNL (50 Group)	0.982	1.000	1.67	1.61
M.I.T. (6 x-section sets) Japanese FP	0.971	0.987	1.66	1.59
M.I.T. (6 x-section sets BNL FP)	0.996	0.994	1.65	1.58

4.3 Gamma and Neutron Heating Analyses

Analysis of non-fission heating was also an important part of the subject investigation of the FMSR core design. The establishment of the thermal energy source distribution, especially in the moderator zones and the blanket regions, where there is either no fission heating, or very low fission heating, will enable one to determine the temperature field within these systems.

4.3.1 Gamma Heating

Gamma sources in a reactor are:

1. Nuclear fission gammas
   a. Prompt fission gammas
   b. Short-lived fission product decay gammas
   c. Long-lived fission product decay gammas
2. Capture gammas
   a. Prompt capture gammas
   b. Post-capture decay gammas
3. Inelastic scattering gammas
4. Gammas from (n, 2n) and (n, charged particles) reactions
5. Annihilation gammas
6. Bremsstrahlung gammas

The mechanisms by which gammas deposit their energy in the reactor medium are:

1. The photoelectric effect
2. Compton scattering
3. Pair production

The computation of gamma energy production and deposition was done by employing the neutron and gamma fluxes generated from one-dimensional transport calculations using the code ANISN [E-1], and a 40-group coupled neutron-gamma cross section library compiled at ORNL [O-1]. The one-dimensional model of the core used in the transport calculations is shown in Fig. 4.3. The S_8P_1 approximation, which has been shown to be acceptable [G-1, K-2], for similar applications, was used in the transport calculations.

The gamma heating rate was normalized to the centerline-core midplane power density of 0.255 MW/liter. In the fast core the heating rate due to gammas is approximately constant, averaging about 16 KW/liter. This is about 6-9% of the fission power density in the same region. In the moderated fuel zones, however, the gamma heating rate varies over the range 15 to 35% of the fission heating rate. This is presumably due to the reduced fission rate in these zones. Gamma heating in the moderator zone lying next to the fast core is rather significant ($\sim$2 kw/liter). This, together with neutron heating will have some influence on the design of the moderator subassembly. It was also found that the heating due to gamma deposition in the fast core, and to a certain extent in the moderated fuel regions, is local. This serves to justify the assumption in the 2DB calculations, that the total energy deposition is localized. Finally, it was also found that leakage of gamma energy from the fast core to the moderator zones can increase

the gamma heating rate in these zones by a factor of 3.5 to 4 compared to purely local deposition. On the other hand, leakage from the outermost beryllium zone decreases the gamma heating rate in the zone by about 40 to 50%.

4.3.2 Neutron Heating

Neutron heating is considered to involve the after effects of elastic scattering, inelastic scattering, nuclear recoil following neutron capture, and nuclear recoil following capture gamma emission. Neutron heating in the fast and moderated core of the FMSR is not important because of its small contribution, and because local deposition can be assumed. In the beryllium zones, however, neutron heating will be significant because of the presence of the moderator, bearing in mind that elastic scattering is the most important mechanism by which neutrons lose their energy.

In the neutron heating calculations, the energy absorption cross sections for the processes of interest were first generated using a 26-group Bondarenko-type cross section set [B-5]. Then the energy deposition resulting from nuclear recoil following neutron capture, inelastic scattering, and capture gamma emission events was calculated using the conservation of momentum principle. The fluxes used in the total neutron heating computations were calculated utilizing the one-dimensional diffusion theory code 1DX[H-1]. The model of the core employed in the 1DX calculations was

similar to that use in the group collapsing calculations in SPHINX (see Fig. 2.4). The normalization factor used in the 1DX calculations was 18.75 MW per axial cm, based on the total core power of 3000 MWt and an active core height of 160 cm.

Neutron heating in the fast core is not significant, varying from ∿0.27 kw/liter to about 0.57 kw/liter. The peak neutron heating rate occurs in the moderator zone adjacent to the fast core--about 5.6 kw/liter. The average neutron heating rate in the same region is approximately 4.0 kw/liter. As was mentioned before, these values of the neutron heating rate, when augmented by gamma heating, might have some influence on the design of the moderator subassembly, particularly if thick structural subdivisions are used.

4.4 Conclusions and Recommendations

The MIT and BNL results are in sufficiently good agreement to conclude that the FMSR concept has been independently validated. Significant differences occur only in regions of low neutronic importance, and even there plausible reasons for the differences can be advanced. The need to reach a definitive consensus on fission product cross section values is clear--this step alone would go a long way toward reduction of the modest differences which do exist between the MIT and BNL results. The MIT results can clearly be improved by use of a larger number of zone-specific cross section subsets. Both the MIT and BNL results could be

improved by refinements in the treatment of resonance self-shielding near core/moderator interfaces. However concern over these fine points can await further iterations on the basic conceptual configuration and fuel management strategy for the FMSR. In this regard, both MIT and BNL tend to predict that the benchmark design is slightly subcritical at beginning-of-cycle. The margin to k = 1.0 is close enough, however, that remediation is foreseeable.

Non-fission heating in unfueled core components has been calculated, and while no obvious problems or surprises were uncovered, once the nature and extent of the moderator inserts are finalized, the energy deposition rate densities should be used to evaluate the thermal/hydraulic and mechanical suitability of actual engineering designs.

Specific recommendations for future work include:

a) Refinement of the present analyses after the conceptual design is updated. Because of the tight schedule imposed on the present work, the various subtasks in the neutronic and photonic calculations were carried out by using a variety of computational tools and cross section data. Thus there is a certain lack of internal consistency which should be exorcised in the longer run.

b) As already noted on several occasions--a consensus fission product cross section set

should be adopted--a goal toward which BNL has already made substantial progress [D-4].

(c) Although outside the charter of the present study, concurrent work on other projects at MIT suggests that the applicability of the following design modifications be evaluated for the FMSR: moderator control rods; use of zirconium hydride in place of beryllium as the moderator; and use of slightly-enriched uranium as the feed stock instead of natural uranium, if a reactivity boost proves essential (or if one could thereby reduce the long in-core residence time of the fuel and the protracted approach to equilibrium). Partial use of thorium may also be of some use, since an epithermal U-233/Th-232 system can be made critical at bred fissile concentrations which are a factor of two lower than for the Pu/U-238 system.

APPENDIX A

Table A.1. Number Densitites of Materials in the Various Zones* at BOEC

Zone 1

Isotope	Number Density
He4	0.1069E-2
Cr	0.2100E-2
Fe	0.9620E-2
Ni	0.1240E-2
U235	0.9703E-4
U238	0.1399E-1
Pu239	0.1995E-4
Pu240	0.1888E-6
Pu241	0.4700E-7
Pu242	0.0

Zone 2

Isotope	Number Density
He4	0.1069E-2
Cr	0.2100E-2
Fe	0.9620E-2
Ni	0.1240E-2
U235	0.7949E-4
U238	0.1382E-1
Pu239	0.1679E-3
Pu240	0.7745E-5
Pu241	0.2195E-5
Pu242	0.6245E-7

Zone 3

Isotope	Number Density
He4	0.1069E-2
Cr	0.2100E-2
Fe	0.9620E-2
Ni	0.1240E-2
U235	0.5348E-4
U238	0.1337E-1
Pu239	0.4674E-3
Pu240	0.3462E-4
Pu241	0.7396E-5
Pu242	0.4993E-6

Zone 4

Isotope	Number Density
He4	0.1069E-2
Cr	0.2100E-2
Fe	0.9620E-2
Ni	0.1240E-2
U235	0.4221E-4
U238	0.1291E-1
Pu239	0.6524E-3
Pu240	0.4922E-4
Pu241	0.6922E-5
Pu242	0.7453E-6

Zone 5

Isotope	Number Density
He4	0.1069E-2
Cr	0.2100E-2
Fe	0.9620E-2
Ni	0.1240E-2
U235	0.3008E-4
U238	0.1240E-1
Pu239	0.8411E-3
Pu240	0.7902E-4
Pu241	0.7521E-5
Pu242	0.1123E-5

Zone 6

Isotope	Number Density
He4	0.1069E-2
Cr	0.2100E-2
Fe	0.9620E-2
Ni	0.1240E-2
U235	0.1637E-4
U238	0.1141E-1
Pu239	0.9987E-3
Pu240	0.1384E-3
Pu241	0.1167E-4
Pu242	0.1744E-5

Zone 7

Isotope	Number Density
He4	0.8000E-3
Be9	0.8628E-1
Cr	0.6750E-3
Fe	0.4730E-2
Ni	0.3300E-4

Zone 6

Isotope	Number Density
He4	0.8000E-3
Be9	0.8628E-1
Cr	0.6750E-3
Fe	0.4730E-2
Ni	0.3300E-4

Zone 9

Isotope	Number Density
He4	0.1069E-2
Be9	0.3778E-1
Cr	0.2100E-2
Fe	0.9620E-2
Ni	0.1240E-2

*The number densities of the heavy metals were calculated using the BOEC fuel inventory for the core (see Table 3-5 in the FMSR Interim Report by BNL Ref. [B-1]).
The units for all entries are nuclei per barn cm.

APPENDIX B

TABULATION OF DATA FOR THE POWER DISTRIBUTION IN THE REFERENCE FMSR

B.1 Tabulated Values of the Fission Power Density and the Gamma Heating Rate for the Gamma Heating Analysis (Section 3.5)

The total power distribution is normalized to the center-line core midplane power density of 255 KW/liter. The ANISN code [E-1] was run (employing a total fission source requirement of 1 fission neutron/sec. per cm. axial length of the core) giving for the unnormalized fission power density at the center of the core a value of 2.600 E-16 kw/liter. The calculated gamma heating rate at the same location, using the flux generated by the ANISN code, is 1.673 E-17 kw/liter. The sum of the above values for the fission power density and the gamma heating rate constitutes 97% of the total power density at the center of the core, that is, 247.35 kw/liter (since it was assumed that the remaining 3% of the total power deposition was due to local neutron heating). Hence, the normalization factor is 247.35/2.7693 E-16, that is: 8.932 E.17.

The data listed in Table B.1 are plotted in Figs. 3.4, 3.5 and 3.6 in Chapter Three.

Table B.1

Fission Power Density, Gamma Production Rate and Gamma Deposition Rate

Mesh Interval	Interval Mid-point Distance from the Core Center (cm.)	Fission Power Density (kw/l)	Gamma Deposition Rate (kw/l)	Gamma Production Rate (kw/l)	Gamma Deposition Rate/ Fission Power (%)	Gamma Deposition Rate/ Gamma Production Rate
1	4.55	2.600 E-16	1.673 E-17	1.594 E-17	6,43	1.05
2	1.36 E1	2.600 E-16	1.672 E-17	1.594 E-17	6.43	1.05
3	2.27 E1	2.604 E-16	1.677 E-17	1.596 E-17	6.44	1.05
4	3.18 E1	2.633 E-16	1.668 E-17	1.596 E-17	6.41	1.05
5	3.89 E1	2.450 E-16	1.634 E-17	1.596 E-17	6.67	1.02
6	4.39 E1	2.458 E-16	1.627 E-17	1.603 E-17	6.62	1.01
7	4.89 E1	2.499 E-16	1.697 E-17	1.626 E-17	6.79	1.04
8	5.43 E1	3.246 E-16	1.941 E-17	1.659 E-17	5.98	1.17
9	6.01 E1	3.213 E-16	1.889 E-17	1.642 E-17	5.88	1.15
10	6.54 E1	1.779 E-16	1.509 E-17	1.467 E-17	8.48	1.03
11	7.03 E1	1.752 E-16	1.442 E-17	1.453 E-17	8.23	0.99
12	7.49 E1	2.258 E-16	1.574 E-17	1.483 E-17	6.97	1.06
13	7.92 E1	2.330 E-16	1.680 E-17	1.527 E-17	7.21	1.10
14	8.33 E1	3.013 E-16	1.796 E-17	1.825 E-17	5.96	0.98
15	8.72 E1	3.086 E-16	1.892 E-17	1.868 E-17	6.13	1.01
16	9.09 E1	3.367 E-16	1.980 E-17	1.897 E-17	5.88	1.04
17	9.45 E1	3.370 E-16	1.938 E-17	1.900 E-17	5.75	1.02

Table B.1 (continued)

Fission Power Density, Gamma Production Rate and Gamma Deposition Rate

Mesh Interval	Interval Mid-point Distance from the Core Center (cm.)	Fission Power Density (kw/l)	Gamma Deposition Rate (kw/l)	Gamma Production Rate (kw/l)	Gamma Deposition Rate/ Fission Power (%)	Gamma Deposition Rate/ Gamma Production Rate
18	9.79 E1	2.272 E-16	1.693 E-17	1.885 E-17	7.45	0.90
19	1.01 E1	2.281 E-16	1.679 E-17	1.893 E-17	7.36	0.89
20	1.04 E2	3.071 E-16	1.849 E-17	1.925 E-17	6.02	0.96
21	1.08 E2	3.124 E-16	1.943 E-17	1.954 E-17	6.22	0.99
22	1.11 E2	3.452 E-16	2.030 E-17	1.976 E-17	5.88	1.03
23	1.14 E2	3.477 E-16	2.083 E-17	1.990 E-17	5.99	1.05
24	1.16 E2	3.612 E-16	2.120 E-17	1.995 E-17	5.87	1.06
25	1.19 E2	3.597 E-16	2.115 E-17	1.988 E-17	5.88	1.06
26	1.22 E2	3.384 E-16	1.939 E-17	2.052 E-17	5.73	0.94
27	1.25 E2	3.360 E-16	1.942 E-17	2.036 E-17	5.78	0.95
28	1.27 E2	3.608 E-16	2.013 E-17	2.020 E-17	5.58	1.00
29	1.30 E2	3.563 E-16	2.031 E-17	1.997 E-17	5.70	1.02
30	1.32 E2	3.521 E-16	2.028 E-17	1.965 E-17	5.76	1.03
31	1.35 E2	3.449 E-16	1.990 E-17	1.925 E-17	5.77	1.03
32	1.37 E2	3.442 E-16	1.908 E-17	1.877 E-17	5.71	1.02
33	1.40 E2	3.247 E-16	1.857 E-17	1.826 E-17	5.72	1.02
34	1.42 E2	3.179 E-16	1.831 E-17	1.775 E-17	5.76	1.03

Table B.1 (continued)

Fission Power Density, Gamma Production Rate and Gamma Deposition Rate

Mesh Interval	Interval Mid-point Distance from the Core Center (cm.)	Fission Power Density (kw/l)	Gamma Deposition Rate (kw/l)	Gamma Production Rate (kw/l)	Gamma Deposition Rate/ Fission Power (%)	Gamma Deposition Rate/ Gamma Production Rate
35	1.44 E2	3.074 E-16	1.777 E-17	1.722 E-17	5.78	1.03
36	1.47 E2	2.927 E-16	1.692 E-17	1.666 E-17	5.78	1.02
37	1.49 E2	2.818 E-16	1.643 E-17	1.613 E-17	5.83	1.02
38	1.51 E2	2.749 E-16	1.630 E-17	1.570 E-17	5.93	1.04
39	1.53 E2	2.662 E-16	1.616 E-17	1.540 E-17	6.07	1.05
40	1.55 E2	2.583 E-16	1.625 E-17	1.539 E-17	6.29	1.06
41	1.58 E2	2.594 E-16	1.689 E-17	1.610 E-17	6.51	1.05
42	1.60 E2	2.792 E-16	1.910 E-17	1.862 E-17	6.84	1.03
43	1.62 E2	3.648 E-16	1.930 E-17	2.654 E-17	5.29	0.73
44	1.64 E2	--	2.250 E-18	6.479 E-19	--	3.47
45	1.66 E2	--	2.012 E-18	6.994 E-19	--	2.88
46	1.68 E2	--	1.880 E-18	6.906 E-19	--	2.72
47	1.70 E2	--	1.816 E-18	6.072 E-19	--	2.99
48	1.72 E2	--	1.811 E-18	4.405 E-19	--	4.11
49	1.73 E2	1.133 E-16	1.280 E-17	1.527 E-17	11.30	0.84
50	1.75 E2	6.343 E-17	9.663 E-18	8.144 E-18	15.23	1.19
51	1.77 E2	5.170 E-17	6.887 E-18	5.440 E-18	13.32	1.27

Table B.1 (continued)

Fission Power Density, Gamma Production Rate and Gamma Deposition Rate

Mesh Interval	Interval Mid-point Distance from the Core Center (cm.)	Fission Power Density (kw/l)	Gamma Deposition Rate (kw/l)	Gamma Production Rate (kw/l)	Gamma Deposition Rate/ Fission Power (%)	Gamma Deposition Rate/ Gamma Production Rate
52	1.78 E2	4.296 E-17	5.619 E-18	4.567 E-18	13.08	1.23
53	1.81 E2	3.068 E-17	5.066 E-18	4.488 E-18	16.51	1.13
54	1.83 E2	3.839 E-17	4.653 E-18	6.041 E-18	12.12	0.77
55	1.85 E2	--	5.336 E-19	1.454 E-19	--	3.67
56	1.86 E2	--	4.880 E-19	1.597 E-19	--	3.06
57	1.88 E2	--	4.677 E-19	1.561 E-19	--	2.96
58	1.90 E2	--	3.343 E-19	4.755 E-20	--	7.03
59	1.92 E2	--	3.358 E-19	3.744 E-20	--	8.97
60	1.93 E2	--	3.537 E-18	4.320 E-18	17.83	0.82
61	1.95 E2	1.984 E-17	2.723 E-18	2.344 E-18	23.87	1.16
62	1.97 E2	1.141 E-17	1.925 E-18	1.543 E-18	21.13	1.25
63	1.98 E2	9.110 E-18	1.536 E-18	1.253 E-18	20.77	1.23
64	2.00 E2	7.395 E-18	1.184 E-18	1.131 E-18	22.04	1.05
65	2.02 E2	5.372 E-18	1.052 E-18	1.485 E-18	16.69	0.71
66	2.04 E2	6.303 E-18	1.171 E-19	2.870 E-20	--	4.08
67	2.06 E2	--	1.089 E-19	3.380 E-20	--	3.22
68	2.08 Eq	--	1.021 E-19	3.030 E-20	--	3.37

Table B.1 (continued)

Fission Power Density, Gamma Production Rate and Gamma Deposition Rate

Mesh Interval	Interval Mid-point Distance from the Core Center (cm.)	Fission Power Density (kw/l)	Gamma Deposition Rate (kw/l)	Gamma Production Rate (kw/l)	Gamma Deposition Rate/ Fission Power (%)	Gamma Deposition Rate/ Gamma Production Rate
69	2.10 E2	--	9.846 E-20	2.231 E-20	--	4.41
70	2.12 E2	2.327 E-18	6.791 E-19	6.618 E-19	29.18	1.03
71	2.15 E2	1.451 E-18	4.391 E-19	3.384 E-19	30.27	1.30
72	2.18 E2	1.094	2.922 E-19	2.390 E-19	26.71	1.22
73	2.21 E2	8.344	2.262 E-20	2.384 E-19	27.11	0.95
74	2.24 E2	--	2.115 E-20	5.680 E-21	--	3.72
75	2.25 E2	--	1.955 E-20	5.906 E-21	--	3.31
76	2.27 E2	--	1.872 E-20	5.353 E-21	--	3.50
77	2.29 E2	--	1.832 E-20	4.129 E-21	--	4.44
78	2.31 E2	4.058 E-19	1.334 E-19	1.367 E-19	32.87	0.98
79	2.34 E2	3.013 E-19	9.575 E-20	7.733 E-20	31.78	1.24
80	2.37 E2	3.321 E-19	7.741 E-20	6.614 E-20	23.31	1.17
81	2.40 E2	4.937 E-19	7.183 E-20	9.212 E-20	14.55	0.78
82	2.44 E2	--	6.542 E-21	7.391 E-21	--	0.89
83	2.50 E2	--	5.538 E-21	1.251 E-20	--	0.44
84	2.55 E2	--	4.788 E-21	1.406 E-20	--	0.34
85	2.61 E2	--	4.202 E-21	1.293 E-20	--	0.32
86	2.69 E2	--	3.277 E-21	9.273 E-21	--	0.35
87	2.78 E2	--	2.121 E-21	4.303 E-21	--	0.50
88	2.87 E2	--	1.239 E-21	8.139 E-22	--	1.52

B.2 Tabulated Values of the Neutron Heating Rate (Section 3.6)

The total core power used in the normalization is 3000 MWt or 18.75 MWT/cm axial, since the active core height is 160 cm.

Table B.2 was used to plot Fig. 3.7 in Chapter Three.

Table B.2

Neutron Heating Rate

Mesh Interval*	Neutron Heating Rate (kw/l)	Mesh Interval	Neutron Heating Rate (kw/l)	Mesh Interval	Neutron Heating Rate (kw/l)
1	0.277 E+0	16	0.445 E+0	31	0.479 E+0
2	0.279 E+0	17	0.458 E+0	32	0.470 E+0
3	0.283 E+0	18	0.469 E+0	33	0.460 E+0
4	0.290 E+0	19	0.479 E+0	34	0.448 E+0
5	0.296 E+0	20	0.486 E+0	35	0.435 E+0
6	0.302 E+0	21	0.492 E+0	36	0.422 E+0
7	0.307 E+0	22	0.497 E+0	37	0.407 E+0
8	0.314 E+0	23	0.501 E+0	38	0.391 E+0
9	0.322 E+0	24	0.505 E+0	39	0.374 E+0
10	0.332 E+0	25	0.508 E+0	40	0.355 E+0
11	0.345 E+0	26	0.500 E+0	41	0.334 E+0
12	0.363 E+0	27	0.500 E+0	42	0.310 E+0
13	0.386 E+0	28	0.498 E+0	43	0.281 E+0
14	0.407 E+0	29	0.493 E+0	44	0.562 E+1
15	0.428 E+0	30	0.487 E+0	45	0.414 E+1

*The distances of the interval midpoints from the center of the core are as given in Table B.1.

Table B.2 (continued)

Neutron Heating Rate

Mesh Interval	Neutron Heating Rate (kw/l)	Mesh Interval	Neutron Heating Rate (kw/l)	Mesh Interval	Neutron Heating Rate (kw/l)
46	0.317 E+1	61	0.413 E-1	76	0.131 E+0
47	0.260 E+1	62	0.354 E-1	77	0.120 E+0
48	0.234 E+1	63	0.324 E-1	78	0.430 E-2
49	0.987 E-1	64	0.316 E-1	79	0.378 E-2
50	0.944 E-1	65	0.284 E-1	80	0.330 E-2
51	0.889 E-1	66	0.547 E+0	81	0.284 E-2
52	0.831 E-1	67	0.392 E+0	82	0.325 E-1
53	0.774 E-1	68	0.297 E+0	83	0.111 E-1
54	0.718 E-1	69	0.246 E+0	84	0.393 E-2
55	0.165 E+1	70	0.968 E-2	85	0.147 E-2
56	0.154 E+1	71	0.8729E-2	86	0.376 E-3
57	0.143 E+1	72	0.773 E-2	87	0.850 E-4
58	0.131 E+1	73	0.680 E-2	88	0.184 E-4
59	0.121 E+1	74	0.153 E+0		
60	0.449 E-1	75	0.141 E+0		

REFERENCES

A-1 D.C. Aldrich, "Parfait Blanket Systems Employing Mixed Progeny Fuels," S.M. Thesis, M.I.T. Nuclear Engineering Department (1976).

A-2 R. Avery, "Coupled Fast-Thermal Power Breeder," Nucl. Sci. Eng. 3, 129 (1958).

A-3 R. Avery, "Theory of Coupled Reactors," Int. Conf. on Peaceful Uses of Atomic Energy, Geneva, p. 182 (1958).

A-4 R. Avery, et al., "Coupled Fast-Thermal Power Breeder Critical Experiment," Int. Conf. on Peaceful Uses of Atomic Energy, Geneva, p. 151 (1958).

A-5 American Nuclear Society, "Proposed American National Standard for the Determination of Thermal Energy Deposition Rates in Nuclear Reactors," ANSI Standard N676 D-2 (September 1975).

B-1 G. J. Fischer and R. J. Cerbone, "The Fast-Mixed Spectrum Reactor Interim Report," Dept. of Nuclear Energy, BNL (Dec. 1978).

B-2 M. Bustraan, "Integral Determination of Neutron Absorption by Fission Products," Review paper to the IAEA Fission Product Nuclear Data Panel, Bologna (Nov. 1973).

B-3 W. P. Barthold and C. P. Tzanos, "Performance Potential of a Reference Fuel in 1200 MWe LMFBR's," Argonne National Laboratory, FRA-TM-104 (Nov. 1977).

B-4 G. J. Brown and M. J. Driscoll, "Evaluation of High Performance LMFBR Blanket Configurations," MITNE-150, COO-2250-4 (May 1974).

B-5 I. I. Bondarenko, Editor, "Group Constants for Nuclear Reactor Calculations," Consultants Bureau, New York (1964).

B-6 M. Bustraan, et al., "Experiences with STEK: Derivation of Fission Product Cross Sections and their Improvement by Statistical Adjustment Using Sample Reactivity Worths," B-26, Proceedings of International Symposium on Physics of Fast Reactors, Tokyo (October 1973).

C-1 J. L. Cook, "Fission Product Cross Sections," AAEC/TM-549 (1970).

D-1 W. J. David, et al., "SPHINX, A One Dimensional Diffusion and Transport Nuclear Cross Section Processing Code," WARD-XS-3045-17 (August 1977).

D-2 M. J. Driscoll, et al., "Safety and Breeding-Related Aspects of Fast Reactor Cores Having Internal Blankets," Proc. Int. Mtg. Fast Reactor Safety and Related Physics, Chicago, IL (Oct. 1976).

D-3 G. A. Ducat, M. J. Driscoll and N. E. Todreas, "Evaluation of the Parfait Blanket Concept for Fast Breeder Reactors," COO-2250-5 (1976).

D-4 C. Durston, Brookhaven National Laboratory, Technical Memorandum-FMSR Log. #37, July, 1979.

E-1 W. W. Engle, Jr., "A Users Manual for ANISN, A One Dimensional Discrete Ordinates Transport Code with Anisotropic Scattering," K-1693, Union Carbide Corporation, Nuclear Division (March 1967).

F-1 W. E. Ford III and D. H. Wallace, "POPOP4, A Code for Converting Gamma-Ray Spectra to Secondary Gamma-Ray Production Cross Sections," CTC-12, Computer Technology Center, Oak Ridge National Laboratory (1969).

G-1 K. N. Grimm and D. Meneghetti, "Application of Gamma Transport Approximations in EBR-II Analysis," ANS Transactions, Vol. 22 (Nov. 1975).

G-2 H. Gruppelaar, et al., "RCN-1 Pseudo Fission-Product Capture Group Cross Sections," RCN-205 (1974).

J-1 Y. Kikuchi, et al., "Fission Product Fast Reactor Constants System of JNDC," JAERI 1248 (Nov. 1976).

K-1 R. B. Kidman, et al., "LIB-IV, A Library of Group Constants for Nuclear Reactor Calculations," LA-6260-MS (1976).

K-2 M. S. Kalra, "Gamma Heating in Fast Reactors." COO-2250-18, MITNE-179 (Feb. 1976).

K-3 J. R. Knight and F. R. Mynatt, "MUG - A Program for Generating Multigroup Photon Cross Sections," CTC-17, Union Carbide Corporation, Computing Technology Center (1970).

K-4 G. R. Keepin, "Physics of Nuclear Kinetics," Addison-Wesley, Reading, Mass. (1965), p. 13, Table 2-1.

L-1 D. B. Lancaster, Personal Communication.

L-2 D. B. Lancaster, "An Assessment of the Use of Internal Blankets in Gas Cooled Fast Breeder Reactors," Ph.D. Thesis, M.I.T., Nuclear Engineering Dept. (February, 1980 - estimated).

L-3 W. W. Little, et al., "2DB, User's Manual, Revision 1," Battelle Memorial Institute, BNWL-954 (1969).

L-4 K. D. Lathrop, "GAMLEG - A Fortran Code to Produce Multigroup Cross Sections for Photon Transport Calculations," LA-3267 (1965).

M-1 R. E. MacFarlane, Los Alamos Scientific Laboratory, Personal Communication.

O-1 Oak Ridge National Laboratory, "40 Group Coupled Neutron and Gamma-Ray Cross Section Data," DLC-23 (April 1974).

P-1 R. A. Pinnock, "Parfait Blanket Configurations for Fast Breeder Reactors," S.M. Thesis, M.I.T., Nuclear Engineering Department (1975).

S-1 P. A. Scheinert and M. J. Driscoll, "Gamma Heating Measurements in Fast Breeder Reactor Blankets," MITNE-164, COO-2250-10 (August 1974).

S-2 J. I. Shin and M. J. Driscoll, "Evaluation of Advanced Fast Reactor Blanket Design," COO-2250-25 (1977).

W-1 P. J. Wood and M. J. Driscoll, "Assessment of Thorium Blankets for Fast Breeder Reactors," MITNE-148, COO-2250-2 (July 1973).

W-2 K. E. Weise and A. Foderaro, "Legendre Polynomial Expansion of the Klein-Nishina Differential Cross Section," Nucl. Sci. Eng., 54, 1, 85-93 (May 1974).